WET-GAS COMPRESSION IN TWIN-SCREW MULTIPHASE PUMPS

A Thesis

by

EVAN CHAN

Submitted to the Office of Graduate Studies of
Texas A&M University
in partial fulfillment of the requirements for the degree of

MASTER OF SCIENCE

December 2006

Major Subject: Petroleum Engineering

WET-GAS COMPRESSION IN TWIN-SCREW MULTIPHASE PUMPS

A Thesis

by

EVAN CHAN

Submitted to the Office of Graduate Studies of
Texas A&M University
in partial fulfillment of the requirements for the degree of

MASTER OF SCIENCE

Approved by:

Chair of Committee,	Stuart L. Scott
Committee Members,	Daulat Mamora
	Charles Glover
Head of Department,	Stephen Holditch

December 2006

Major Subject: Petroleum Engineering

ABSTRACT

Wet-Gas Compression in Twin-Screw Multiphase Pumps.

(December 2006)

Evan Chan, B.S., Brown University

Chair of Advisory Committee: Dr. Stuart L. Scott

Multiphase pumping with twin-screw pumps is a relatively new technology that has been proven successful in a variety of field applications. By using these pumps to add energy to the combined gas and liquid wellstream with minimal separation, operators have been able to reduce capital costs while increasing overall production. In many cases, such as subsea operations, multiphase pumping is the only viable option to make remote wells economic.

Despite their many advantages, some problems have been encountered when operating under conditions with high gas volume fractions (GVF). Twin-screw multiphase pumps experience a severe decrease in efficiency when operating under wet-gas conditions, GVF over 95%. Field operations have revealed severe vibration and thermal issues which can lead to damage of the pump internals, requiring expensive maintenance. The research presented in this thesis seeks to investigate two novel methods of improving the performance of twin-screw pumps under wet-gas conditions.

The first involves increasing the viscosity of the liquid stream. We propose that by increasing the viscosity of the liquid phase, the pump throughput can be increased. Tests were conducted at high GVF using guar gel to increase the viscosity of the liquid phase. Along with results from a multiphase pump model the pump behavior under wet-gas conditions with increased liquid viscosity was evaluated. The experimental results indicate that at high GVF, viscosity is not a dominant parameter for determining pump performance. Possible reasons for this behavior were proposed. These results were not predicted by current pump models. Therefore, several suggestions for improving the model's predictive performance were suggested.

The second method is the direct injection of liquid into the pump casing. By selectively injecting liquid into specific pump chambers, it is believed that many of the

vibration issues can be eliminated with the added benefit of additional pressure boosting capacity. Since this method requires extensive mechanical modifications to an existing pump, it was studied only analytically. Calculations were carried out that show that through-casing liquid injection is feasible. More favorable pressure profiles and increased boosting ability were demonstrated.

DEDICATION

I dedicate this work to my family.

ACKNOWLEDGEMENTS

I would like to thank Dr. Scott for his guidance and for making this work possible. I would also like to thank Jason and Hemant with whom I shared many hours at Riverside.

TABLE OF CONTENTS

CHAPTER Page

LIST OF FIGURES

FIGURE Page

FIGURE Page

FIGURE Page

FIGURE Page

LIST OF TABLES

TABLE Page

CHAPTER I
INTRODUCTION

Multiphase pumping is a relatively new technology that allows the energy of an unprocessed wellstream of oil, water, gas, and other produced material such as sand to be increased, thus allowing it to be moved to a central processing facility. This eliminates the need for production site processing equipment thereby decreasing capital costs associated in efficiently producing an oil and gas field. Removing auxiliary equipment also reduced the environmental impact by minimizing installation size and eliminating flaring in some cases.

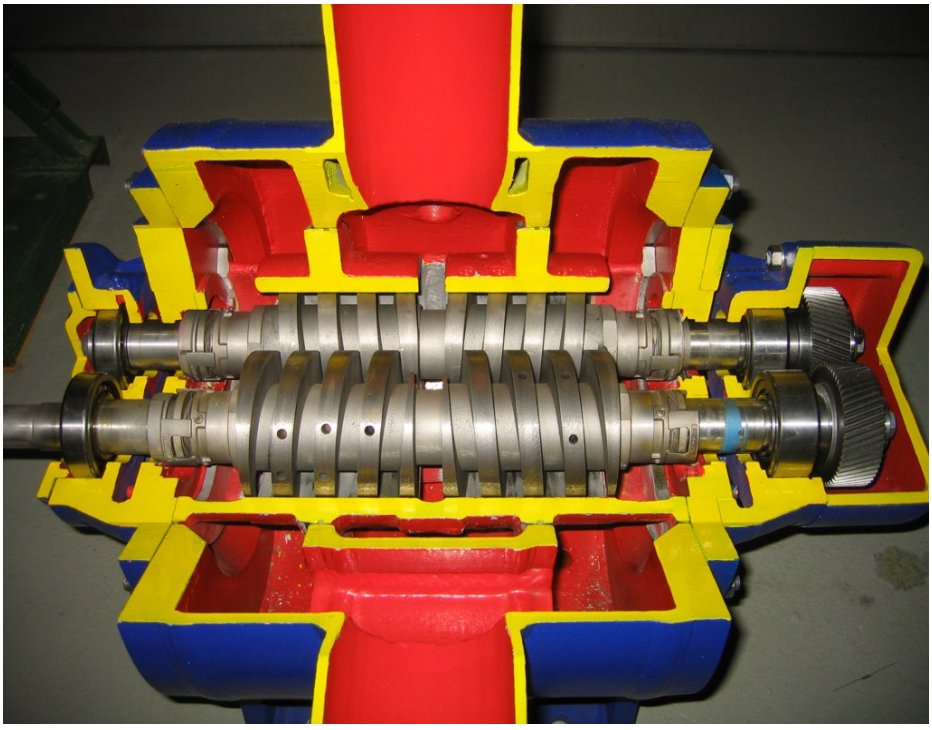

Fig. 1.1 – Cut-away view of twin-screw pump internals (after Scharf *et al.*[2]).

This thesis follows the style and format of *SPE Production and Facilities*.

Though there are several types of multiphase pumps, twin-screw pumps are currently the most widely used.[1] Twin-screw pumps are rotary positive displacement pumps consisting of two intermeshing screws which form a series of chambers. As the screws rotate, these chambers normally move from the suction ends of the pump towards the discharge in the center. This action moves the fluid from the low pressure suction side of the pump to the higher pressure discharge. **Fig. 1.1** illustrates the internal components of a typical twin-screw pump.

Twin-screw pumps are thought to be ideal for multiphase conditions because of the small amount of shear they impart on the fluid, their ability to handle high gas volume fractions (GVF), and their ability to tolerate some amount of solids contaminating the fluid stream. They are generally favored because of their relatively high flow capacity and pressure boosting capability. Originally designed to move highly viscous liquids, twin-screw pumps have only relatively recently been applied in the oilfield to move oil, water, and gas mixtures directly from the well to reduce backpressure on the well, thus increasing production rates and total recovery. Martin and Scott[3] showed that in cases in which the well was backpressure limited, multiphase pumping can have a dramatic effect, increasing well productivity and recoverable reserves.

Twin-screw pumps have been applied in a variety of different operational situations. The simplest application is as an alternative to conventional production methods where a multiphase pump can take the place of a separation system, single-phase liquid pump, and gas compressor, thereby lowering capital costs and installation size. Wilkinson[4] and Dick & Speirs[5] have shown that twin-screw pumps have proven useful for reducing annulus gas pressure during steam-flood operations in the Canadian oil sands, eliminating the need for multiple scrubbers and separators, heat exchangers, and gas compressors.

Additionally, twin-screw pumps show great promise in subsea applications where they provide a means of boosting production from remote wells to existing platforms or onshore facilities. Scott[1] has outlined four basic categories of subsea processing which represent the current state and future of subsea multiphase production, ranging from basic subsea boosting to advanced subsea processing systems. Subsea boosting is one of the largest growth areas for multiphase pumping. In many subsea fields multiphase pumping

is the only economical method of production as water depths and step-out lengths increase.

These applications are all examples of instances where the GVF of the production stream can routinely reach 94 – 100%. At such high GVF, multiphase pumping is often reclassified as wet-gas compression. In these cases, pump manufacturers recommend that GVF be limited to 95% to ensure pump operability. This necessitates the use of a liquid recycling system consisting of a downstream separator to capture some liquid for recirculation. For this thesis, a GVF of 95% or above will be considered as wet-gas compression.[6,7]

The reason for limiting GVF to 95% is that field operations under wet-gas conditions have revealed significant vibration and thermal issues which can lead to damage of the pump internals and expensive repairs and maintenance. The project outlined in this thesis investigates novel methods of improving the performance of twin-screw pumps under wet-gas conditions. The twin-screw pump model developed by Martin[7] was used as a tool for evaluating these ideas along with experimental data.

Twin-screw pumps represent large investments in equipment costs. Individual pumps units can cost up to several million US dollars. This large initial cost is the prime reason for the slow acceptance of multiphase pumping technology even when significant cost savings can be projected in the long run. The relative immaturity of the technology presents another obstacle since the reliability of the equipment can be questionable at times. This research is aimed at making twin-screw pumps a more economic piece of oilfield equipment. By improving gas throughput and reliability, we can make twin-screw pumps more attractive to the industry as an alternative to traditional production methods.

The first method investigated involves increasing the viscosity of the liquid phase. By increasing the liquid viscosity, it is hoped that pump throughput can be increased. The second method is the direct injection of liquid into the pump casing. By selectively injecting liquid at certain points on the pump, it is believed that many of the vibration issues can be eliminated with the added benefit of additional pressure boosting capacity. Since this method requires extensive mechanical modifications to an existing pump, it will be studied only theoretically. These two novel ideas were first described by Singh.[6,7]

This thesis is divided into seven chapters. Chapter II is a literature review focusing on modeling of twin-screw pumps and some unique problems encountered under wet-gas conditions. Understanding how these pumps are modeled is vital in understanding the operating principles on which they function, therefore enabling an investigator to attempt to modify a pumps performance and behavior. Chapter III discusses approaches to wet-gas compression and presents the two new ideas for improving twin-screw pump performance under wet-gas conditions, high viscosity liquid circulation and through-casing injection. Chapter IV diagrams the experimental facility that was used to test the high viscosity liquid circulation concept and the matrix of tests performed. Chapters V and VI present the results of work done to investigate the feasibility of the two concepts presented. Chapter VII summarizes the conclusions and recommendations of the total work. Additionally, a study of twin-screw pump clearance sizes using the Martin pump model is presented in Appendix A.

CHAPTER II
LITERATURE REVIEW
TWIN-SCREW PUMP MODELS

This chapter focuses on modeling of twin-screw pumps as a means of understanding pump behavior in order to understand the causes and possible remedies of some of the problems encountered in wet-gas compression. The application of twin-screw pumps to multiphase-flow conditions has created a number of complications. Interactions between the different phases and the inherently complex nature of the system have necessitated the development of mathematical models to predict how parameters such as screw geometry, clearance sizes, suction pressure, viscosity, and GVF affect pump performance. Mechanistic models are a vital tool for applying and studying these types of pumps. However, these models fail to predict some of the problems encountered when twin-screw pumps operate at under wet-gas conditions. These problems are not

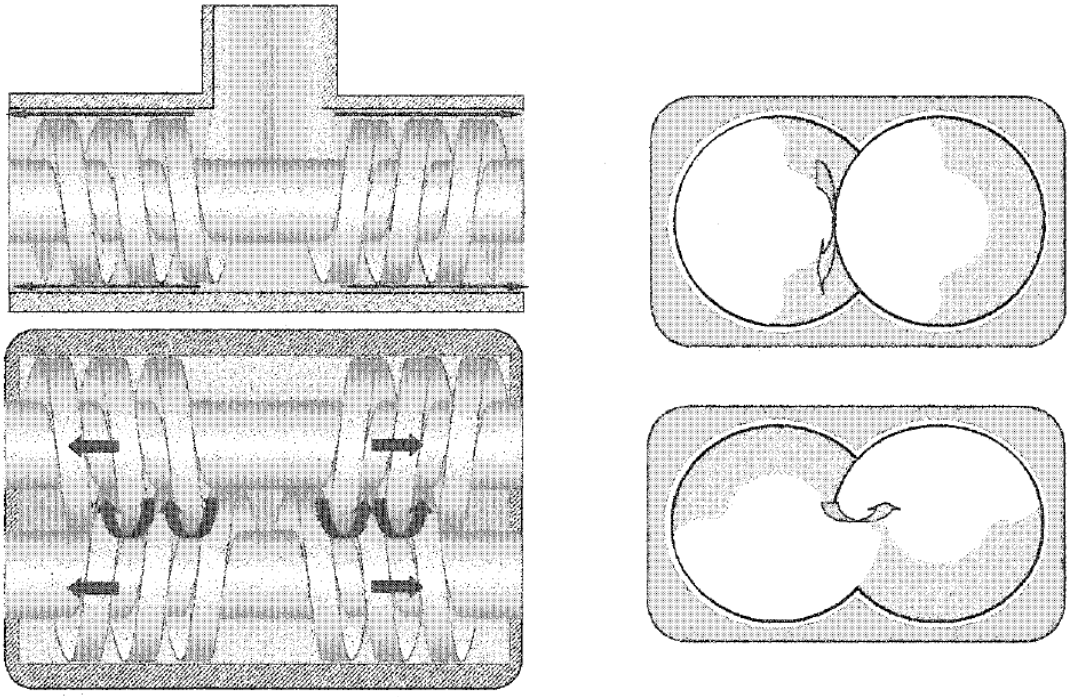

Fig. 2.1 – Screw intermeshing and slip flow paths (after Martin[8,9]).

predicted by the current pump models because they are based in part on assumptions known to be invalid at high GVF. Currently, no twin-screw pump models exist that were designed specifically with wet-gas compression in mind.

All current twin-screw pump models are based around the modeling of backflow through the pump. Since the two screws of a pump do not touch, flow paths exist through the small gaps formed. The pressure differential between the discharge and suction sides of the pump causes backflow to occur. Backflow within the pump, also known as slip flow, is a key factor in the operation of twin-screw pump since it is this slip flow that seals and compresses the gas phase in each chamber. Most researchers have therefore based their modeling efforts on understanding slip flow. **Fig. 2.1**, above, illustrates the flow paths formed by the intermeshing screws. This chapter will attempt to show the evolution of twin-screw pump models. Discussion of the various pump models will be handled in the order presented by Scott[1] on **Table 2.1**.

Table 2.1 – Summary of twin-screw pump models (after Scott[1]).

Model	Developer	Funded	Year	Capabilities	Comments
U. of Erlangen	Letter & Wincek	Leistritz	1993	mechanistic	requires detailed geometry and solution algorithm poorly defined
JNOC	Egashira, Shoda, Tochikawa and Furukawa	JNOC	1996	empirical	correlations for slip may not extend to other pumps
Texas A&M University	Martin & Scott	BP, ChevronTexaco, Marathon	2003	mechanistic	uses easy to obtain combine slip concept
Flowserve	Prang & Cooper	Flowserve	2004	mechanistic	requires detailed geometry
U. of Hannover	Rausch, Vauth, Brandt & Mewes	Bornemann / German Federal Ministry for Education & Research	2004	thermodynamic	neglects slip and requires detailed geometry

2.1 Vetter *et al.* (1993)

In two papers, Vetter *et al.*[10,11] outlined a mechanistic twin-screw pump model based on modeling backflow between the various pump clearances within the pump. This model is considered a landmark work and is the basis for most other work done on the modeling of twin-screw pumps. Vetter and his colleagues made the key simplification of approximating the pump as an infinite series of fluid-filled cylinders moving towards the middle of the pump.

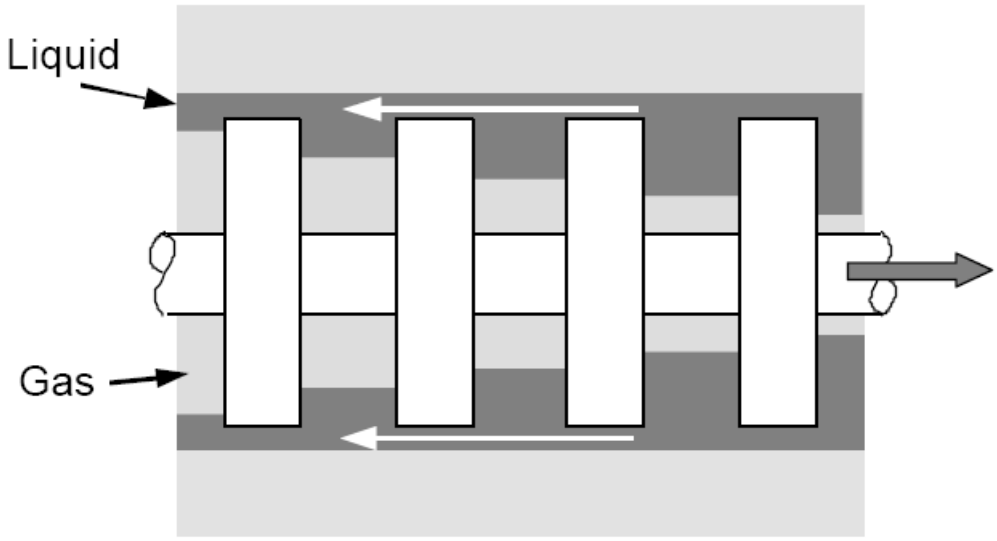

Fig. 2.2 – Simplified twin-screw model (after Vetter *et al.*[10,11]).

As seen in **Fig. 2.2**, the model assumes phase separation due to centrifugal forces from the spinning screws. This is an important assumption since it allows for the slip flow in the clearances to be calculated as single phase liquid, pressure driven flow. Therefore, the liquid filled clearances act as a seal against gas leakage out of the pump chambers.

For this model, several precise measurements of screw geometry are required in order to calculate the actual size of each of the different clearances in the pump. Using tests conducted with pure liquid and locked screws, the contribution of the various

clearances were measured. The circumferential gap between the screw and the pump casing was found to contribute the most to internal slip flow, accounting for approximately 80% of the total.

The slip flow itself behaves like a piston, compressing the gas as it enters the previous chamber. This gas compression process is assumed to be isothermal up to 96% GVF, although no non-isothermal solution is given for GVF above this limit. The assumption of liquid sealing in the clearances is recognized as a simplification and does not reflect real conditions at high GVF.

In their second paper, Vetter *et al.* recognize that the assumption of liquid filled clearances is not valid for GVF above 85%. They propose equations for adjusting the fluid density and viscosity to reflect effect of gas and liquid mixture flowing through the clearances are presented. The developed model was validated by running water-air mixtures through a test pump.

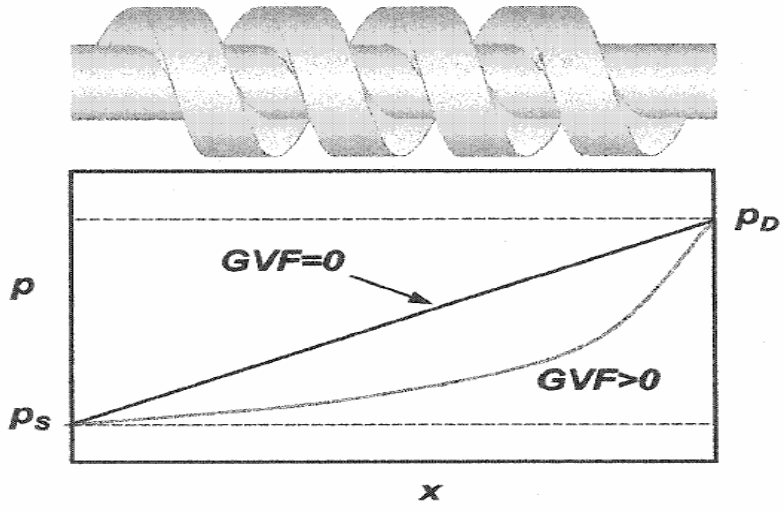

Fig. 2.3 – Pressure profiles for single and two phase pumping (after Vetter *et al.*[10,11]).

An interesting observation made was the shape of the pressure profiles along the screw of the pump. As shown in **Fig. 2.3**, during single-phase flow the pressure profile is linear. This means that each chamber of the pump is contributing equally to the overall pressure boost provided by the pump. However for two-phase flow, the pressure profile is no longer linear. As GVF increases, the compression occurring becomes more concentrated in the chambers closer to the discharge.

Vetter *et al.*[10,11] also discussed spindle shaft deformation resulting from differential pressure differences along the shaft. According to them, the degree of shaft deformation or deflection is independent of whether the pump is operating under single-phase or two-phase conditions. Shaft deformation or deflection is an important feature that would be incorporated into future models.

2.2 Egashira *et al.* (1996)

Egashira *et al.*[12] took an empirical approach to modeling backflow in twin-screw pumps. Using experimental data, they proposed an equation to calculate the pressure profile along the screw.

$$\left(\frac{p_i - p_s}{p_d - p_s}\right) = \left(\frac{i}{n_t + 1}\right)^{\gamma} \tag{2.1}$$

This equation is a curve fit based on the parameter γ, which is adjusted to fit experimental data. This curve fit is based on a single test pump so it may not be applicable to other pump designs. Egashira *et al.*[12] also identified the various pump clearances through which slip flow occurs and showed that the amount of slip flow is mainly a function of differential pressure, GVF, and shaft rotational speed.

Experimental data provided by Egashira *et al.*[12] also confirms earlier experiments about the nature of the pressure profile along the pump screws. As GVF increases the pressure profile in the pump becomes more and more nonlinear. They also note that the profile becomes steeper as of the pump speed and multiphase fluid compressibility increase. The experiments conducted used water and air as test fluids.

A unique feature of the work described by Egashira *et al.*[12] is their description of possible backflow flow patterns. They describe three different patterns detailing the type of flow, either pure water or an air and water mixture, in each of the four clearances they

define. The first pattern consists of pure water flow in the circumferential clearance because of phase separation from centrifugal forces with a multiphase mixture in each of the internal clearances. The second and third patterns are pure water or air and water mixtures in all clearances, respectively.

2.3 Martin and Scott (2003)

The Martin and Scott[8,9] model was developed to meet the need for a twin-screw pump model for petroleum engineers. To properly design a twin-screw pump into a production system, a complete set of pump tables is required. Though these tables can sometimes be obtained from the pump manufacturer, an independent tool for predicting pump performance was still needed. Previous models required detailed measurements of screw geometry in order to calculate the size of the clearances. However, pump manufacturers are usually unwilling to disclose these measurements since they are regarded as trade secrets. To get around this limitation, Martin and Scott[8,9] introduced a system for calculating an effective clearance size based on pure-water performance data using linear regression.

Martin and Scott[8,9] were also the first to validate their pump model for liquids with high viscosity using guar gel. Higher viscosity was observed to decrease slip rate. The Martin and Scott[8,9] model was also the first model to be confirmed to work with different pump designs. Experiments were conducted with two different pumps and data from two others was matched successfully.

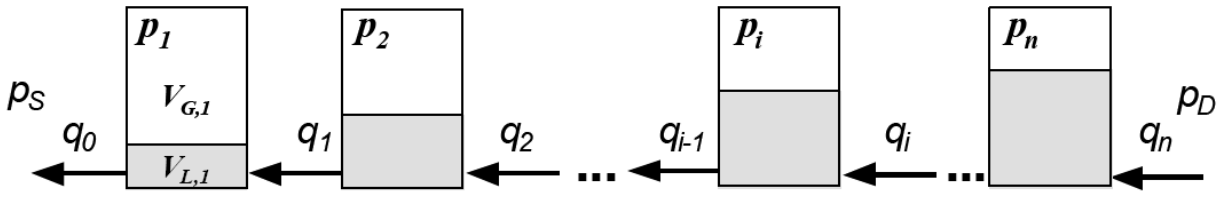

Fig. 2.4 – Simplified pump model (after Martin[8,9]).

A key component of this model is the gas compression module. As shown in **Fig. 2.4**, the pump is modeled as a series of independent chambers that are connected by slip flow from one chamber to the previous chamber. The slip flow moves in the opposite direction of the chambers as they are translated through the pump. This is similar to the Vetter *et al.*[10,11] model.

A set of moving control volumes is defined around each chamber, Fig. 2.4, which allows for a set of equations to be written defining the pump behavior.

$$\begin{aligned}
V_s \cdot \left(\frac{p_s \cdot Z_1}{p_1 \cdot Z_s} - 1 \right) + \left(q_1 - q_0 \right) \cdot \Delta t = 0 \\
V_1 \cdot \left(\frac{p_1 \cdot Z_2}{p_2 \cdot Z_1} - 1 \right) + \left(q_2 - q_1 \right) \cdot \Delta t = 0 \\
\vdots \\
V_{i-1} \cdot \left(\frac{p_{i-1} \cdot Z_i}{p_i \cdot Z_{i-1}} - 1 \right) + \left(q_i - q_{i-1} \right) \cdot \Delta t = 0 \\
\vdots \\
V_{n-1} \cdot \left(\frac{p_{n-1} \cdot Z_D}{p_D \cdot Z_{n-1}} - 1 \right) + \left(q_n - q_{n-1} \right) \cdot \Delta t = 0
\end{aligned} \tag{2.2}$$

In this system of equations the volumes, V, and the slip flow rates, q, are all functions of pressure. Therefore, the pressure in each chamber must be solved simultaneously. The Martin and Scott model utilized a Newton-Raphson algorithm to solve for these pressures. Total slip flow through the entire pump and therefore the pumping rate can then be calculated.

2.4 Cooper & Prang (2004)

Cooper & Prang[13] proposed a twin-screw pump model based on similar methods to previous models. However, Cooper & Prang[13] clearly stated the assumptions made to make a volumetric slip flow model possible. Two of the main assumptions are:

1. Complete liquid sealing in the clearances.
2. Liquid in the pump sufficient to carry away any heat generated so that the pump is considered an isothermal system.

Cooper & Prang[13] acknowledge that the assumption of liquid seals is invalid but necessary. They too noted that at high GVF, the amount of gas compression occurring becomes concentrated towards the discharge side of the pump. This imbalance causes a severe pressure differential across the pump screws that may cause some vibration problems observed in field operations. The source of these vibrations may be spatial variation of the clearances, also termed spindle shaft deflection by other authors, caused by the differential pressure causing the screw to come into contact with the pump casing. Additionally, shaft deflection can dramatically change the shape of the circumferential clearance leading to increased slip flow, especially in the laminar flow regime.

Cooper & Prang[13] also discussed the effect of viscous heating on liquid viscosity. They were able to validate their model for pure liquid high viscosity flow as well as high GVF multiphase flow. Cooper & Prang[13] observed increased volumetric efficiency with the pump operating with higher viscosity liquids. Therefore, they note that changes in operating conditions over time that may result in a decrease in liquid viscosity could dramatically reduce twin-screw pump efficiency. This supports the need for better pump models since for engineers to properly design a pump for the entire life of a well, pump performance must be known for a variety of possible field conditions.

2.5 University of Hannover (2004)

In a paper from the University of Hannover, Rausch *et al.*[14] approached the modeling problem by combining a mass balance with an energy balance. For the first time, the system was considered adiabatic instead of isothermal. Though it was known that heat was generated in the pump from compression and viscous effects, it was always assumed as a simplification that there was enough fluid in the pump to carry away most of the heat. However, while the authors again acknowledge that the fluid in the clearances may not be completely liquid, they are still forced to make this assumption. The authors suggest that adoption of multiphase slip flow model is necessary to expand model validity to wet-gas conditions. The model also considered internal recirculation of liquid which is a design feature of some pumps.

Instead of a series of fluid filled cylinders as described in previous models, this thermodynamic model describes twin-screw pump operation as two main components:

1. Individual chambers are modeled as moving volumes of mass and energy.
2. The gaps or clearances are streams where mass and energy are interchanged between the chambers.

Therefore the pump is modeled as a series of mass and energy balances over a moving control volume. Two different mass balances are proposed, one for the inlet chamber, termed the first open chamber, and one for the closed chambers. The conditions at which the fluid first enters the pump and the “filling process” it causes necessitate the need for a different set of equations at the inlet.

Energy balances over each closed chamber are made assuming adiabatic conditions and neglecting the kinetic energy of the slip flows and wall friction. This allows for accurate calculations of the temperature in each chamber under non-isothermal conditions. The energy balance given was made for constant volume chambers, although the authors briefly mentioned the effect of progressive pitch screws. Having screws with a progressive pitch would result in smaller chamber volumes and what the authors termed a “built in compression”.

2.6 Model Comparisons and Thermal Issues

The Vetter, Cooper & Prang, and Hannover models were designed for use by pump designers. As such, they require many different measurements of pump clearances which may not always be available. As an alternative, Martin created a new twin-screw pump model designed for use by petroleum engineers. The regression analysis used to calculate effective pump clearances from pump performance data and is much more user friendly while maintaining acceptable accuracy of prediction. Because of these factors, the Martin model will be used for this research.

Singh[6,7] examined temperature increases within twin-screw pumps during periods of high GVF. He concluded that the assumption of an isothermal pump system is invalid at GVF above 94%. From experimental data, Singh developed a thermodynamic model that predicts temperature rise in twin-screw pumps at high GVF conditions. Toma[15] has presented field cases in which thermal effects such as flash boiling are the main cause for destructive vibrations in the pump. Flash boiling results from the superheating of small liquid droplets which fall into the gas phase. This directly refutes the assumption of an isothermal system. Toma also showed evidence that in some cases pump volumetric efficiency can exceed one.

The high pressure differentials observed across the screw during high GVF can cause severe deflection of the screw shafts. Though all the pump models mentioned above accounted for some deflection, whether or not the deflection is severe enough to cause the screws to touch is unknown but may account for some of the vibrations and loss of efficiency observed.

CHAPTER III
METHODS FOR WET-GAS COMPRESSION

This chapter focuses on methods for producing wet gas. Starting with conventional techniques and moving on to new developments for wet-gas compression with twin-screw pumps, the issues and solutions to the unique problems encountered with wet-gas are explained. The two methods for improving twin-screw pump performance proposed by Singh[6,7] and investigated in this thesis are also presented. To understand the methods presented, the concept of volumetric efficiency must first be defined.

3.1 Volumetric Efficiency

According to Martin[8,9], the maximum theoretical flow rate, q_{TH}, of a twin-screw pump is simply a function of the pump's displacement per revolution, D, and the pump rotational speed, N. Pump displacement is dictated by screw geometry.

$$q_{th} = D \cdot N \tag{3.1}$$

Although slip flow, q_{slip}, through the pump creates a seal and compresses the gas under two-phase conditions, it nevertheless subtracts from the theoretical flow rate. Therefore the actual flow rate, q, is:

$$q = q_{TH} - q_{slip} \tag{3.2}$$

Since the slip flow is a pressure driven flow through the internal clearances, as differential pressure across the pump increases, slip flow will increase resulting in a drop in actual flow rate. It is useful to define the volumetric efficiency, η_v, of the twin-screw pump as:

$$\eta_v = \frac{q}{q_{TH}} = \frac{q_{TH} - q_{slip}}{q_{TH}} \tag{3.3}$$

From this definition we can see that any method of increasing the total flow rate through the pump at given pump speed will improve volumetric efficiency.

3.2 Conventional Methods

The traditional method of boosting the pressure of a wet-gas stream is to use a series of scrubbers and separators to create individual liquid and gas flow lines. The liquid stream is then boosted using single-phase liquid pumps, while the gas stream is compressed using dry-gas compressors. **Fig. 3.1** and **Fig. 3.2** illustrate the reduction in process equipment possible by switching to a multiphase system to produce heavy oil and annulus gas in a cyclic steam-flood application. An interesting feature of a multiphase system is the ability to conserve system heat, preserving the mobility of the extremely viscous bitumen.

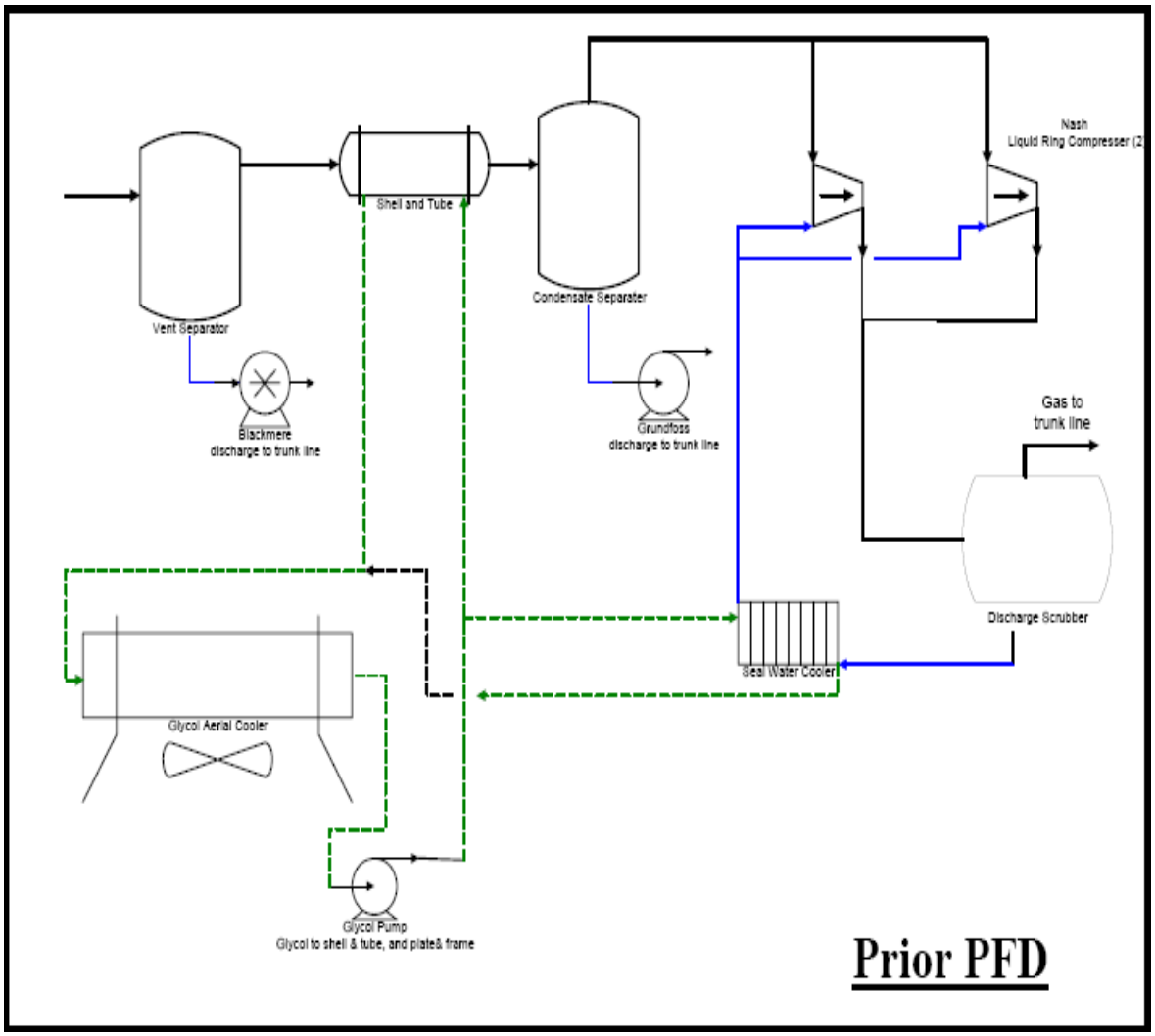

Fig. 3.1 – Conventional production process flow diagram(after Dick and Speirs[5]).

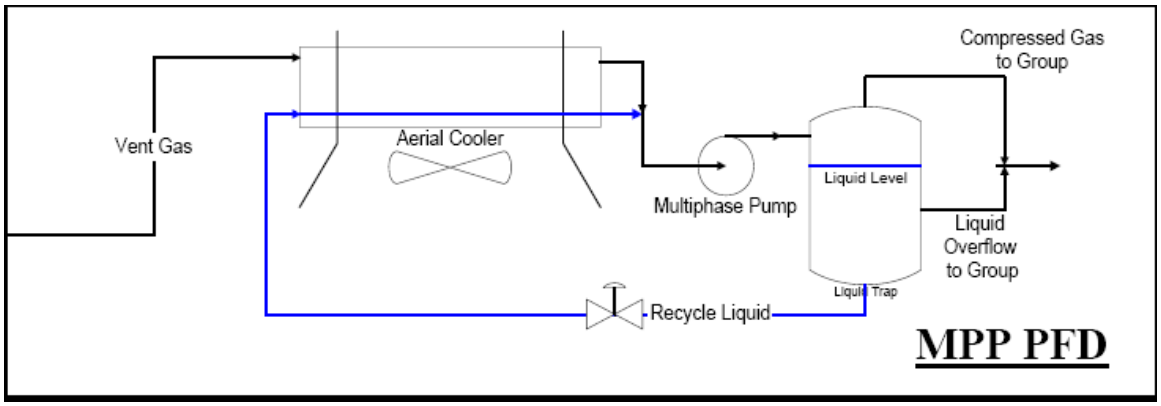

Fig. 3.2 – Multiphase production process flow diagram (after Dick and Speirs[5]).

3.3 Digressive Screws

A new development for improving twin-screw pump efficiency at high GVF is a new generation of screws for high GVF operations introduced by Bornemann. These "digressive" screws feature varying pitch along the screw, resulting in smaller and smaller chamber volumes as the fluid approaches the discharge of the pump.[2]

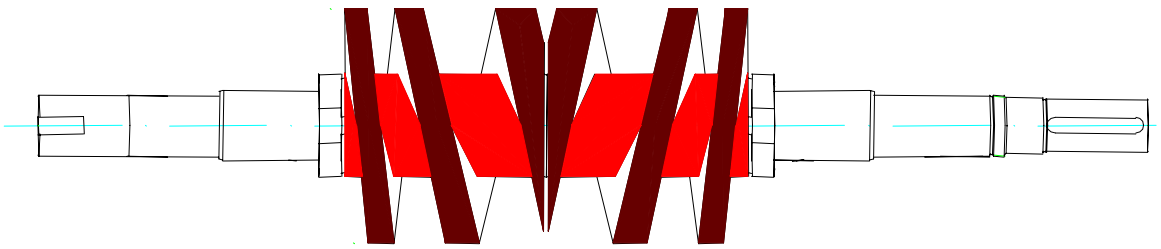

Fig. 3.3 – Diagram of digressive screw.

Fig. 3.3 shows a diagram of the digressive screw design. In this case, the fluid moves from the suction at the center to the discharge out at both ends. Since the chamber volumes become progressively smaller, less liquid slip is needed to compress the gas present. This is advantageous since at high GVF there may not be enough liquid present to properly seal and compress the gas phase. Tests with this new screw design have

demonstrated a significant increase in flow capacity, efficiency, and a decrease in power consumption over conventional screw designs at high GVF, **Fig. 3.4**.

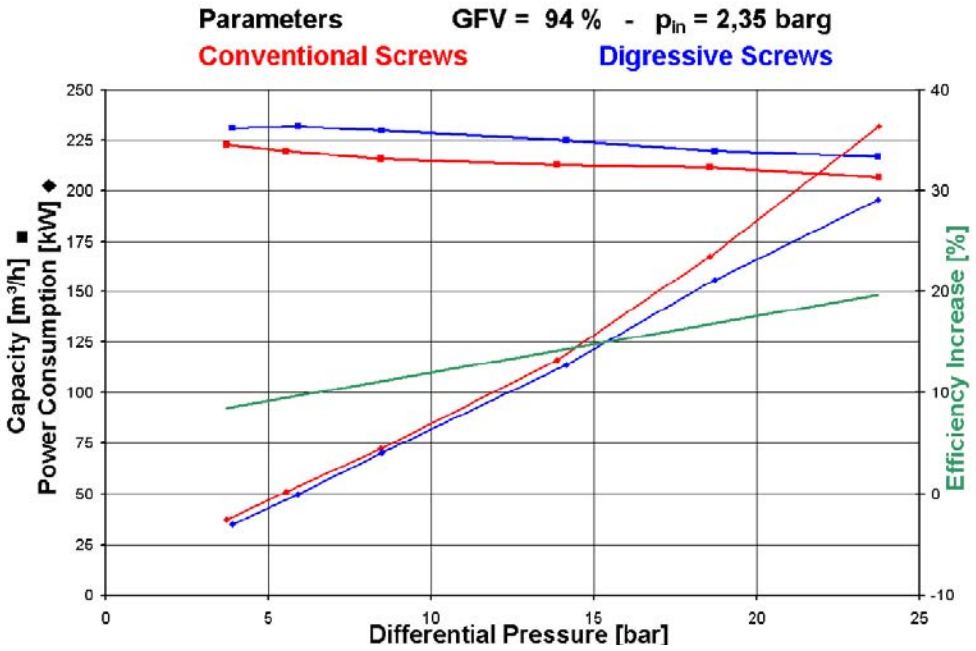

Fig. 3.4 – Digressive screw test results (after Rohlfing and Muller-Link[16]).

Though the results are promising, methods of achieving this improvement without the need to replace screw sets have been proposed. Even with these new screws, a GVF of 95% is recommended to ensure that there is sufficient liquid in the pump.

3.4 High Viscosity Fluid Circulation

Singh[6,7], Martin[8,9], and Cooper & Prang[13] have all presented evidence that shows that increasing the viscosity of the liquid phase reduces slip flow leading to higher volumetric efficiency, **Fig. 3.5**.

Martin suggested that the lower slip flow with higher viscosity fluids would decrease the amount of volume taken up by slip liquid in the suction end of the pump. This would enable more fluid to be taken into the pump at high GVF conditions. **Fig. 3.6** presents in an illustration of this concept.

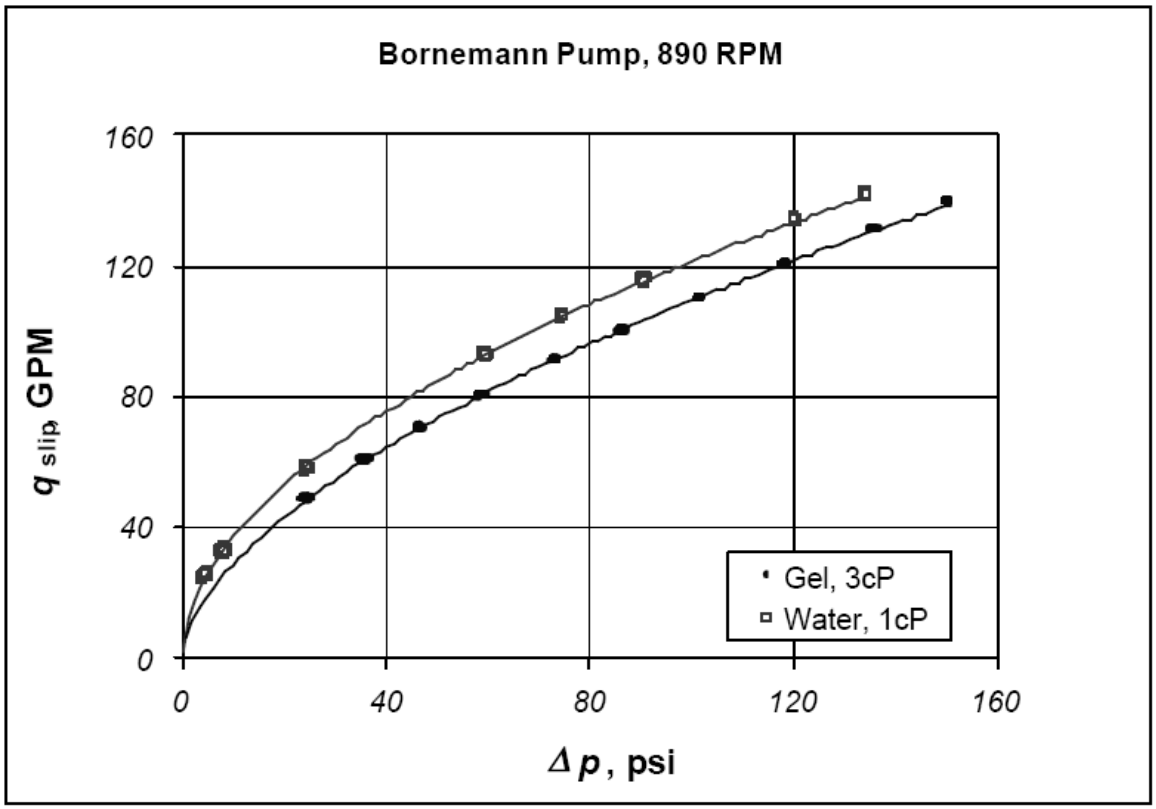

Fig. 3.5 – Viscosity effects on liquid flow rate (after Martin[8,9]).

Singh therefore tested various liquid viscosities at high GVF all the way to 100% on a Bornemann MW 6.5zk-37 twin-screw pump. The Bornemann pump was selected because of the recirculation chamber integrated into its design which allows for more liquid to be retained in the pump at high GVF. This recirculation chamber allows the pump to maintain operation at 100% GVF for a short period of time.

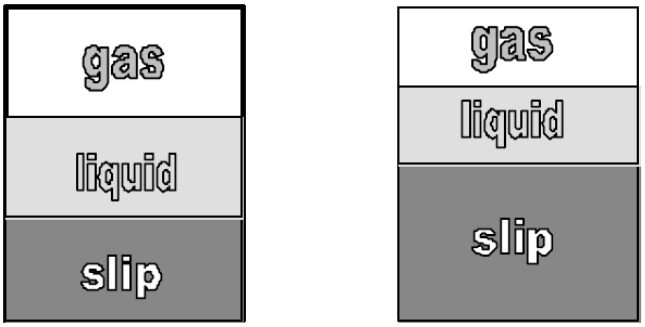

Fig. 3.6 – Reduced slip allows for more gas flow (after Martin[8,9]).

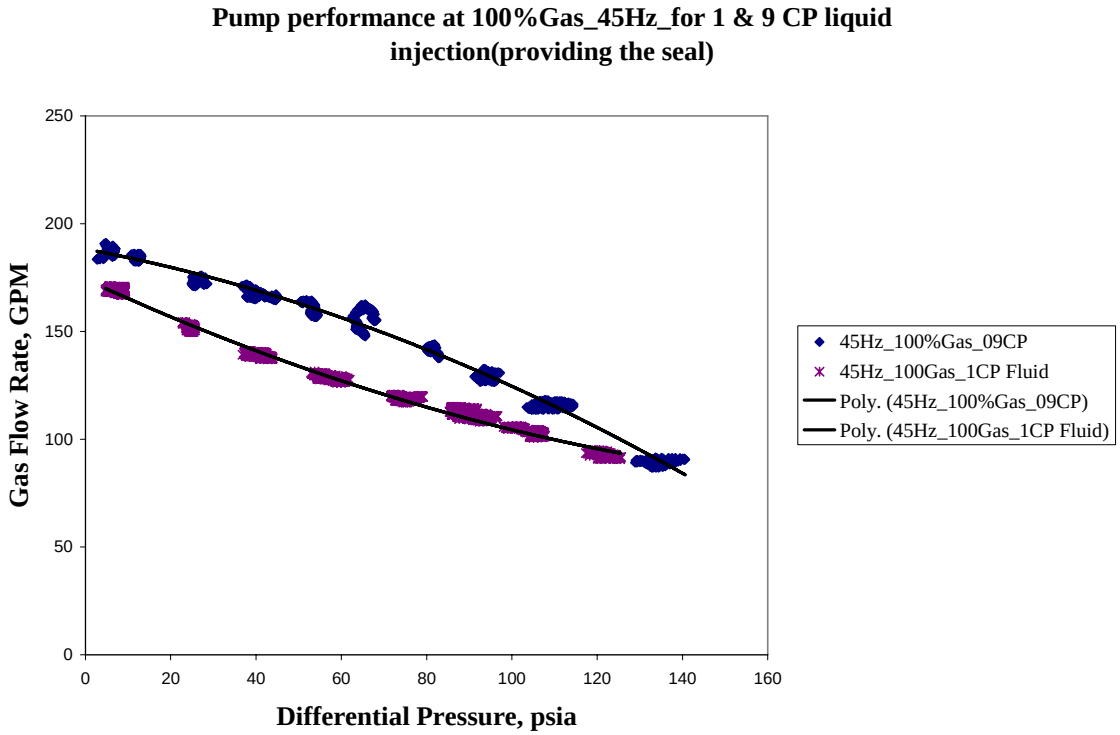

Fig. 3.7 – Gas flow rate versus differential pressure for different liquid viscosities, pump speed 1350 RPM (after Singh[6,7]).

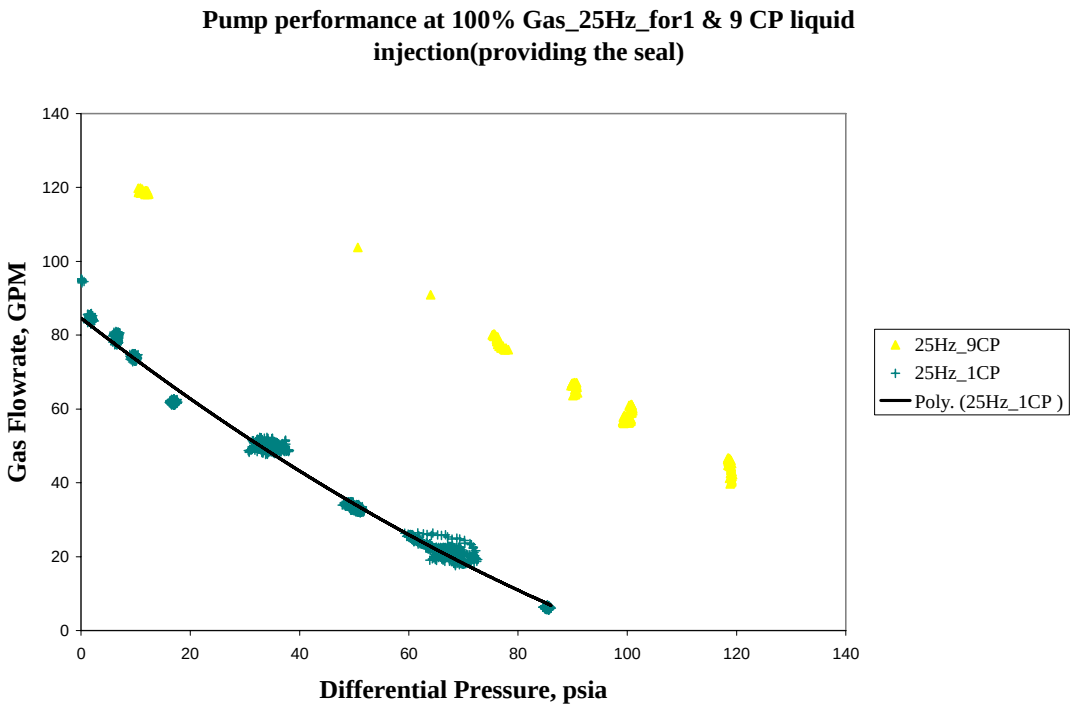

Fig. 3.8 – Gas flow rate versus differential pressure for different liquid viscosities, pump speed 750 RPM (after Singh[6,7]).

Fig. 3.7 and **Fig. 3.8** show the test results presented by Singh. There is significant gain in gas flow rate when circulating a higher viscosity fluid. An increase in liquid viscosity for 1 cP to 9 cP produces up to a 22% increase in gas flow rate when the pump is rotating at 1350 RPM. The increase in flow rate drops off at higher differential pressures. This drop off is not observed when the pump is rotating at a slower speed. Similar behavior was observed in another data set obtained from Nuovo Pignone[17].

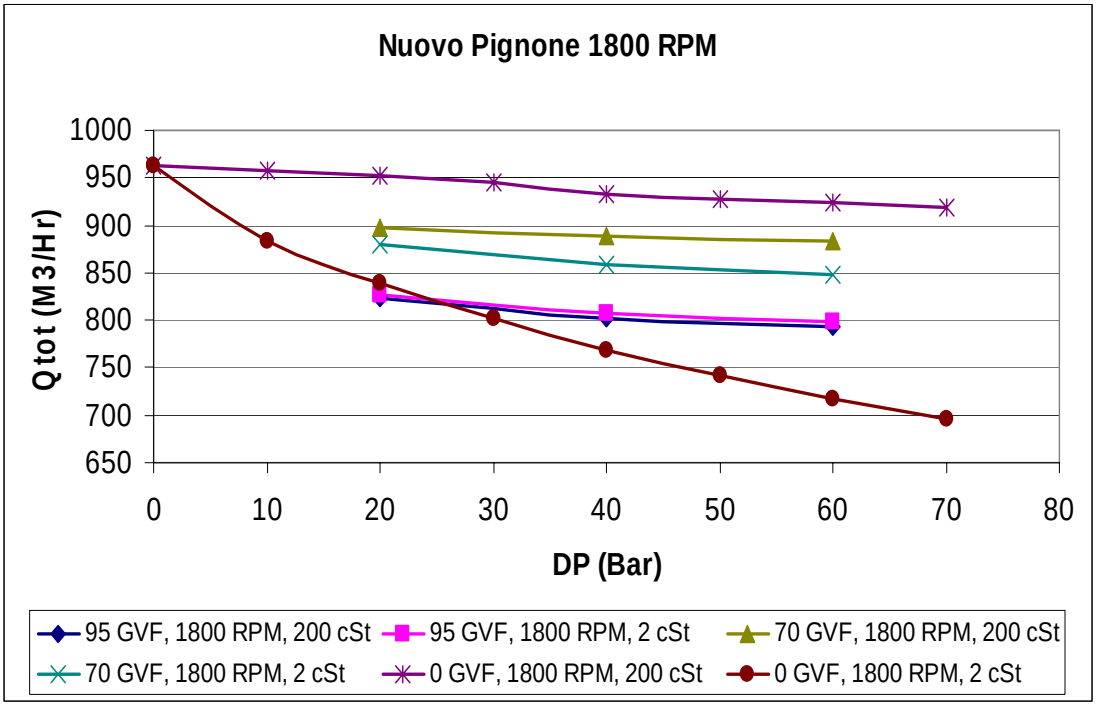

Fig. 3.9 – Nuovo Pignone, total flow rate versus differential pressure for different liquid viscosities, pump speed 1800 RPM.

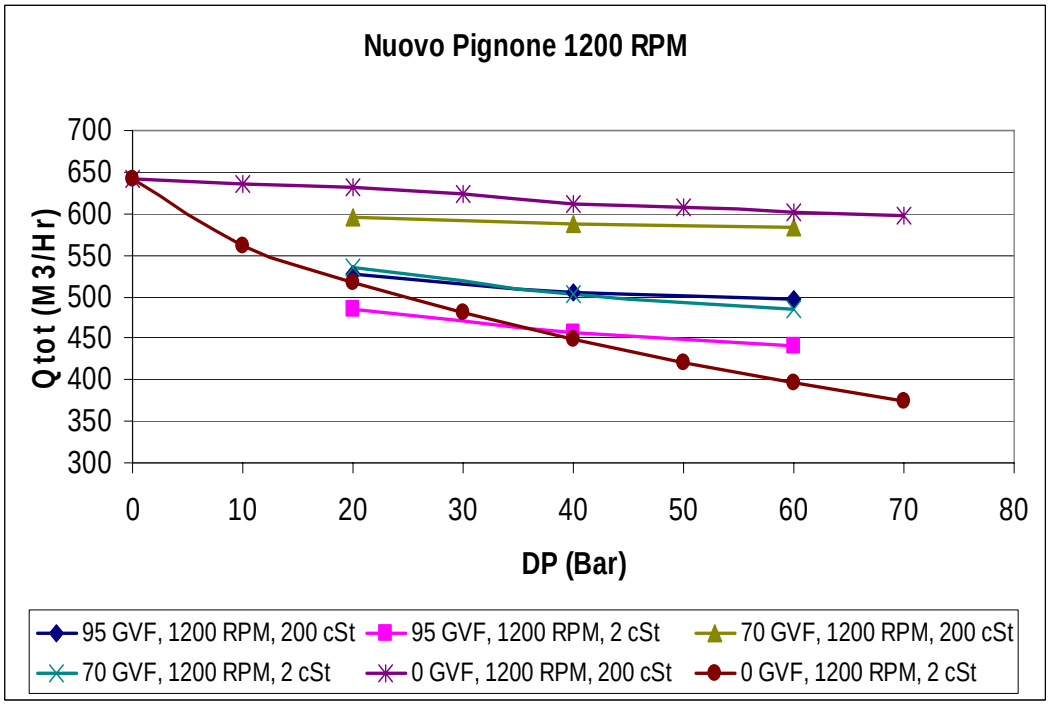

Fig. 3.10 – Nuovo Pignone, total flow rate versus differential pressure for different liquid viscosities, pump speed 1200 RPM.

Fig. 3.9 shows the results of experiments conducted with a 2 and 200 cSt fluid at a pump speed of 1800 RPM. At a GVF of 95%, there is a slight decrease in total flow rate with increasing viscosity. In **Fig. 3.10**, the pump speed is slower at 1200 RPM. In that case, there is a large increase in total flow rate with increasing viscosity. **Fig. 3.11** summarizes the differences.

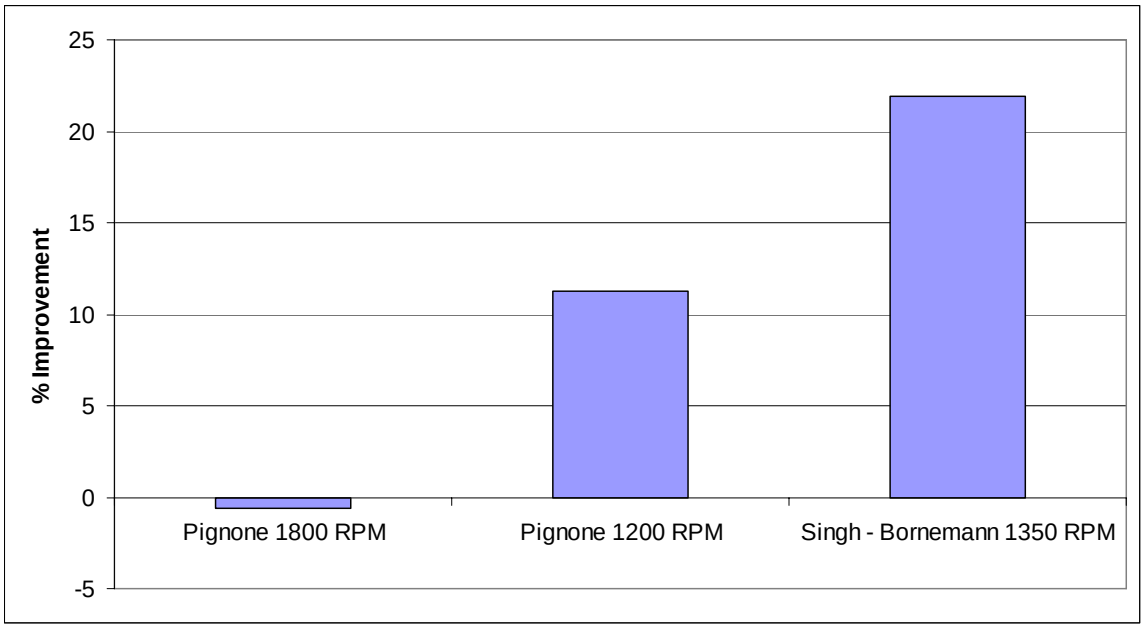

Fig. 3.11 – Improvement in total flow rate with increased viscosity.

From the results of his experiments, Singh proposed a system where the viscosity of the liquid phase would be artificially increased. Since liquid is already captured for re-circulation to maintain a minimum GVF, an additive could be introduced to increase the viscosity. Flow assurance fluids which are often used to prevent hydrate formation or corrosion could also provide another source fluid for increasing the viscosity.

3.5 High Viscosity Test Matrix

The results presented in the previous section warrant further study and are the motivation for the work presented in this thesis. More data at high liquid viscosity and GVF are needed. Therefore, new experiments were conducted using the same Bornemann pump used by Singh. The test parameters are given in **Table 3.1**.

Table 3.1 – High viscosity test matrix.

Viscosities (cP)	GVF (%)	Pump Speeds (RPM)
1	0	1350
9	70	1700
24	95	
40	100	
50		

Liquid viscosity will be increased using guar gel because of its availability and ease of use. The viscosity that can be tested is limited by the charging pumps used to move the liquid from the holding tank. The viscosity is measured using a Fann 35 rotary viscometer. For this model viscometer the apparent viscosity is measured at a speed of 600 RPM, which is equivalent to a shear rate of 1022 1/sec. The apparent viscosity at this shear rate will be used through the rest of this thesis. The apparent viscosity is calculated by:

$$\text{Apparent Viscosity, } \mu \text{ [cP]} = (600 \text{ rpm dial reading})/2 \qquad (3.4)$$

The gel used is shear and temperature thinning. This will cause its effect within the pump to be somewhat diminished. However, Singh used the same type of gel and achieved encouraging results. There are currently no sources of data about the shear rates encountered in the clearances of a twin-screw pump, so a direct comparison with the viscosities measured by the viscometer is not possible. The small size of the clearances and the amount of flow through them should certainly produce shear rates higher than 1022 1/sec. A full characterization of the guar gel and an estimation of shear rates encountered in the pump clearances will be given in the next chapter.

3.6 Through-Casing Injection

Singh also proposed injecting liquid through the pump casing, directly into the pump chambers. This injected liquid would help maintain the seal around the chambers and could facilitate control of the internal pressure profile. By increasing the amount of liquid in a specific chamber in the pump, we could increase the pressure in that chamber and allow an operator to create a more favorable linear pressure profile. This is similar to the operating concept of the digressive screw design, but instead of decreasing the chamber volume mechanically, it will be attempted hydro dynamically

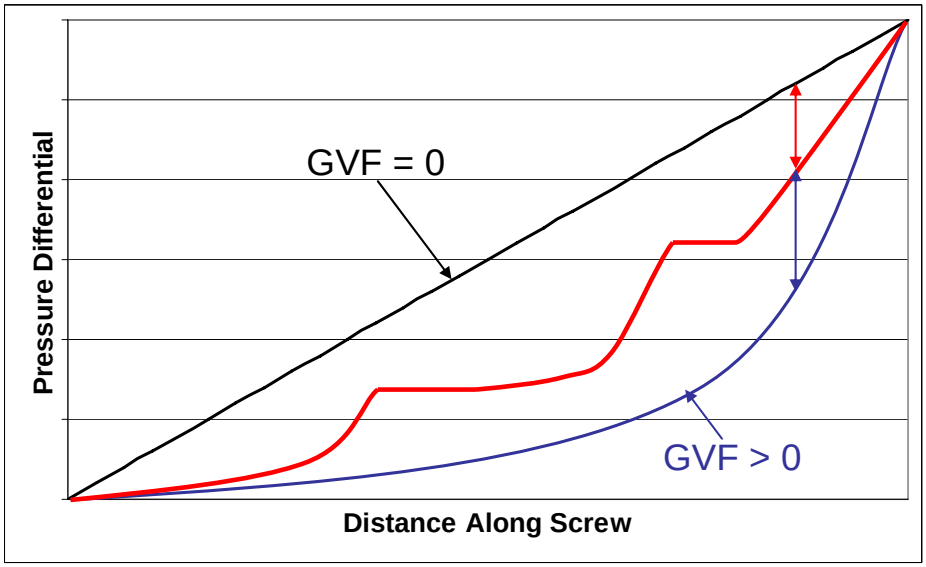

Fig. 3.12 – Theoretical pressure profile with through-casing injection.

Fig. 3.12 shows the type of pressure profile that is thought to be possible using through-casing injection. The compression ratio of the chambers closer to the discharge is reduced and the chambers near the suction side of the pump now contribute to the overall pressure boost. By eliminating sudden changes in pressure within the pump, it is thought that some of the vibration issues encountered can be eliminated. This method may be able to increase the total boosting capacity of the pump since the pressures in the

pump chambers will be increased. Since this method requires significant modifications to an expensive piece of machinery, it will be examined only theoretically in this thesis.

The implementation through-casing injection presents many mechanical challenges. Injecting fluid into a chamber rotating in excess of 1800 RPM will be difficult. At any given time when injecting at a single point along the pump casing, the outer portion of the screw may block the injection port, **Fig. 3.13**. A timing system or a wider slot for injection must be developed before any field trials may be conducted.

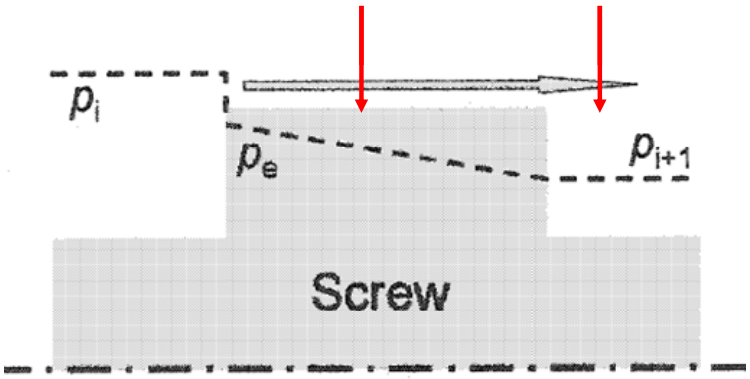

Fig. 3.13 – Diagram of injection timing problem.

CHAPTER IV
EXPERIMENTAL FACILITY

This chapter is a description of the multiphase field laboratory at the Texas A&M Riverside campus. This facility was used for all the experiments described in this thesis. The remote location of the Riverside campus, approximately 15 miles from College Station, allows for the testing of real pieces of oilfield equipment that would not be possible in a normal research setting.

Riverside is a field-scale experimental test facility which features two full-size twin-screw multiphase pumps. The smaller of the two pumps is a Bornemann MW-6.5zk-37. This pump has a capacity of 10,000 bbl/day with a maximum pressure boost of 250 psig. An important feature of this pump is its internal recirculation chamber. This allows for some of the liquid at the discharge to be moved back to the suction end of the pump. **Fig. 4.1** shows a side view of the Bornemann pump. The discharge from the pump is upwards to help retain liquid. The recirculation chamber can be seen branching off from the discharge.

Fig. 4.1 – Bornemann MW-6.5zk-37 twin-screw pump with internal recirculation chamber.

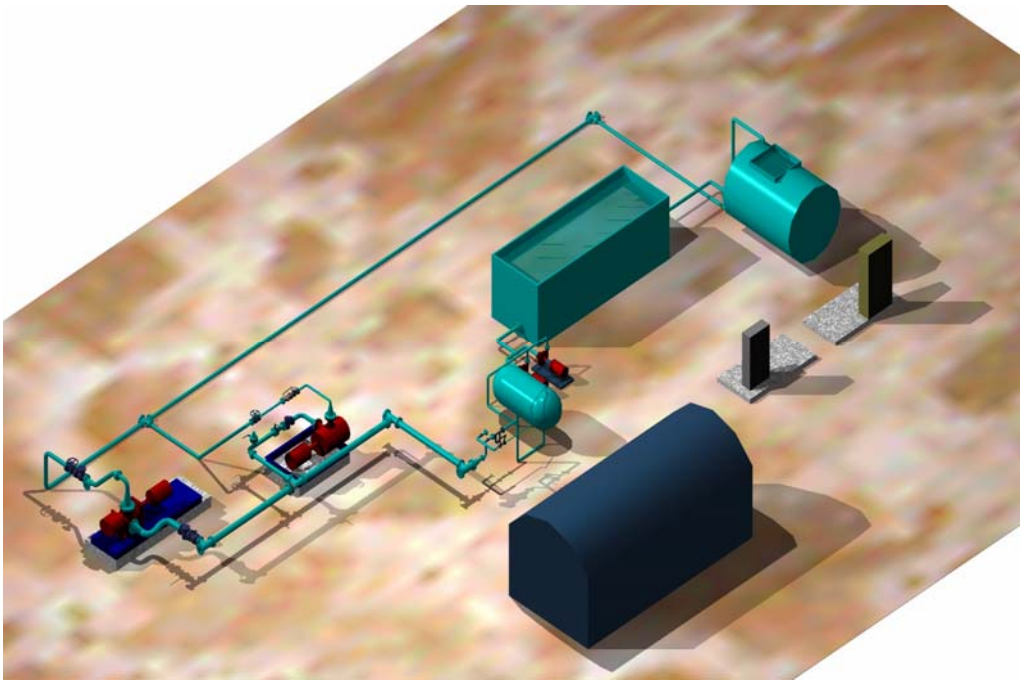

Fig. 4.2 – Rendition of Riverside test facility (Martin[8,9]).

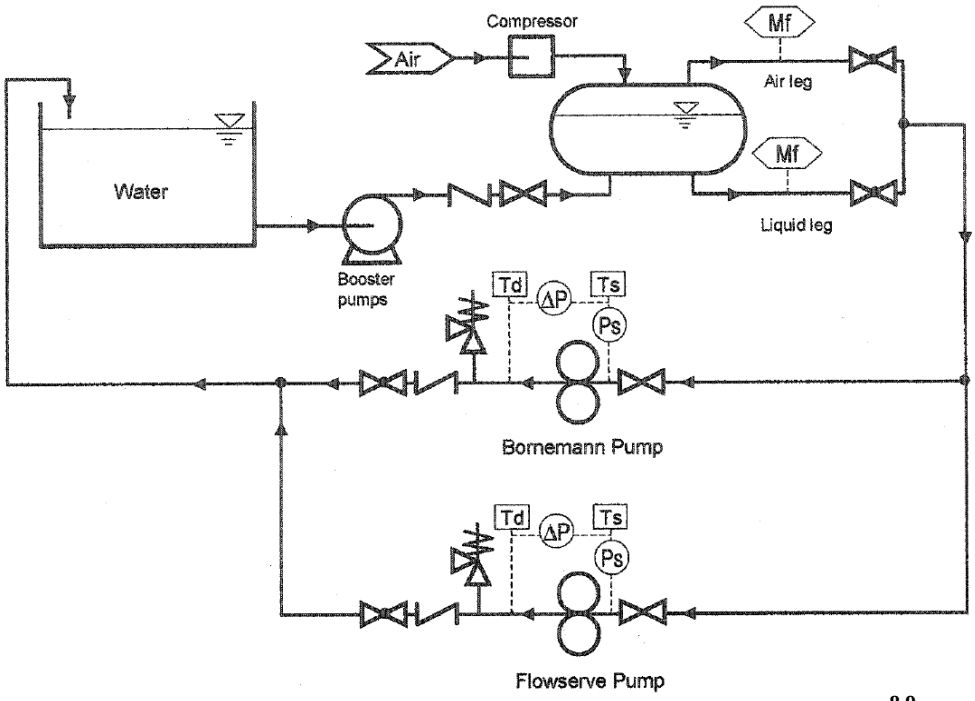

Fig. 4.3 – Flow diagram of Riverside test facility (after Martin[8,9]).

The Bornemann pump is driven by a 50 hp electric motor with a maximum speed of 1800 RPM. Power is supplied by a variable frequency drive (VFD) with speed control using a Kimo MotorMaster frequency inverter. The facility also features a Flowserve LSIJS pump with its own VFD drive. This pump was not used in this work.

4.1 Flow Loop Description

Fig. 4.2 and **Fig. 4.3** show a rendition and flow diagram of the flow loop at the Riverside facility. Water or gel is pumped from a storage tank using two 15 hp centrifugal charging pumps, shown in **Fig. 4.4**. Twin-screw pumps do not generate their own suction, so fluid must be supplied to them at some elevated pressure. The pumps are configured to operate in series or in parallel, depending on whether higher pressures or flow rates are required.

Fig. 4.4 – Centrifugal charging pumps.

Air from a 185 CFM compressor is stored in a pressure vessel, **Fig. 4.5**. For testing at high GVF, the liquid is also pumped into this vessel. Doing this allows the pressure of each phase to equalize and greatly reduces any slugging effects from phase mixing. Liquid is then allowed to flow from the bottom of the vessel while the air comes from the top.

Fig. 4.5 – Pressure equalization vessel.

The separate air and liquid lines are then passed into a metering section. Mass flow rates are measured using MicroMotion Elite series Coriolis meters. A three inch meter, model CMF300M355NUR, is used for the liquid while a one inch meter, Model CMF100M329NU, is used for the gas. These types of meters are highly accurate with errors of +/- 0.10% for liquid flow rates and +/- 0.50% for gas flow rates. Valves at the metering section allow the flow rate of liquid and gas sent to the twin-screw pump to be adjusted. The GVF of the flow stream sent to the pump is adjusted in this way. After metering, the liquid and air lines are combined at a mixing tee. The metering section and mixing tee are shown in **Fig. 4.6**.

The combined flow stream then moves through either a six or four inch flow line to the Bornemann pump. Two Weed 201 Direct Immersion RTDs provide temperature measurements at both the suction and discharge ends of the pump. These devices have an accuracy of +/- 0.54^{o}F. Rosemount model 3051 pressure transducers are used to measure the suction and discharge pressures. These pressure sensors have an accuracy of +/- 0.075%.

Fig. 4.6 – Metering section and mixing tee.

After moving through the pump, the fluids are flowed back to the storage tank in a three inch flow line. A globe valve, shown in **Fig. 4.7**, is located near the end of the flow loop which can be adjusted to simulate backpressure and increase the differential pressure (Δp) across the pump.

Fig. 4.7 – Backpressure control valve.

4.2 Data Acquisition

Signals from the flow meters, temperature sensors, and pressure transducers were captured using a computer with a National Instruments PCI data acquisition board. LabView 7 software was used to record data. Mass flow rates from the Coriolis meters were used along with pressure and temperature data to calculate GVF, which is measured at suction conditions. Since multiphase flow is inherently unstable, data at a each Δp measured was recorded for a extended period of time and then averaged.

4.3 Viscosity Control

Guar gel is mixed as a liquid concentrate in the storage tank at various concentrations corresponding with the viscosity desired. A small five horsepower centrifugal pump is used to roll the tank, ensuring thorough mixing. **Fig. 4.8** shows the relationship between gel concentration (lb/gal) and viscosity (cP) measured at four different shear rates.

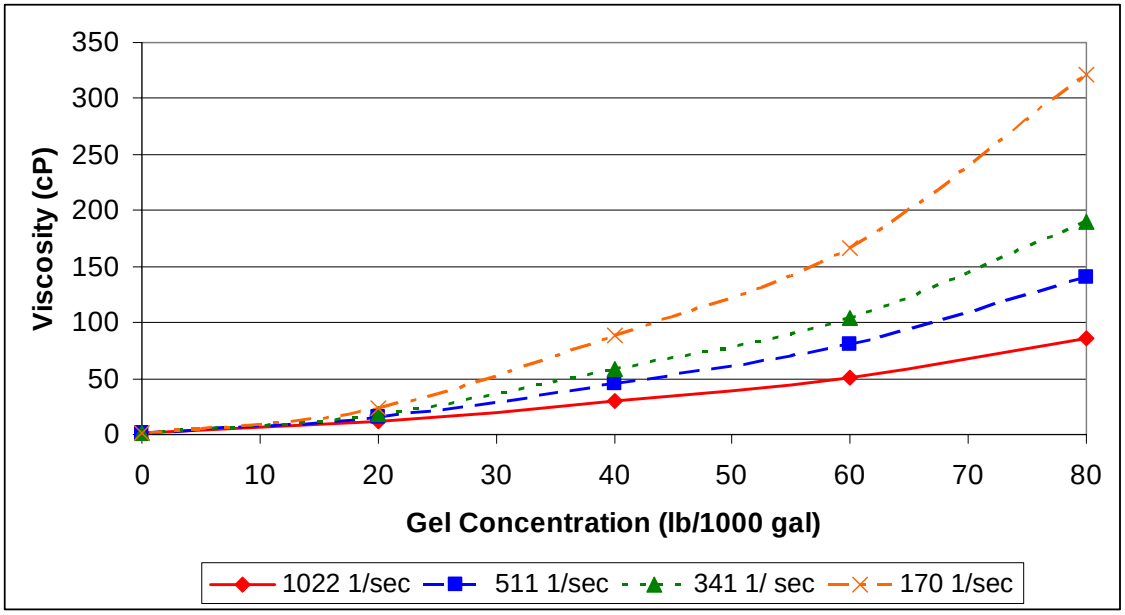

Fig. 4.8 – Gel concentration versus viscosity at different shear rates.

Viscosity was measured using a Fann 35 rotary viscometer with the four shear rates presented in Fig. 4.8 corresponding to viscometer speeds of 600, 300, 200, and 100 RPM, respectively. Samples were taken out of the storage tank periodically and tested to ensure constant viscosity and gel concentration. The gel is a non-Newtonian pseudoplastic fluid. The viscosity of the fluid, μ, can represented as a function of shear rate, γ, in the form of:

$$\mu = K\left(\gamma\right)^{n-1} \tag{4.1}$$

In this equation K is the flow consistency index while n is the flow behavior index. A Newtonian fluid has an n value of one. To determine n for the guar gel used in the experiments presented in this thesis, shear rate data obtained from a viscometer is plotted versus apparent viscosity for each of the different gel concentrations, **Fig. 4.9**.

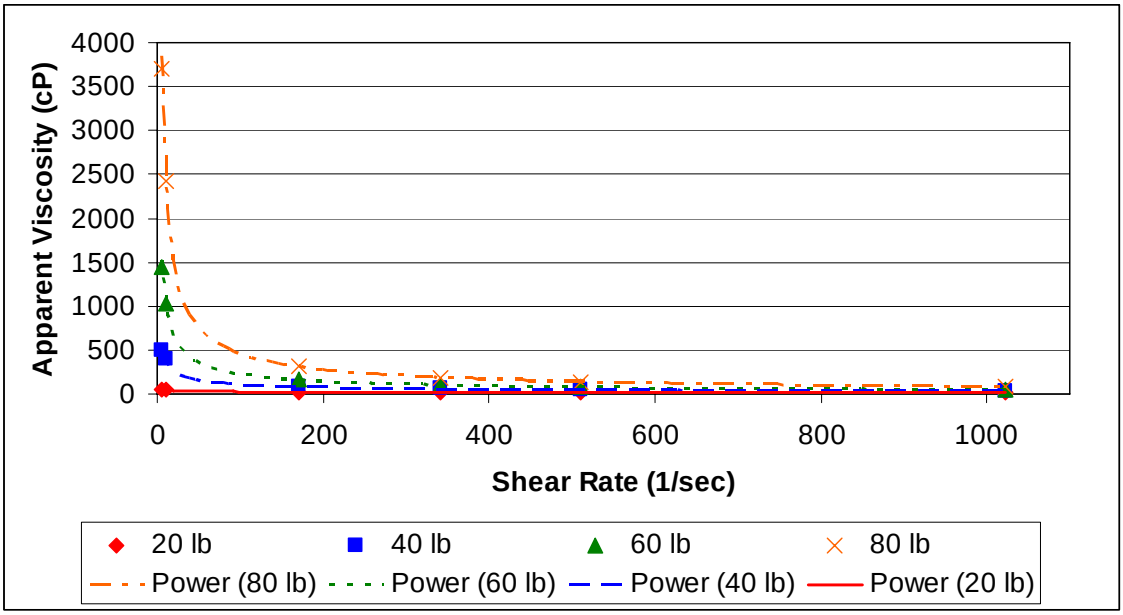

Fig. 4.9 – Apparent viscosity (cP) versus shear rate (sec^{-1}) for different gel concentrations.

It is clear from **Fig. 4.9** that this gel exhibits power law behavior. Curve fits on data from viscometer measurements are performed to calculate K and n, **Table 4.1** summarizes the results. As expected, the gel becomes more non-Newtonian as gel concentration increases.

Table 4.1 – Values of flow consistency index, *K*, and flow behavior index, *n*, for gels of different concentrations.

Gel Concentration (lb/1000 gal)	Flow Consistency Index, *K*	Flow Behavior Index, *n*
20	88.8	0.720
40	1295.3	0.466
60	4321.3	0.361
80	12363.0	0.284

The shear thinning behavior observed in Fig. 4.9 presents the problem of decreased effectiveness of the gel in the high shear clearances in the pump. An estimation of the shear rates encountered within a twin-screw pump can be made by approximating the flow through the circumferential clearance, the gap between the outer part of the screw and the pump casing, as single phase liquid flow through a thin channel. Using measurements of the screw diameter and circumferential clearance, the area of the clearance can be calculated. Martin[6] gives values for the external screw diameter, D_c, and the effective circumferential clearance, for the Bornemann pump. Using the shape of the circumferential clearance presented in Fig. 2.1, a circumferential area, A_c, in ft^2 consisting of two circular areas can be calculated as:

$$A_c = \frac{2\pi \cdot \left(\left(D_c + c_c \right)^2 - D_c^2 \right)}{144} \tag{4.2}$$

The screw measurements and the calculated area are given below in **Table 4.2**.

Table 4.2 – Clearance measurements and calculated area.

D_c (in.)	c_c (in.)	A_c (ft_2)
5.24	0.0109	0.004989

Using slip flow rates calculated from the Martin model, the velocity of the fluid in the clearance can be calculated. The slip flow rates given by the model are in both directions so it is divided by two. Addionally, Vetter *et. al.*[10,11] determined that 80% of the slip flow passes through the circumferential clearance.

$$v = 0.002228 \cdot \left(\frac{0.8 q_{slip}}{2 A_c} \right) \tag{4.3}$$

Assuming no slip flow at the wall, the shear rate can be calculated by:

$$\gamma = \frac{12v}{c_c} \tag{4.4}$$

Table 4.3 summarizes the shear rates encountered in the circumferential clearance of the Bornemann pump for different differential pressures and slip flow rates. The large amount of slip flow and the extremely narrow clearances contribute to estimated shear rates that are much higher than those observed in the viscometer.

Table 4.3 – Calculated shear rates at different slip flow rates.

	q_{slip} (GPM)	v (ft/sec)	γ (sec^{-1})
ΔP = 150 psi	169.26	30.23	33283.90
ΔP = 100 psi	130.82	23.37	25724.39
ΔP = 50 psi	91.08	16.27	17910.98

Extrapolated viscosities from the data shown in Fig. 4.9 at the calculated shear rates for different concentration gels are given below in Table 4.4. Eq. 4.1 was used with the values of *K* and *n* from Table 4.1.

Table 4.4 – Extrapolated gel viscosities.

γ (sec-1)	20 lb gel μ (cP)	40 lb gel μ (cP)	60 lb gel μ (cP)	80 lb gel μ (cP)
33283.90	4.81	4.98	5.57	7.14
25724.39	5.17	5.71	6.57	8.59
17910.98	5.72	6.93	8.28	11.13
1022	11.3	30.3	50.3	85.5

It is clear that the high shear rates in the pump significantly reduce the viscosity of the gel. However, even with the high shear rates the viscosity is not completely reduced to that of water. The gel should still have some effect on pump performance.

CHAPTER V
HIGH VISCOSITY CIRCULATION

This chapter presents the results and discussion of all work done on high viscosity liquid circulation in twin-screw pumps at high GVF. Tests conducted with pure liquid will be presented to demonstrate the effect of elevated viscosity on this type of pump. The results of the extensive tests conducted under wet-gas conditions will then be shown and compared to model predictions.

It is common to express pump flow rates at suction conditions. All flow rates given in this chapter are at suctions conditions. Liquid flow rate is calculated by dividing the mass flow rate (lb/min) by the liquid density (lb/gal) both values given by the Coriolis meter.

$$q_l = \dot{m}_l \times \rho_l \tag{5.1}$$

Gas flow rates are calculated in a similar way except that the real gas law is used to calculate the density at suction conditions. The gas in this case is assumed to be an ideal gas.

$$q_g = \dot{m}_g \times \rho_g \tag{5.2}$$

$$\rho_g = \frac{Mp_{suction}}{zRT_{suction}} \tag{5.3}$$

Total flow rate is simply the gas and liquid flow rates added together.

$$q_t = q_l + q_g \tag{5.4}$$

5.1 Pure Liquid Tests

Tests with pure liquid, 0% GVF, at various viscosities were conducted to quantify the effect of increased viscosity on pump performance. Pump curves showing flow rate in gallons per minute versus differential pressure (psi) across the pump are presented. The full results of these tests are shown below in **Fig. 5.1** and are similar to previously published data. Viscosities reported were measured at a shear rate of 1022 sec^{-1}.

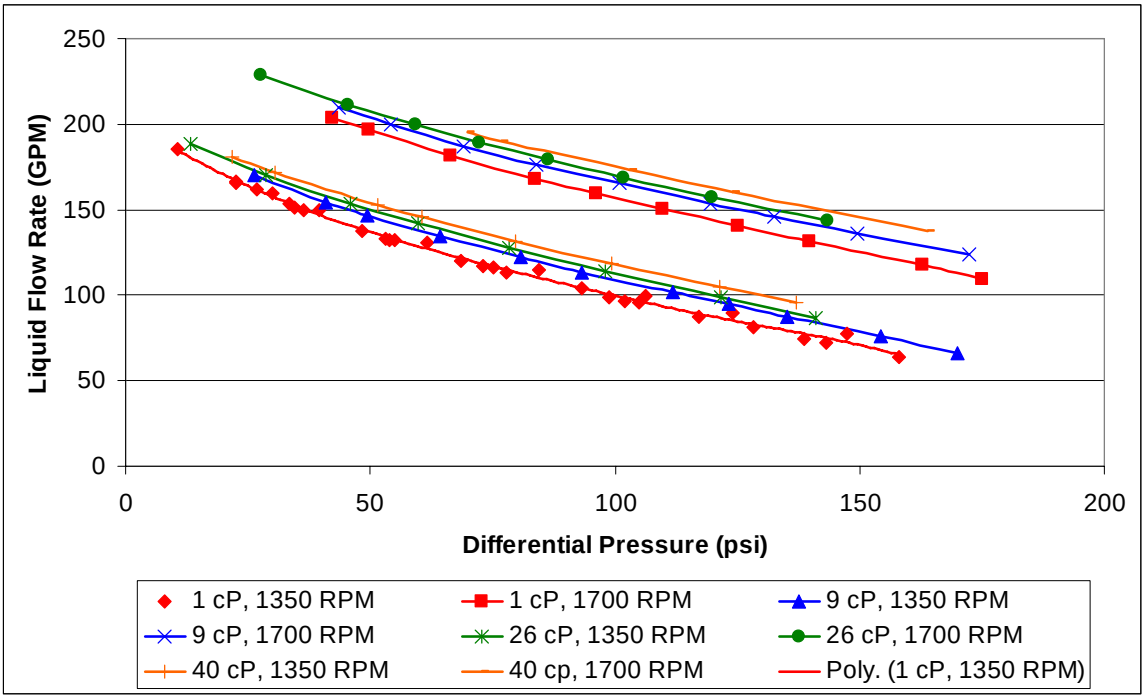

Fig. 5.1 – Liquid flow rate (GPM) versus differential pressure (psi) for four different viscosities and two pump speeds.

Higher differential pressure results in increased slip flow which in turn results in lower flow rate through the pump. Therefore volumetric efficiency decreases with increasing differential pressure. As expected, the higher pump speed produces higher flow rates. Slip rate is known to be independent of pump speed. Therefore, volumetric efficiency increases as pump increases, **Fig. 5.2**.

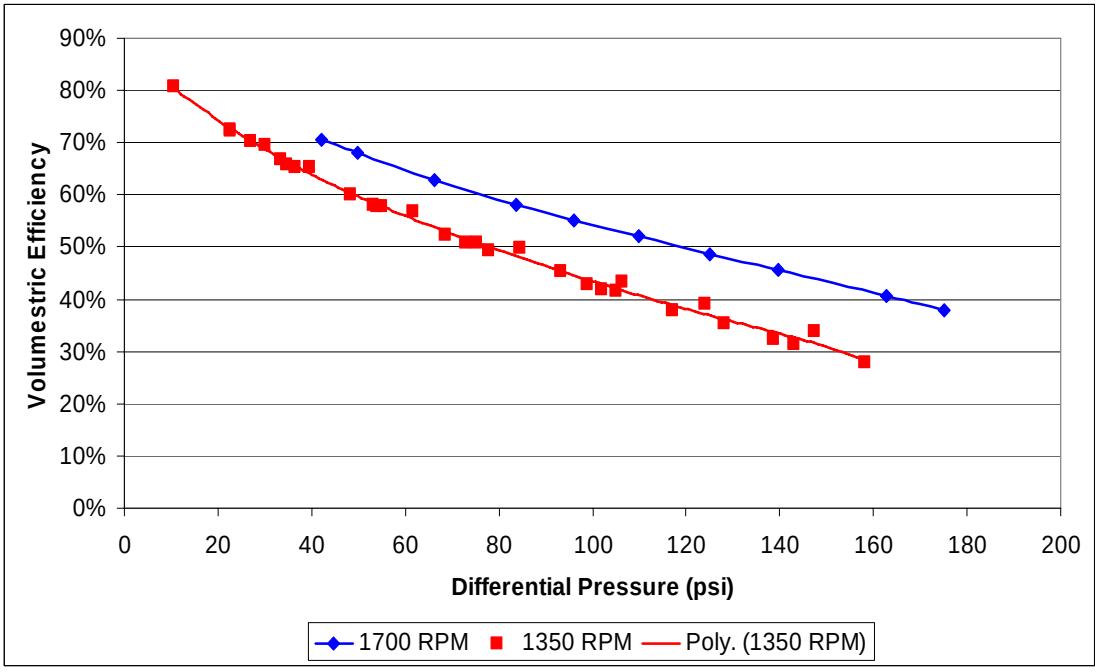

Fig. 5.2 – Volumetric efficiency (%) versus differential pressure (psi) at 1350 and 1700 RPM, liquid viscosity 1 cP.

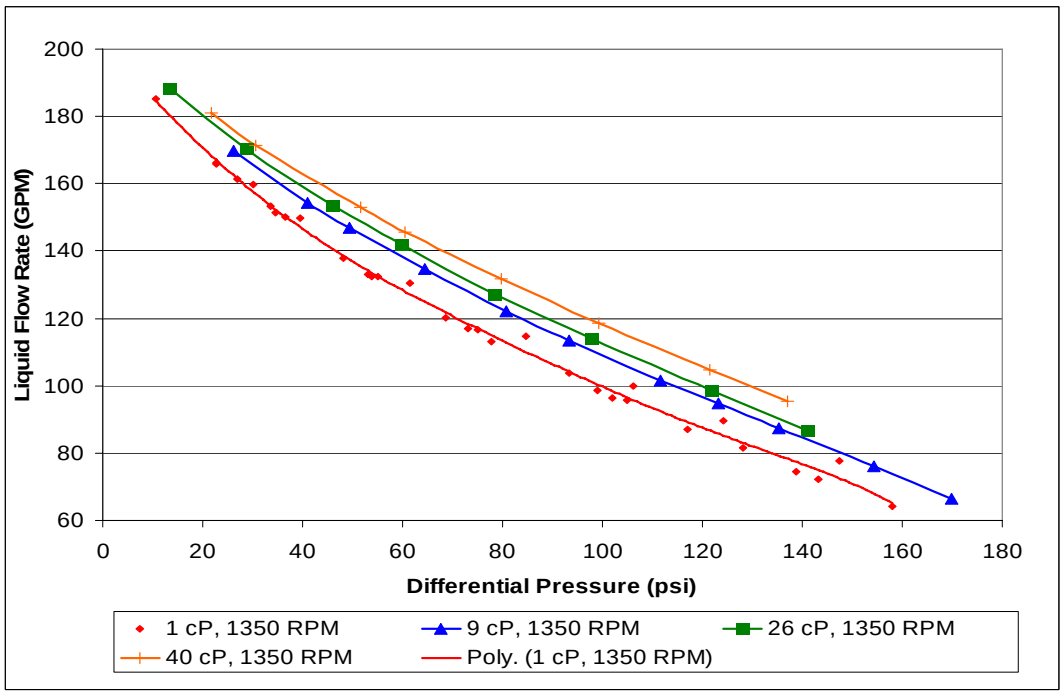

Fig. 5.3 – Liquid flow rate (GPM) versus differential pressure (psi) for four different viscosities at 1350 RPM.

Fig. 5.3 shows the same results for 1350 RPM pump speed only, the effect of increased viscosity can be seen more clearly. **Fig. 5.4** shows the calculated slip rate as a function of differential pressure. Viscosity clearly has a significant effect in reducing slip rate. Therefore, the volumetric efficiency of the pump increases as viscosity is increased. At 1700 RPM, increasing viscosity has a similar effect as at 1350 RPM, **Fig. 5.5**.

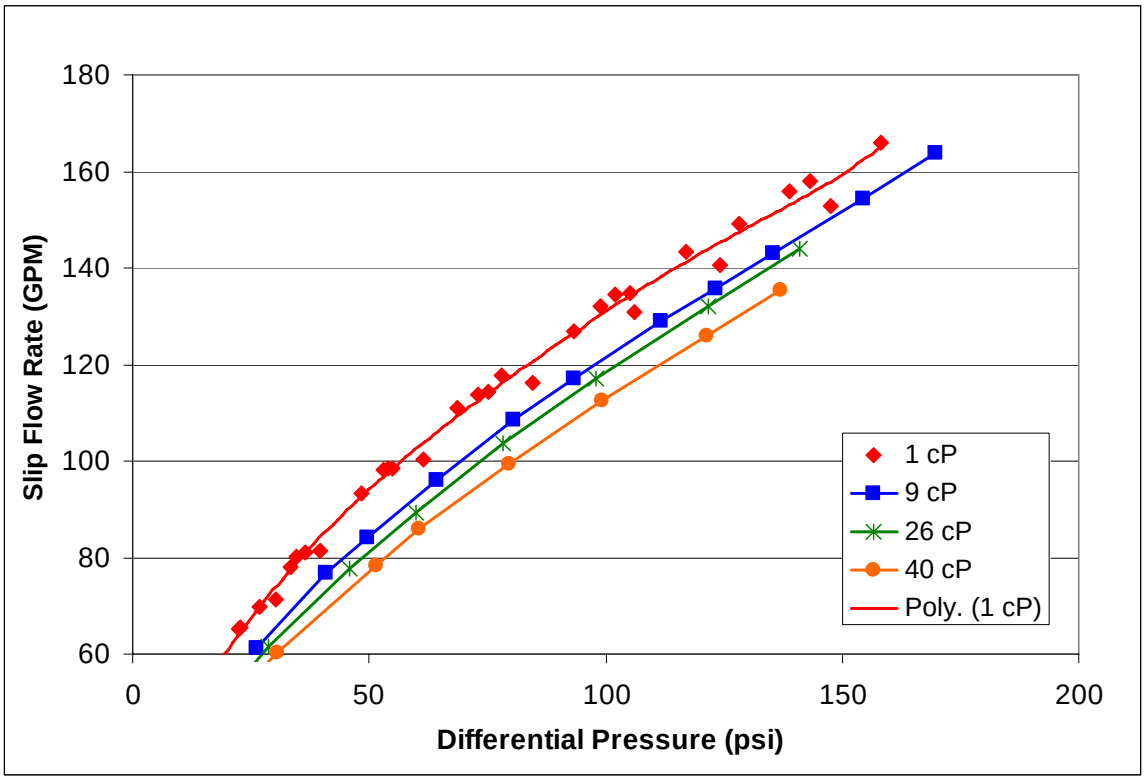

Fig. 5.4 –Slip flow rate (GPM) versus differential pressure (psi) for four different viscosities at 1350 RPM.

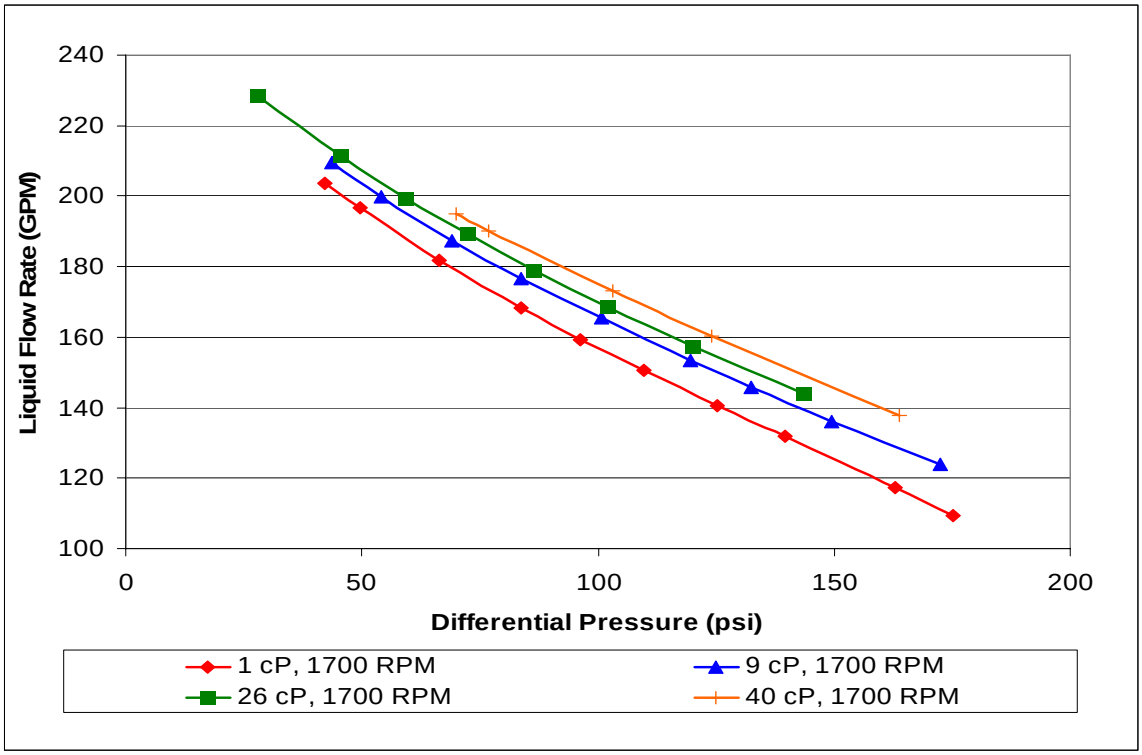

Fig. 5.5 – Liquid flow rate (GPM) versus differential pressure (psi) for four different viscosities at 1700 RPM.

5.2 100% GVF Tests

In attempt to reproduce the results of the experiments conducted by Singh[6,7], tests were conducted at 100% GVF using a 1 and 9 cP liquid. Pure liquid was flowed through the pump for an extended period of time. The liquid flow was then cut-off and compressed gas was then sent through the pump, leaving only the fluid left inside the pump to maintain the seals and provide compression. To ensure that the results are comparable, the same Bornemann twin-screw pump and gel used by Singh was used for this set of tests.

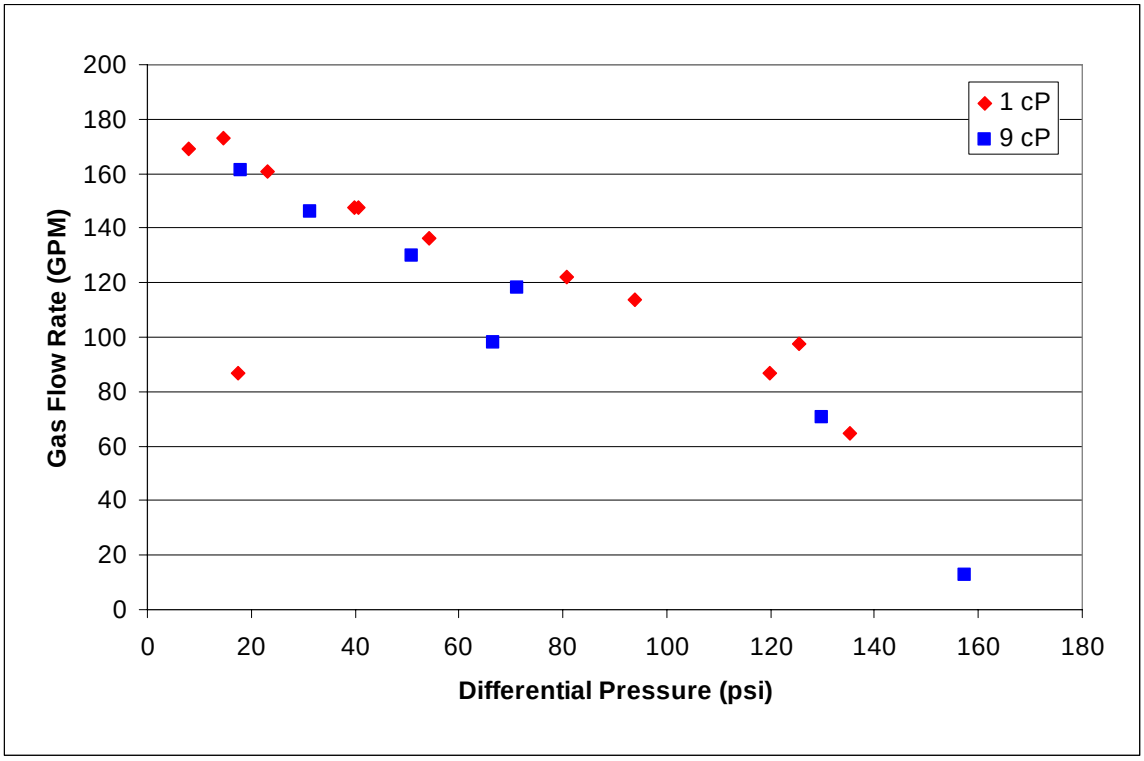

Fig. 5.6 – Gas flow rate (GPM) versus differential pressure (psi) , 100% GVF for a 1 cP and 9 cP fluid.

As shown in **Fig. 5.6**, we were not able to replicate the gain in gas flow rate observed by Singh. There is no significant increase in gas throughput resulting from the increase in viscosity. The gas flow rate with a 9 cP liquid providing the compression is actually somewhat lower than that for a 1 cP liquid in the pump.

There is one point on Fig. 5.6 which demonstrates a significant problem when conducting tests are 100 % GVF. The outlying point where the gas flow rate is much lower than the others at its differential pressure range is what results when there is insufficient liquid to maintain gas compression within the pump. Pump operability was observed to be sustainable for only 12 – 16 minutes at a time.

5.3 GVF Progression

The majority of tests were conducted at 0%, 70%, and 95% GVF. Because of the inherent instability of testing at 100% GVF and since most pump installations are maintained at a maximum GVF of 95% no further tests were conducted with pure gas. Pump behavior under wet-gas conditions was evaluated at 95% GVF. Tests were conducted at 70% GVF to provide comparison to a mostly gas but not wet-gas condition.

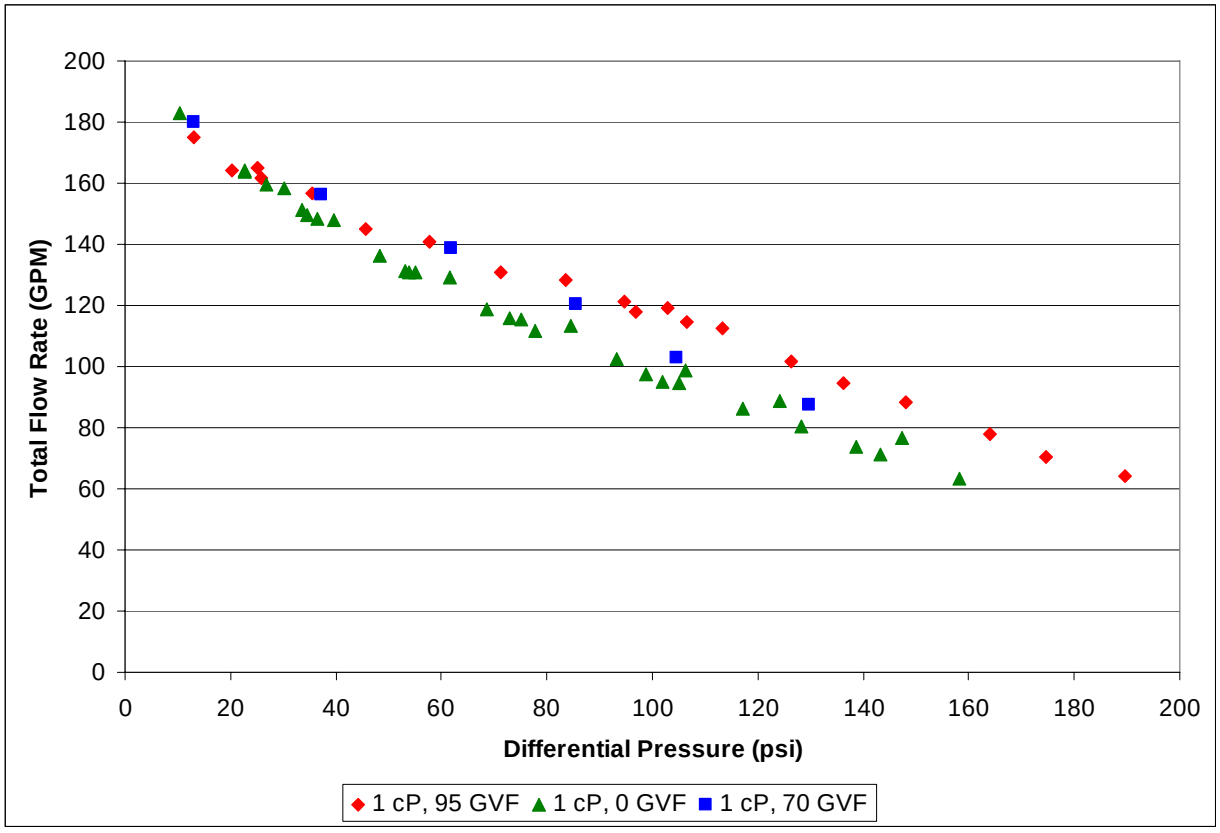

Fig. 5.7 – GVF progression, total flow rate (GPM) versus differential pressure (psi), 1 cP fluid at 1350 RPM.

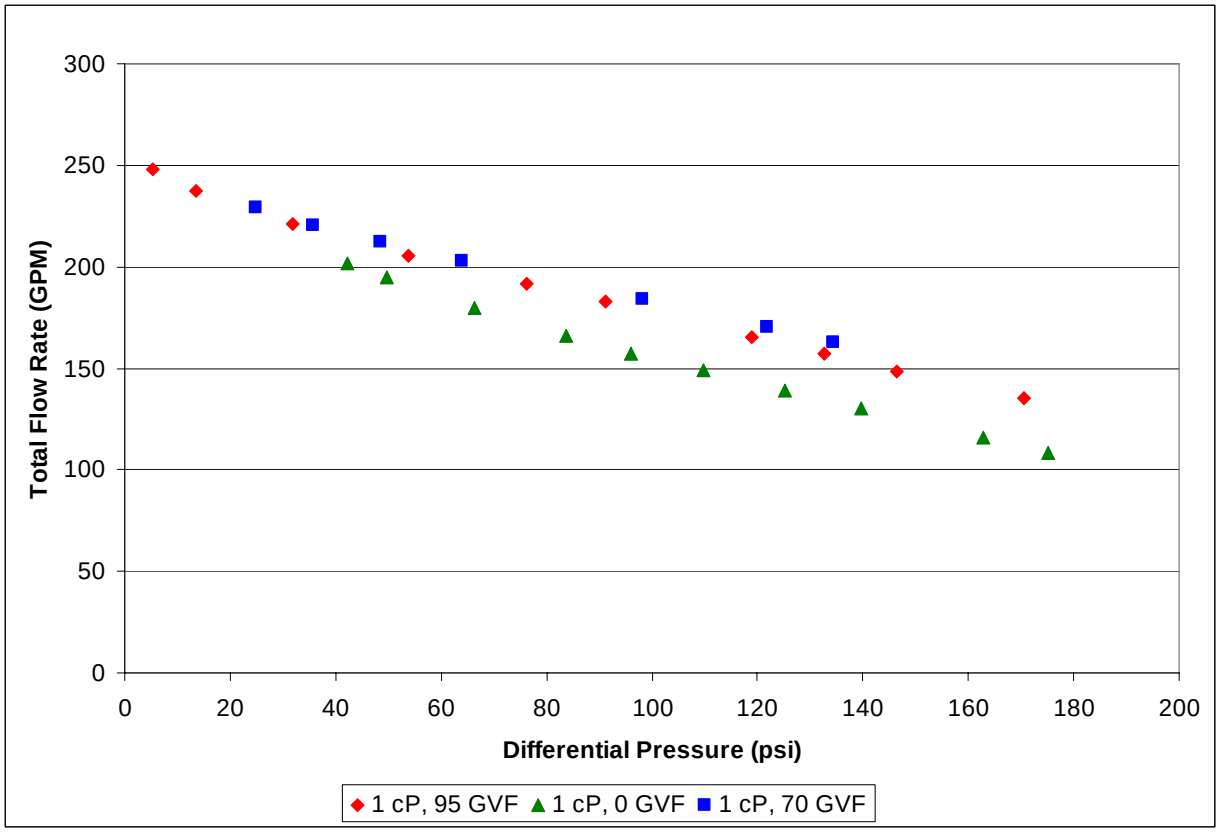

Fig. 5.8 – GVF progression, total flow rate (GPM) versus differential pressure (psi), 1 cP fluid at 1700 RPM.

Figs 5.7 and **Fig. 5.8** show pump curves at different GVF for 1350 and 1700 RPM pump speeds, respectively. At 1350 RPM, there is a slight increase in total flow rate flow and therefore a slight increase in volumetric efficiency. This is due to gas compression enabling more gas to be taken into the pump. The effect at 1700 RPM is similar, but the difference between 70 and 95% GVF is negligible with the 70% GVF slightly higher. This suggests that there is a limit to the gas compression phenomena that is being reached at the higher pump speed.

5.4 Speed Comparison

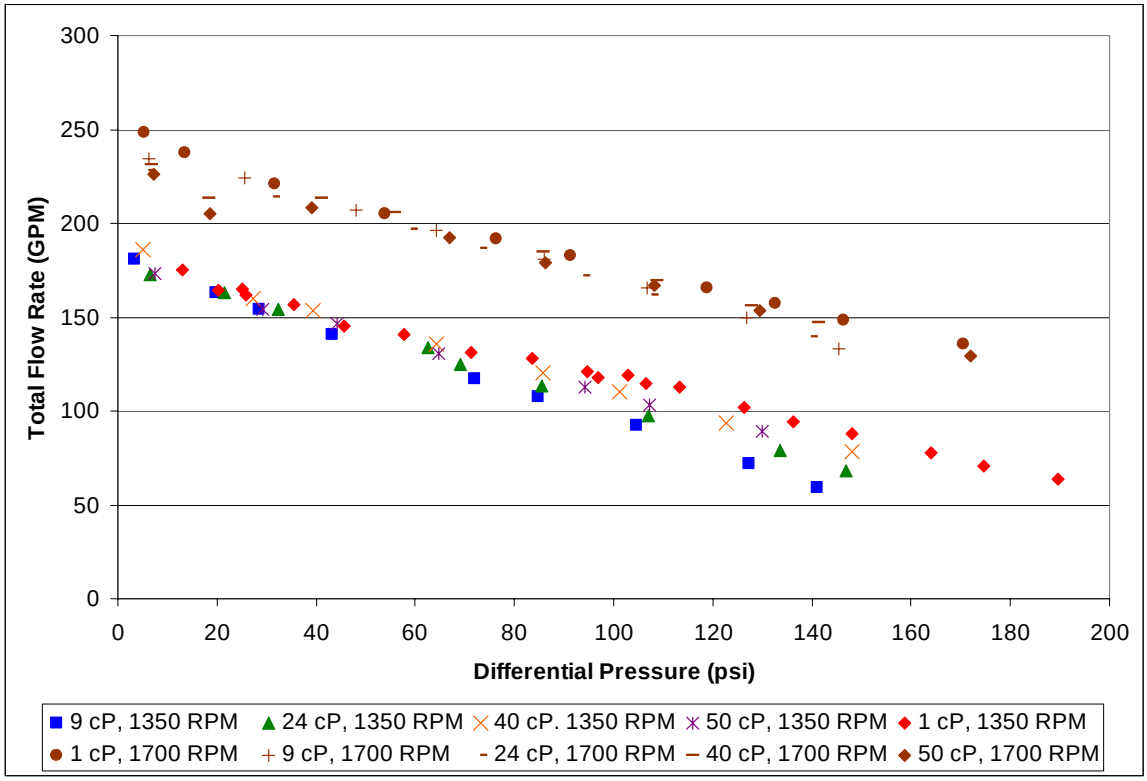

Fig. 5.9 – Speed comparison, total flow rate (GPM) versus differential pressure (psi), 95% GVF.

As speed increases total flow rate is expected to increase. This is confirmed by the data presented in **Fig. 5.9**. Increase in flow rate is a constant offset from the lower to higher speed. This provides further evidence that slip rate is independent of pump speed.

5.5 Wet-gas Compression Tests

If our current models for gas compression within twin-screw pumps is correct we would expect in increase in flow rate with increasing viscosity due to decreased slip flow. As fig. **5.10** illustrate, this is not the case.

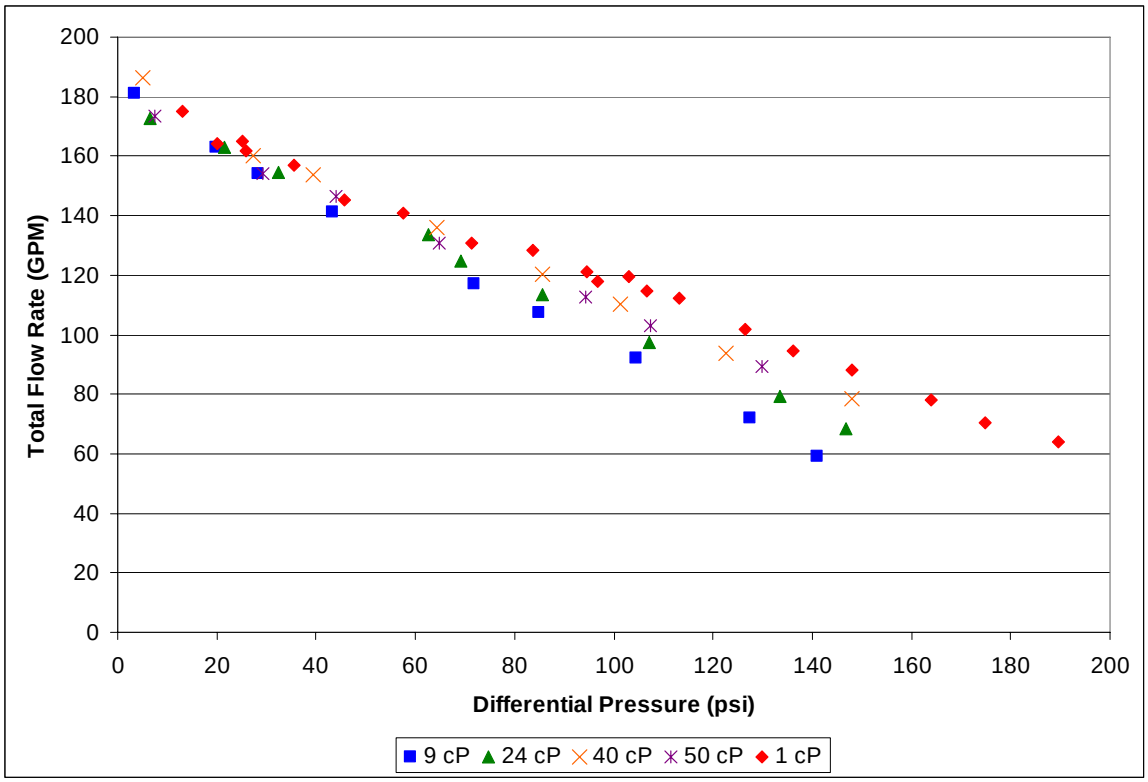

Fig. 5.10 – Total flow rate (GPM) versus differential pressure (psi), 95% GVF, 1350 RPM.

At a pump speed of 1350 RPM, no increase in total flow rate was observed with increased viscosity. At small differential pressures, pump performance is unchanged as viscosity increases. Around 60 psi differential pressure pump performance drops as a result of increasing viscosity; this difference becomes more apparent as differential pressure increases. An interesting phenomenon is that the poorest performance came as a result of the use of a 9 cP liquid. As viscosity increases further, the performance gradually increases towards the pump curve established with pure water.

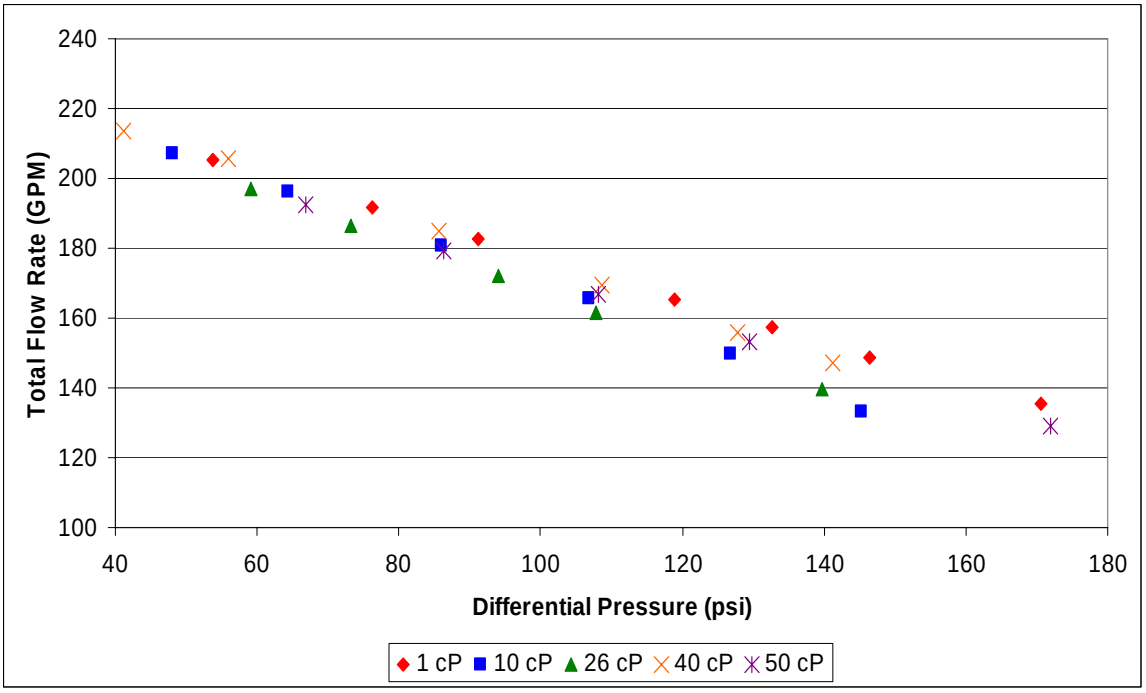

Fig. 5.11 – Total flow rate (GPM) versus differential pressure (psi), 95% GVF, 1700 RPM.

At 1700 RPM, **Fig. 5.11**, pump behavior with increasing viscosity is similar to that observed at 1350 RPM. At the higher pump speed the spreading of the curves at higher GVF is smaller and begins later at a differential pressure of approximately 120 psi.

To determine whether more liquid in the pump would produce the expected performance, further tests at 70% GVF were conducted. The results are shown in **Fig. 5.12**. Similar performance to the tests conducted under wet-gas conditions was observed.

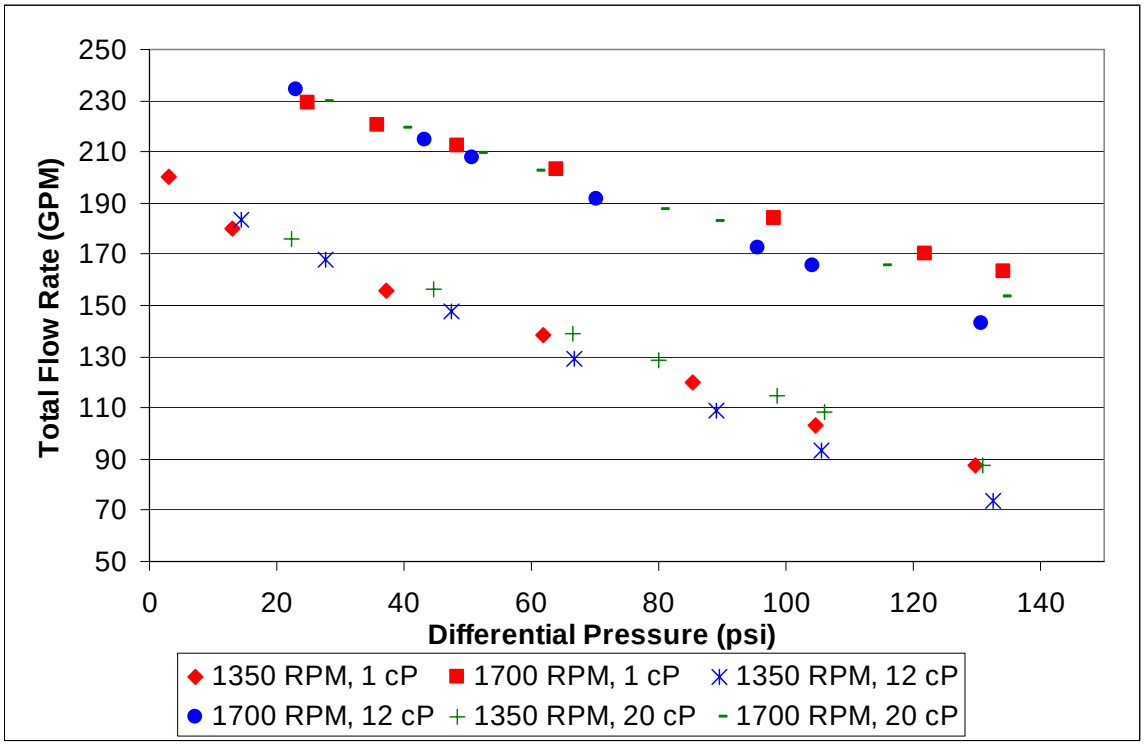

Fig. 5.12 – Total flow rate (GPM) versus differential pressure (psi), 70% GVF, 1350 and 1700 RPM.

5.6 Model Verification

To understand twin-screw pump behavior in the context of the new experimental data presented in the previous section. An attempt to match predictions of pump performance produced by the model presented by Martin[8,9] to the data obtained by the experiments was made.

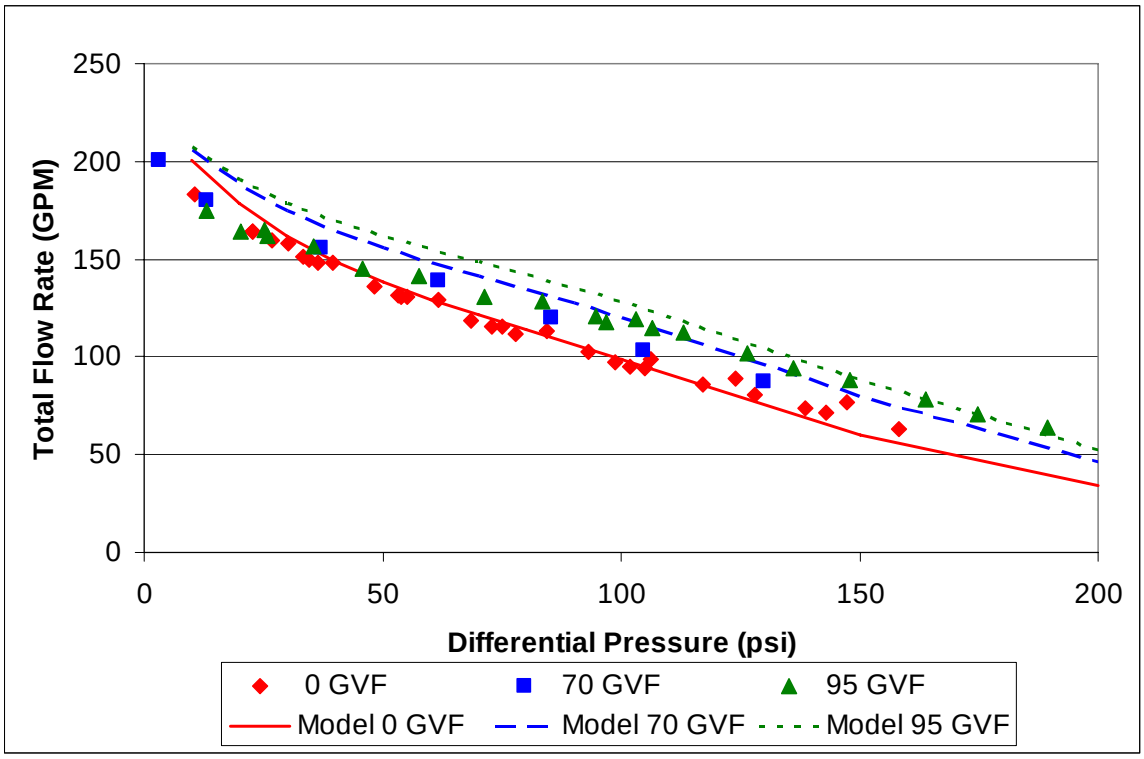

Fig. 5.13 – Model match, total flow rate (GPM) versus differential pressure (psi), 1350 RPM, 1 cP liquid.

Fig. 5.13 is a match with water as the liquid phase. In this case the experimental data confirms the conclusions made by Martin that the model is able to make accurate predictions of pump behavior at 0, 70, and 95% GVF.

Fig. 5.14 is the base case at 0% GVF and a 1 cP liquid. The model match is excellent since the linear regression used to obtain the effect clearance size is based on given data at this same condition. We are essentially giving the model this solution from which other predictions at new operating situations are made.

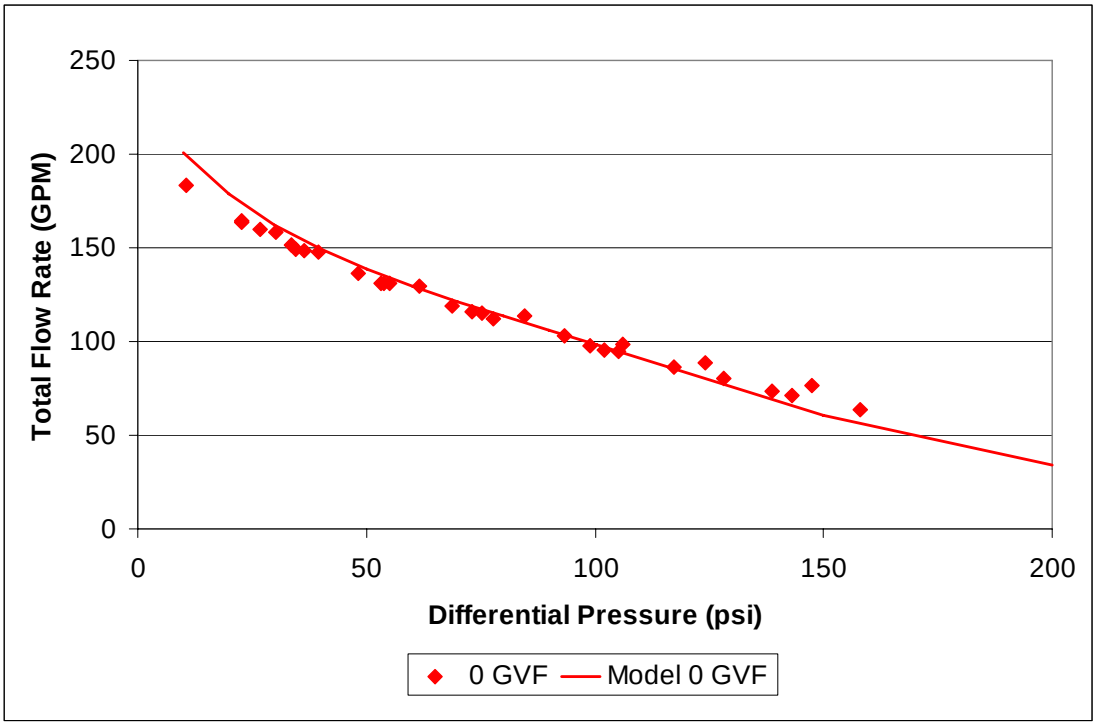

Fig. 5.14 – Model match, total flow rate (GPM) versus differential pressure (psi), 0% GVF, 1350 RPM, 1 cP liquid.

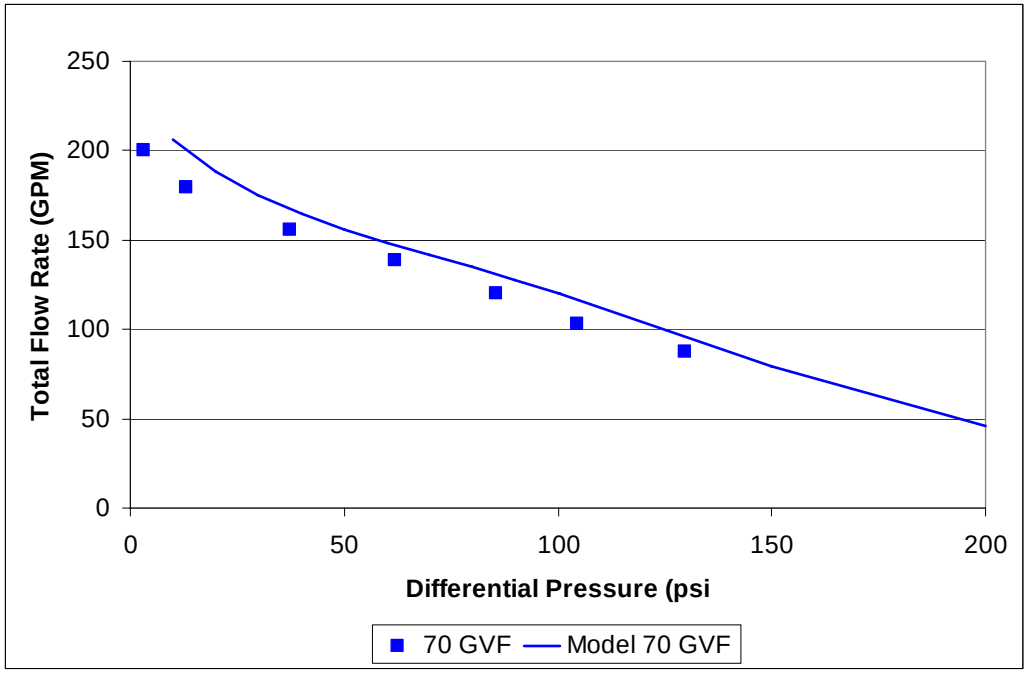

Fig. 5.15 – Model match, total flow rate (GPM) versus differential pressure (psi), 70% GVF, 1350 RPM, 1 cP liquid.

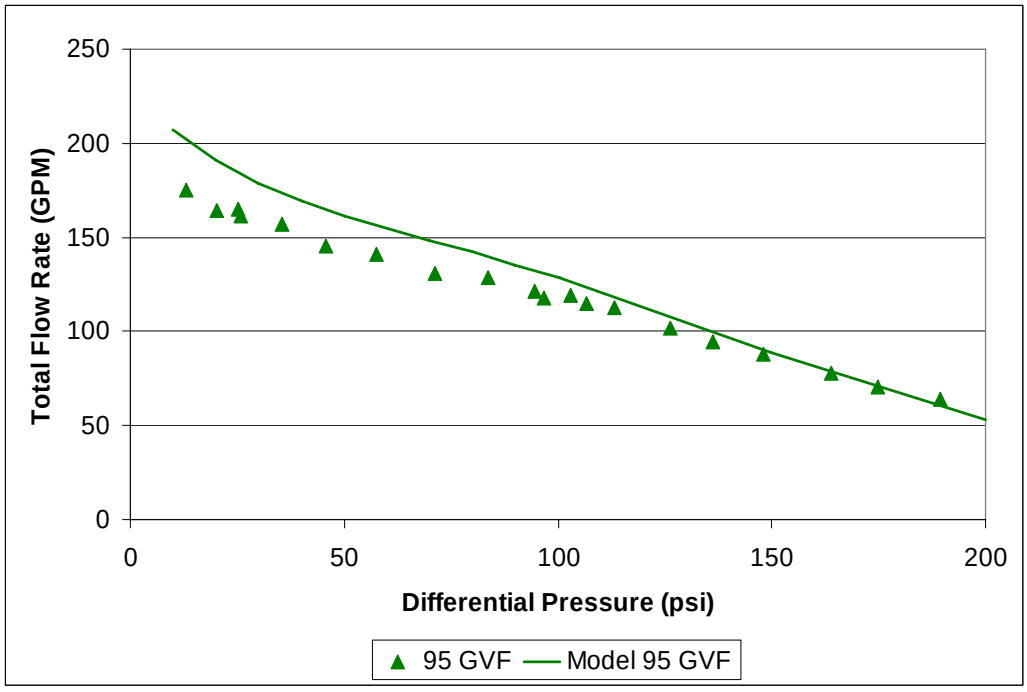

Fig. 5.16 – Model match, total flow rate (GPM) versus differential pressure (psi), 95% GVF, 1350 RPM, 1 cP liquid.

Fig. 5.15 and **Fig. 5.16** are the model matches at 70 and 95% GVF. In both cases, there is a slight amount of overestimation by the model. The overestimation is more severe at lower differential pressures and for higher GVF.

When the liquid viscosity is increased to 9 cP, the model begins drastically overestimating pump performance at all GVF, **Fig. 5.17**. An increasing trend in total flow rate is predicted by the model with increasing GVF. This trend is opposite to what was observed experimentally with a drop in performance with increasing starting at higher differential pressures.

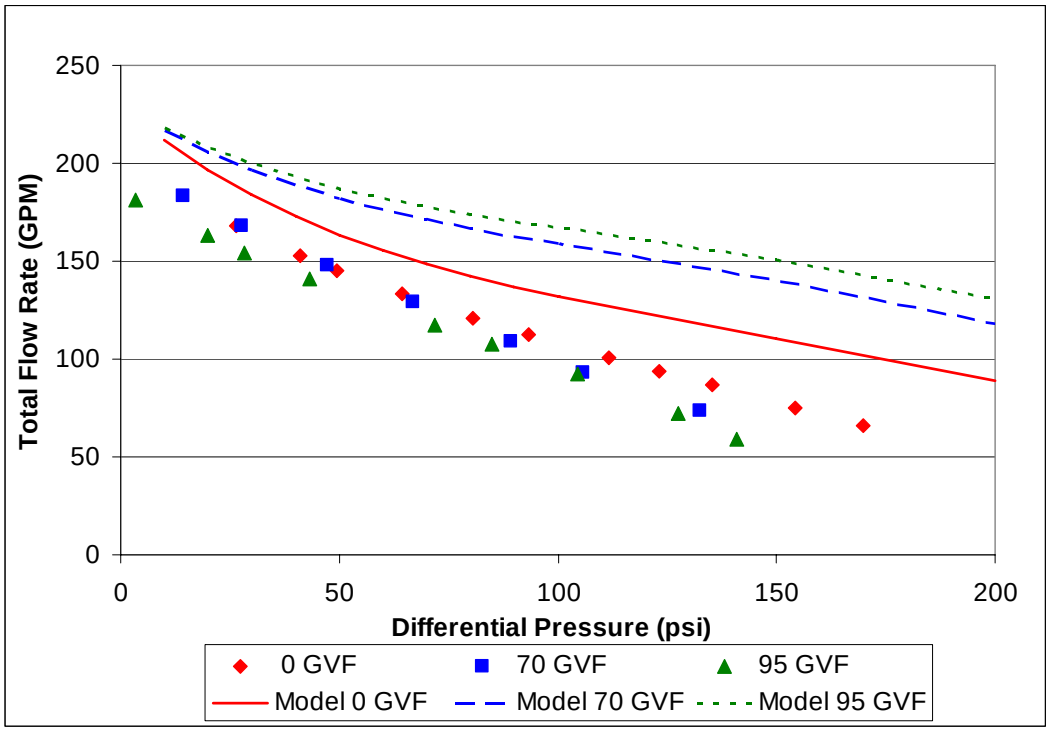

Fig. 5.17 – Model match, total flow rate (GPM) versus differential pressure (psi), 1350 RPM, 9 cP liquid.

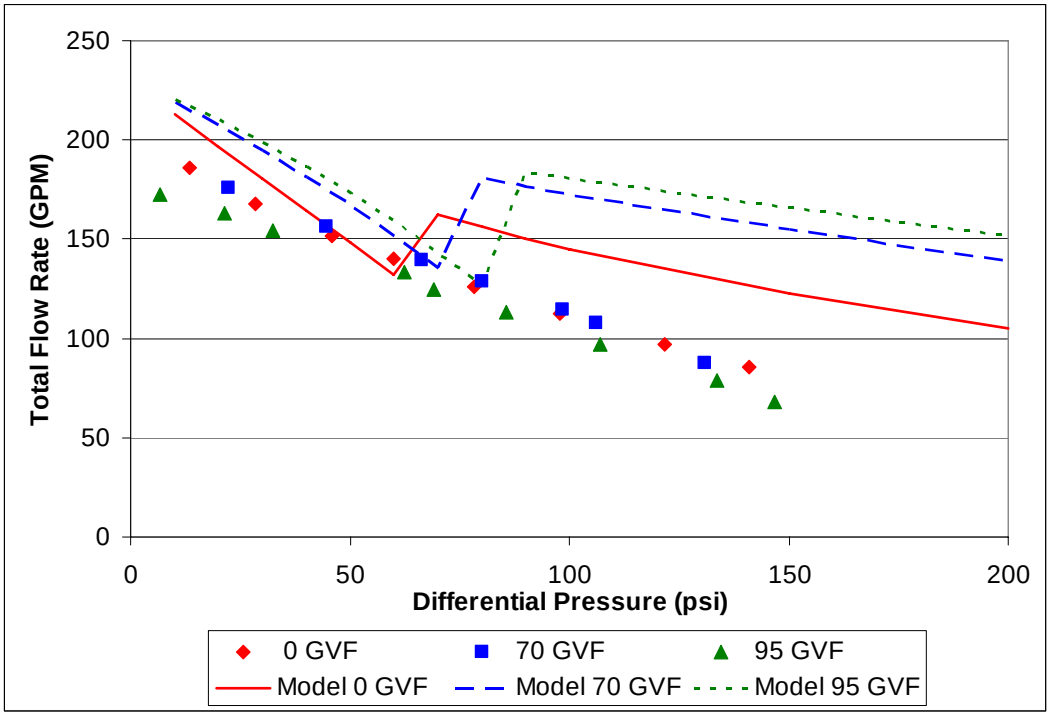

Fig. 5.18 – Model match, total flow rate (GPM) versus differential pressure (psi), 1350 RPM, 24 cP liquid.

Fig. 5.18 is an attempt to match data at 24 cP. The model begins experiencing severe difficulties, predicting a sharp discontinuity for the pump curve at each GVF. These discontinuities are the result of a predicted transition between laminar and turbulent flow.

Assuming that there is a problem with flow regime transitions, a match was attempted using only the laminar or turbulent solution. The laminar solution produced an unsatisfactory match. First overestimating and then underestimating pump performace, **Fig. 5.19**.

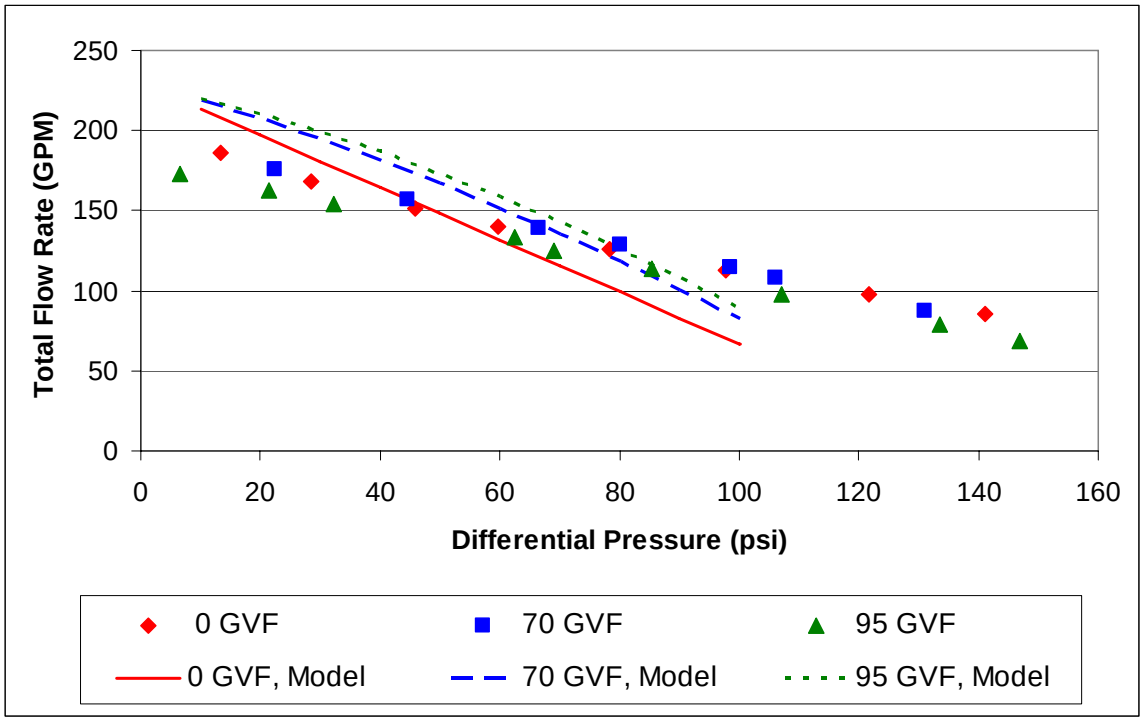

Fig. 5.19 – Model match, total flow rate (GPM) versus differential pressure (psi), 1350 RPM, 24 cP liquid, laminar flow only.

The turbulent solution was even more inaccurate. In all cases the predicted pump curve was much higher than the experimental data, **Fig. 5.20**. Therefore, the conclusion can be made that the poor matches at this viscosity are not caused purely by the flow regime transition, though it is certainly one of the more glaring issues.

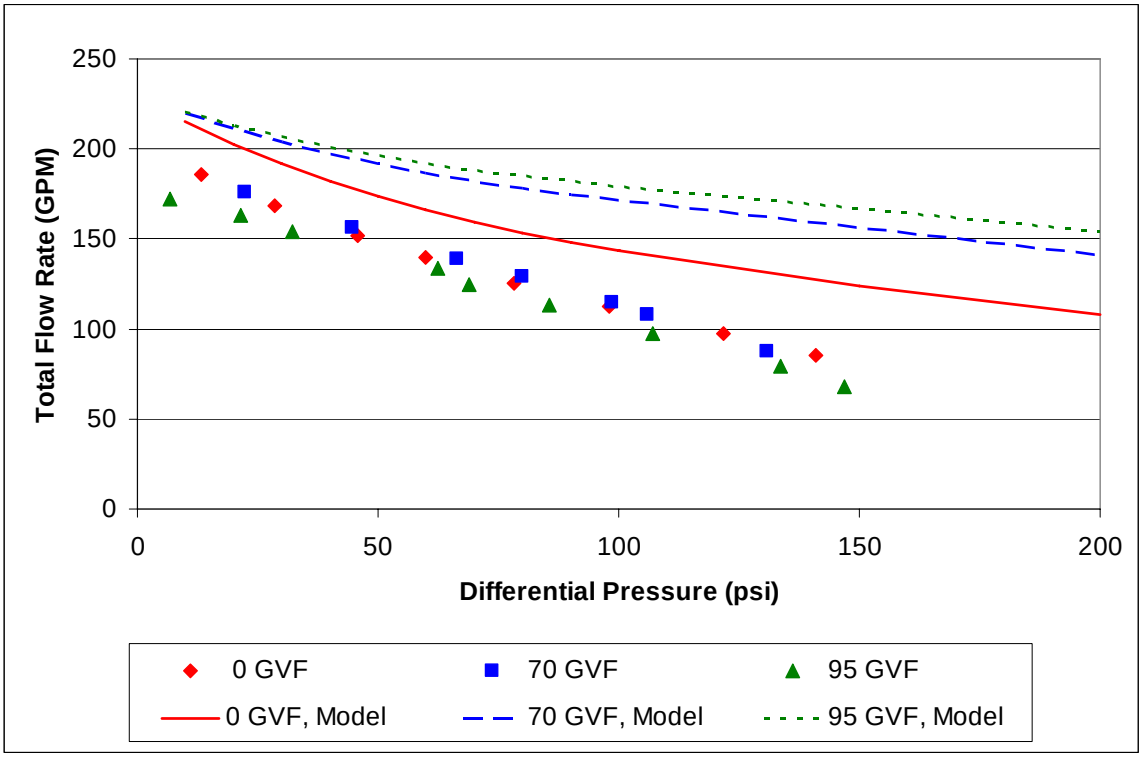

Fig. 5.20 – Model match, total flow rate (GPM) versus differential pressure (psi), 1350 RPM, 24 cP liquid, turbulent flow only.

5.7 Viscosity Correction

Part of the reason that increased liquid viscosity is not having the expected effect may be the non-Newtonian and temperature thinning properties of the gel used. The shear imparted on a fluid within a twin-screw pump is thought to be small. Nevertheless, some shear is being applied on the fluid as it moves through the narrow clearances. Additionally, temperature increases due to viscous effects and gas compression further reduce the effectiveness of the gel.

Since the Martin model does not have the ability to compensate for temperature and shear effects using fluid rheology data. An attempt to determine the actual liquid viscosity in the pump was made by matching pure liquid data with model prediction made with lower viscosities. **Fig. 5.21** shows that data of a 9 cP gel corresponds to viscosity slightly under 2 cP in the model.

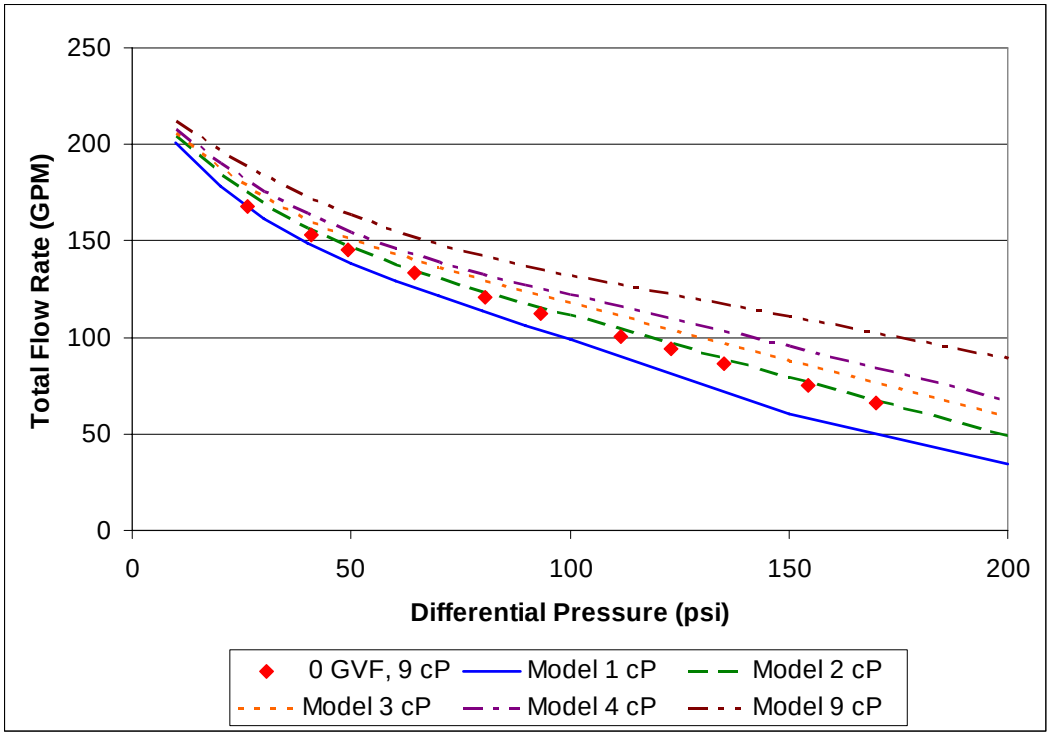

Fig. 5.21 – Viscosity match, total flow rate (GPM) versus differential pressure (psi), 1350 RPM, 9 cP.

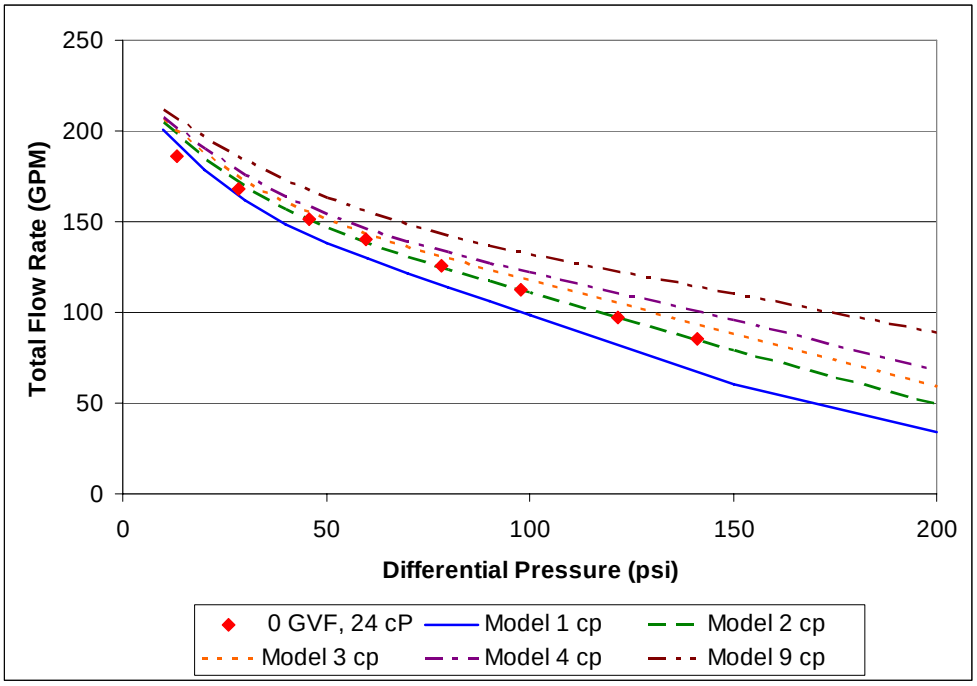

Fig. 5.22 – Viscosity match, total flow rate (GPM) versus differential pressure (psi), 1350 RPM, 24 cP.

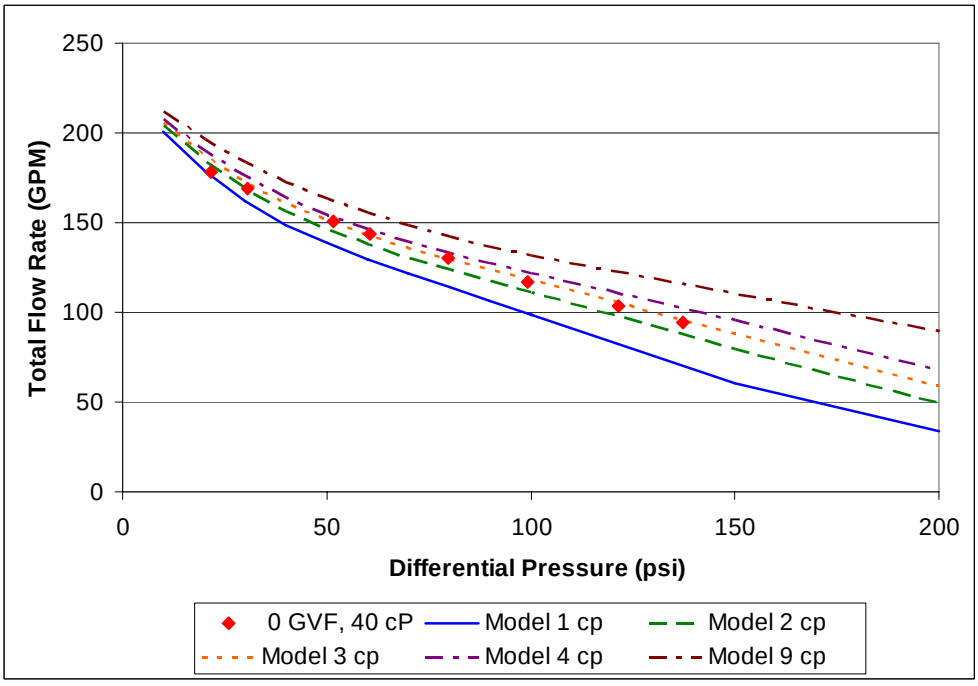

Fig. 5.23 – Viscosity match, total flow rate (GPM) versus differential pressure (psi), 1350 RPM, 40 cP.

Figs. 5.22 and **Figs. 5.23** display the viscosity matching results for data with 24 and 40 cP liquids, respectively. These viscosities correspond to liquid viscosities of approximately 2 and 3 cP in the model. A corrected viscosity match can now be made at 95% GVF.

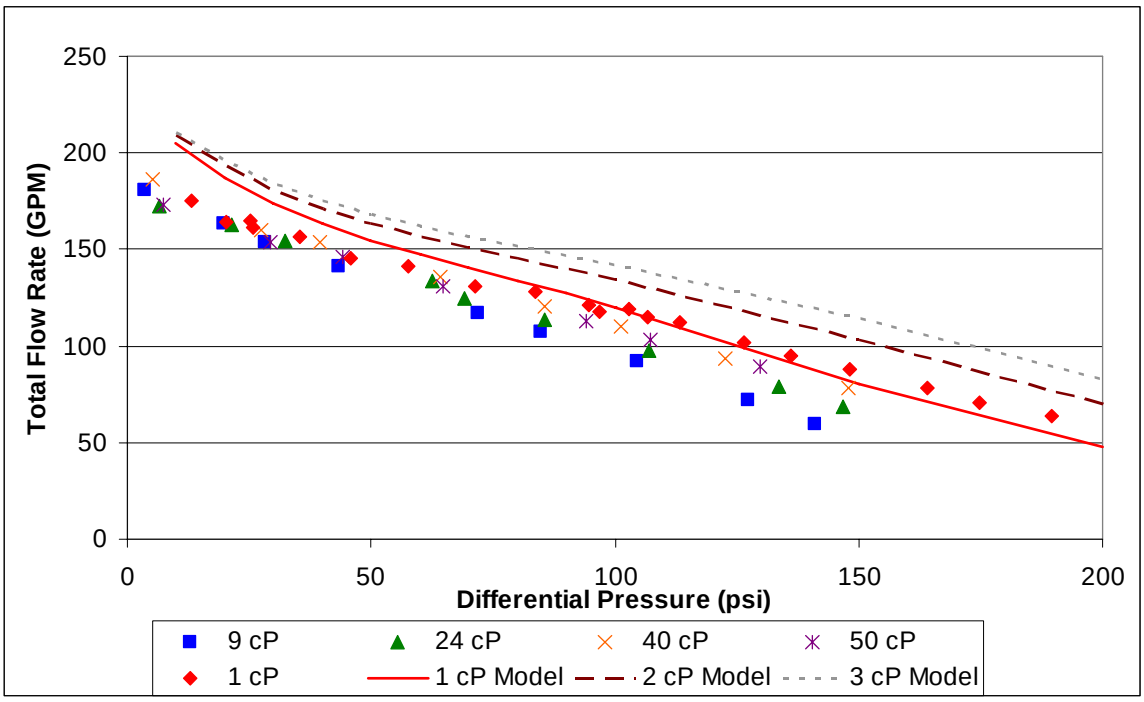

Fig. 5.24 – Corrected viscosity match, total flow rate (GPM) versus differential pressure (psi), 1350 RPM, 95% GVF

Fig. 5.24 shows the corrected viscosity match. The model is still unable to accurately predict pump performance at 95% GVF with elevated viscosity. The model predicts small increases in total flow rate with increasing viscosity which is not reflected in the experimental data.

5.8 Conclusions and Recommendations

New data obtained at high GVF does not confirm earlier findings. Instead of an increase in pump flow rate with higher viscosity there is no change and even a drop in total flow rate and volumetric efficiency. The new data suggest that at high GVF, viscosity is not a dominant parameter. Though the thinning behavior of the gel reduces the effect that it has on the pump system, it does not completely explain the trends observed.

What is likely is that at high GVF, the liquid sealing around the chambers is being lost, resulting in multiphase flow in the clearances. This would explain why the Martin model which assumes pure liquid slip flow cannot provide adequate predictions. The need for models to include multiphase flow effects in the clearances has been mentioned before both by Prang & Cooper[13] and Rausch[14].

We can conclude that for the Martin model to work under wet-gas conditions it must be modified to use real fluid property data to adjust the viscosity in each chamber. The model must also be able to account for multiphase flow in the clearances. A partial solution to this problem has been presented by Vetter *et al.*[10] in the form of an effective viscosity based on gas density and liquid viscosity.

Additionally, the recirculation chamber of the Bornemann pump must be taken into account. Internal liquid recirculation would lower the actual GVF in the pump which may reduce any performance differences resulting from high GVF. Rausch *et al.*[14] were able to design this pump feature into their model.

More tests should be conducted at higher differential pressures. Since some spreading of the data was observed at higher differential pressures, going to even higher differential pressures may produce interesting results. Discharge pressure from the Bornemann pump may be limited by the piping at the Riverside facility. Testing at viscosities higher than 50 cP should be performed. Currently our ability to test higher viscosities is limited by the capacity of the centrifugal charging pumps. Testing with a non-Newtonian and temperature resistant fluid would minimize shear and temperature effects on pump performance and allow for less convoluted data.

CHAPTER VI
THROUGH-CASING INJECTION

This chapter presents the results and discussion of all work done on determining the feasibility of the through-casing injection concept. Since experimental testing of through-casing injection would require significant modifications to an expensive piece of machinery, this problem could only be approached theoretically.

6.1 Injection Theory

The method used to model gas compression in twin-screw pumps was presented in Chapter II. **Eq. 2.2** is the system of equations that is solved to determine the pump's internal pressure profile at a given set of conditions. To simulate injection, the simplest approach would be to model the injection as an additional slip flow term. A portion of the modified system of equations can then be rewritten as:

$$V_{i-1} \cdot \left(\frac{p_{i-1} \cdot Z_i}{p_i \cdot Z_{i-1}} - 1 \right) + \left(q_i - q_{i-1} + q_{inj} \right) \cdot \Delta t = 0 \qquad (6.1)$$

Where the additional injection flow rate, q_{inj}, would be inserted depends on into which chamber or chambers injection is desired. Implementing this injection term would require the computer program solving the Martin model to be reworked. However a good approximation of pump behavior with injection can be obtained using a simpler method. Data on pump pressure profiles and liquid volumes in each chamber can be adjusted to simulate injection.

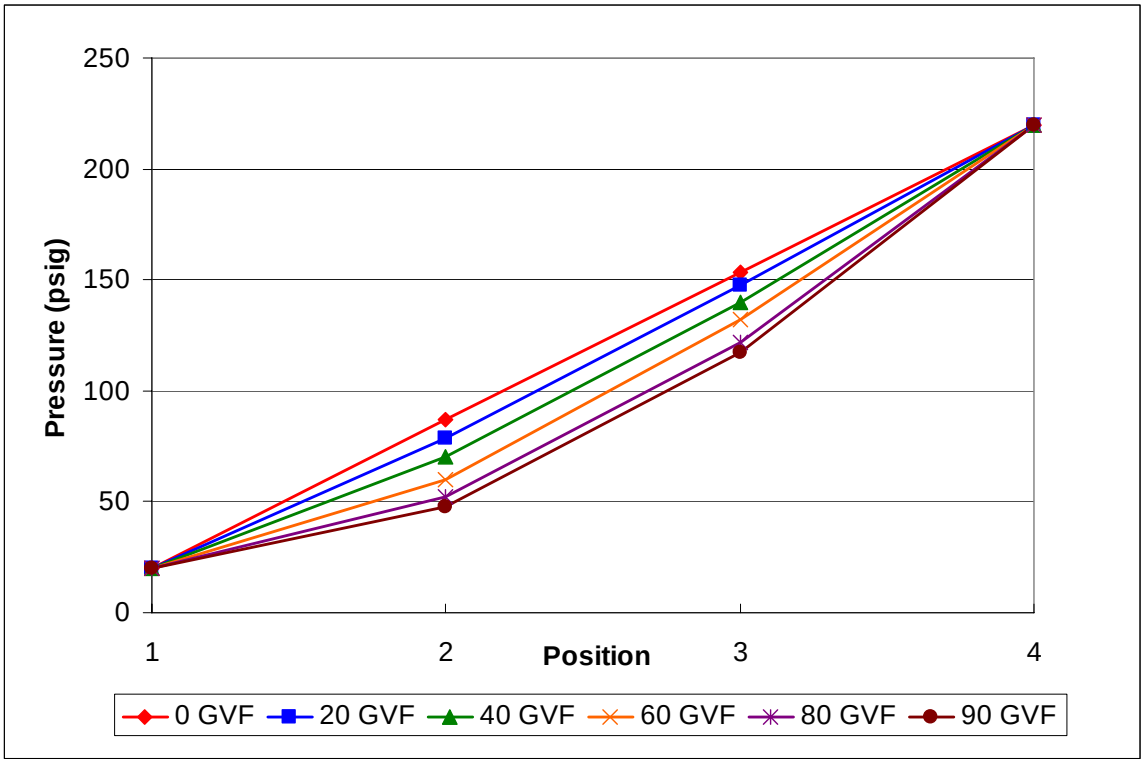

Fig. 6.1 – Pressure profiles (psig), differential pressure 200 psi, 1800 RPM (after Martin[8]).

Fig. 6.1 presents pressure profile solutions given by the Martin model for the Bornemann pump operating at a differential pressure of 200 psi and a pump speed of 1800 RPM for different GVF. As the GVF increases the pressure profile becomes increasingly nonlinear. The Bornemann pump has four chambers on each half of the each of the two screws. This corresponds to four identical sets of four chambers moving from the suction to the discharge, Fig. 2.1. Each of the chambers is indexed 1 through 4 with position 1 being the suction and position 4 being the discharge.

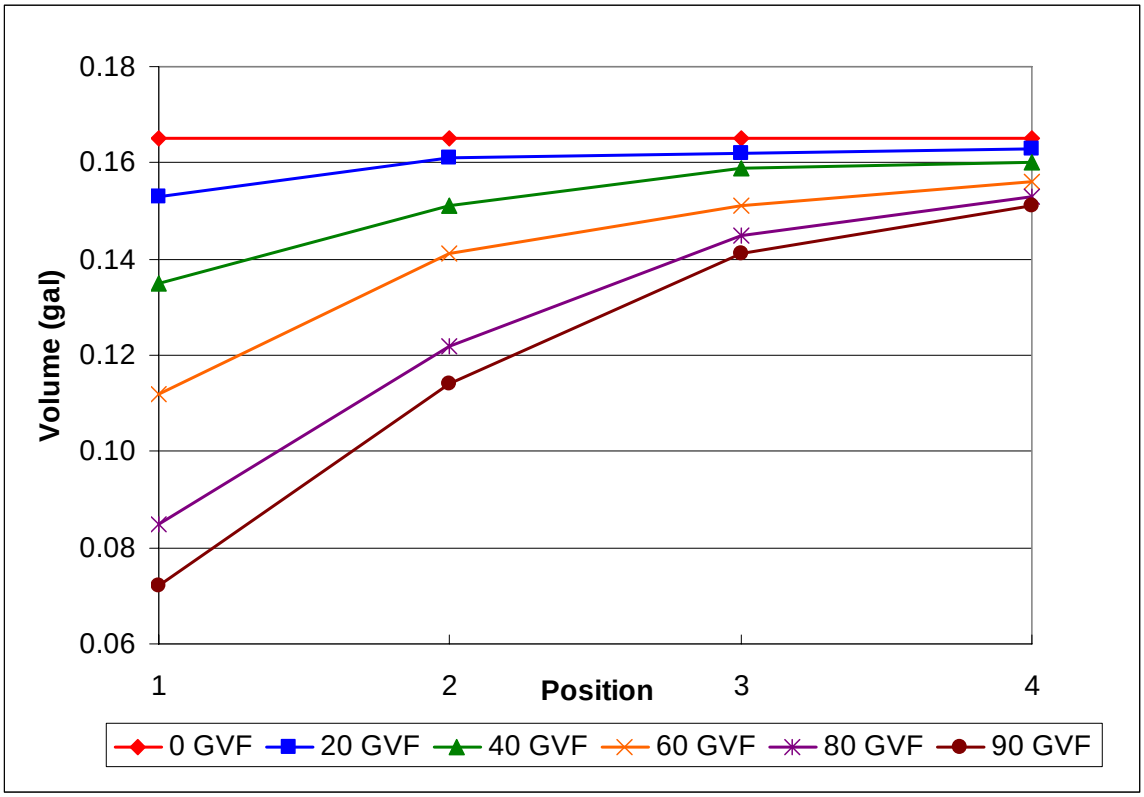

Fig. 6.2 – Liquid volume in chambers (gal), differential pressure 200 psi, 1800 RPM (after Martin[8]).

Fig. 6.2 shows the liquid volume in each chamber corresponding to the pressure shown in Fig. 6.1. When GVF is 0% each chamber is completely filled with liquid, therefore the liquid volume is constant. The volume of each chamber is 0.165 gallons. As GVF increases less liquid is present in the pump resulting in lower liquid volumes. The step change in liquid volume from position to position increases dramatically as GVF increases.

The change in liquid volume is due to slip flow from the next position. After each rotation of the screws each position is advanced through the pump by one. We can assume that any gain in liquid volume comes from the slip flow. The amount of volume change resulting from slip is therefore a known quantity.

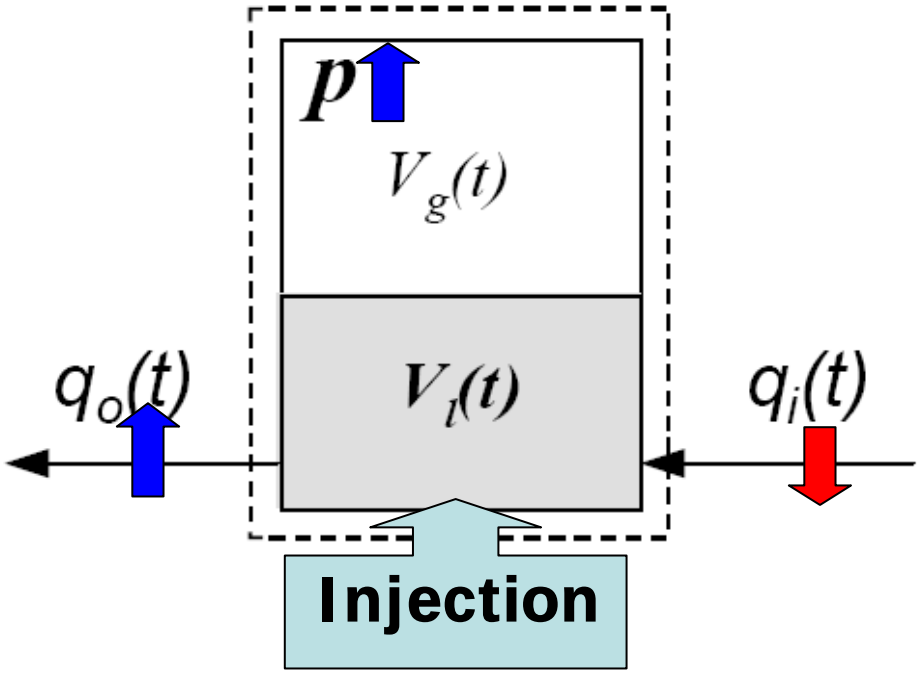

Fig. 6.3 – Simplified injection model.

If each chamber in the pump is modeled as a piston with the liquid phase compressing the gas phase, injection into this piston would increase the liquid volume thereby increasing the overall pressure. Since the slip flow rates into and out of the chamber are only functions of pressure, new slip flow rates can be calculated, **Fig. 6.3**. For turbulent flow the slip flow can be calculated as:

$$q_{slip} = C \cdot \Delta p^{0.57} \tag{6.2}$$

In the preceding equation, the characteristic clearance, *C*, can be assumed as constant. Therefore, a proportional change in slip flow resulting from the injection can be formulated as:

$$\frac{q_{slip,inj}}{q_{slip}} = \left(\frac{p_{2+inj} - p_1}{p_2 - p_1} \right)^{0.57} \tag{6.3}$$

Using these two simple equations, the flow out of the chamber upstream and into the downstream chamber from the chamber in which we are injecting can be adjusted for a given increase in pressure in the injected chamber. The resulting changes in volume will then allow a new pressure profiles to be calculated.

Given a specific pressure increase in the injected chamber, the volume and therefore the flow rate necessary to cause the increase in pressure can be calculated. The flow rate is calculated by simply multiplying the volume of injection needed by the pump speed. The amount of power needed for injection can then be easily calculated:

$$hp = \frac{Q\Delta P}{1714} \tag{6.4}$$

In this equation the flow rate, Q, is given in gallons per minute and the pressure head, ΔP, in psi. The calculated power values are subject to injection pump efficiency. Injection pressure needed is calculated assuming injection fluid initially at atmospheric pressure to give a worse case scenario. Taking fluid pressurized liquid from the suction or discharge side would dramatically decrease the amount of power needed. If liquid at suction pressure were used, no additional boosting would be needed since the discharge pressure is higher than the injection pressure. If liquid were taken from suction then a minimal amount of power would be needed since the pressure difference between positions 1 and 2 is small. In some cases using fluid from the suction would decrease the power needed by half.

6.2 Feasibility Study

For this study injection will occur at position 2 only. Injection at this position should create a more linear pressure profile by adding compression to chambers which previously contributed little at high GVF. **Fig. 6.4** shows the calculated pressure profiles starting from the base case of 90% GVF with no injection and adding various pressure increases in position 2 resulting from injection.

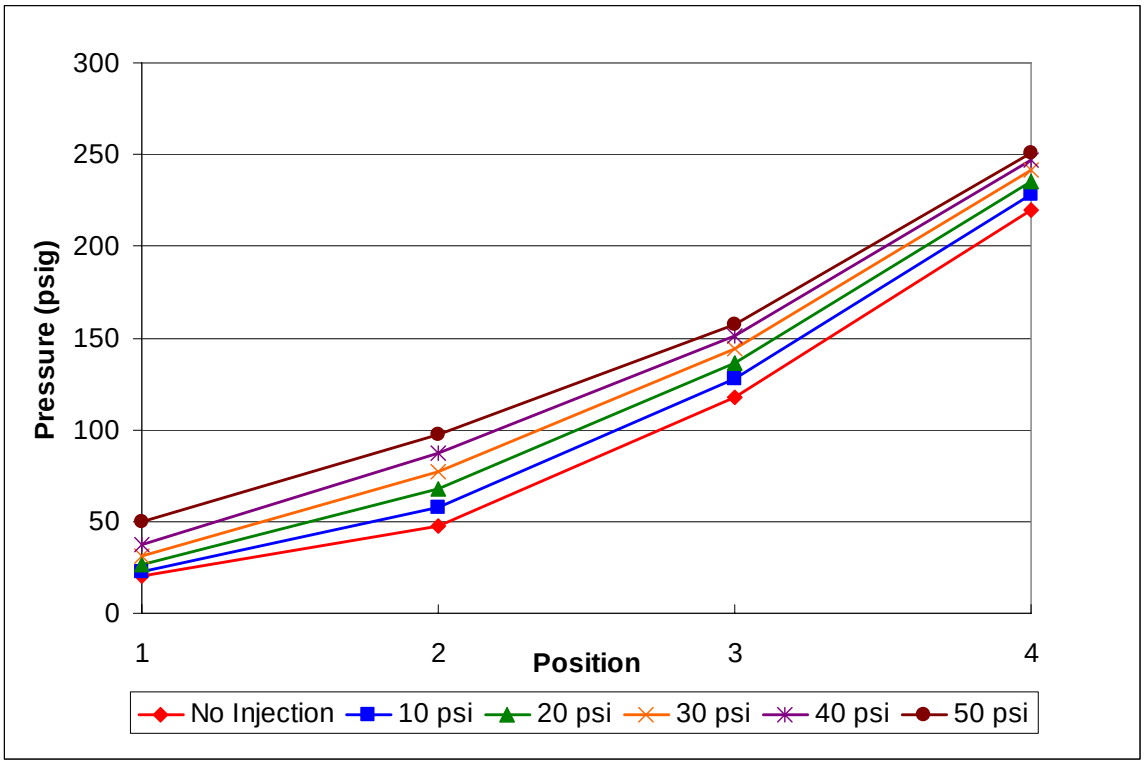

Fig. 6.4 – Pressure profiles (psig) with injection, 90% GVF, differential pressure 200 psi, 1800 RPM.

As the pressure in position 2 is increased, a corresponding increase in discharge pressure at position 4 is observed. The pressure profile also becomes slightly more linear with increasing injection. The suction pressure is also affected in this model since it is considered a closed chamber. In actuality, the suction pressure may not change.

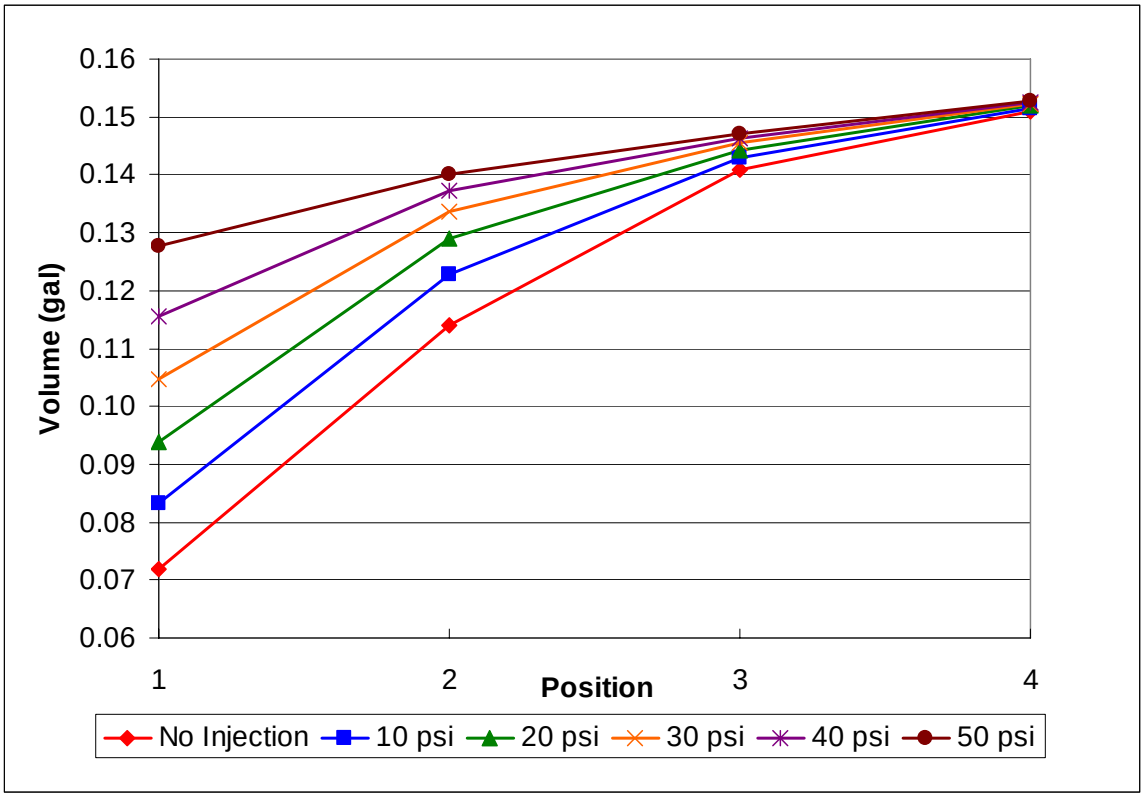

Fig. 6.5 – Liquid volume in chambers (gal) with injection, 90% GVF, differential pressure 200 psi, 1800 RPM.

Corresponding liquid volumes in the chambers increase as expected as we introduce more liquid into the pump, **Fig. 6.5**. As more liquid is injected the liquid volumes begin to approach a more even profile. The liquid volume at position 4 provides a limiting parameter to injection. Eventually, no more liquid and subsequently no more pressure can be introduced at the discharge.

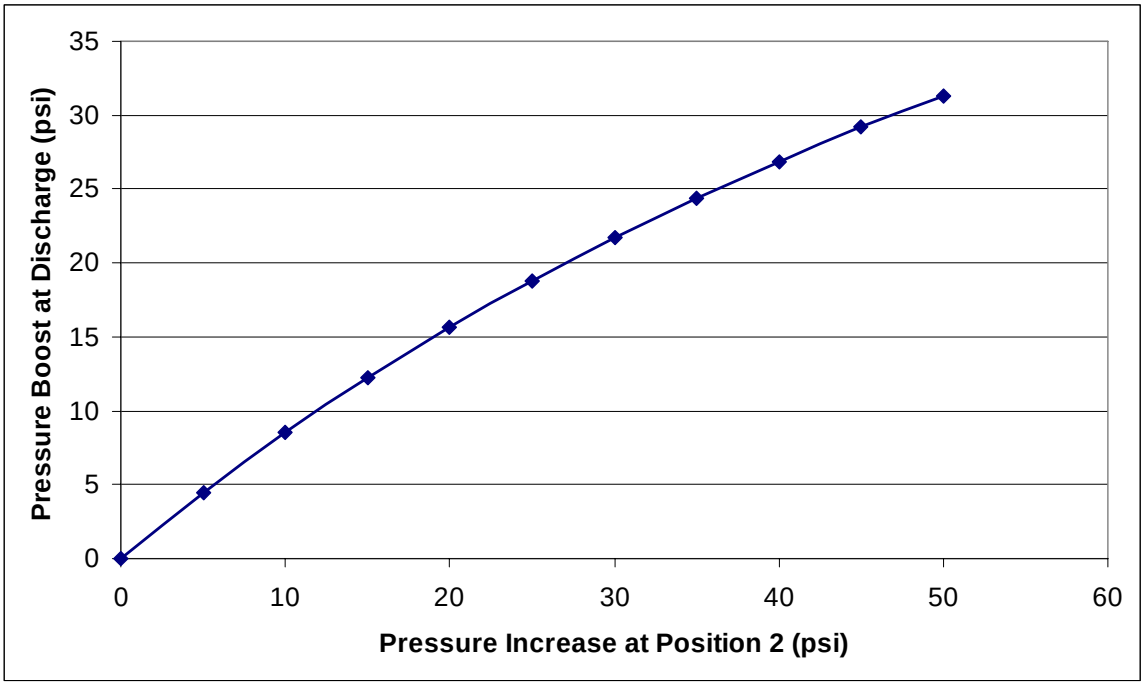

Fig. 6.6 – Pressure boost at position 2 (psi) versus pressure boost at discharge (psi), 90% GVF, differential pressure 200 psi, 1800 RPM.

As pressure is introduced into position 2 the total pressure boost at the discharge increases at a declining rate, **Fig. 6.6**. An injection pressure increase of 50 psi will result in a total pressure boost of only 31 psi.

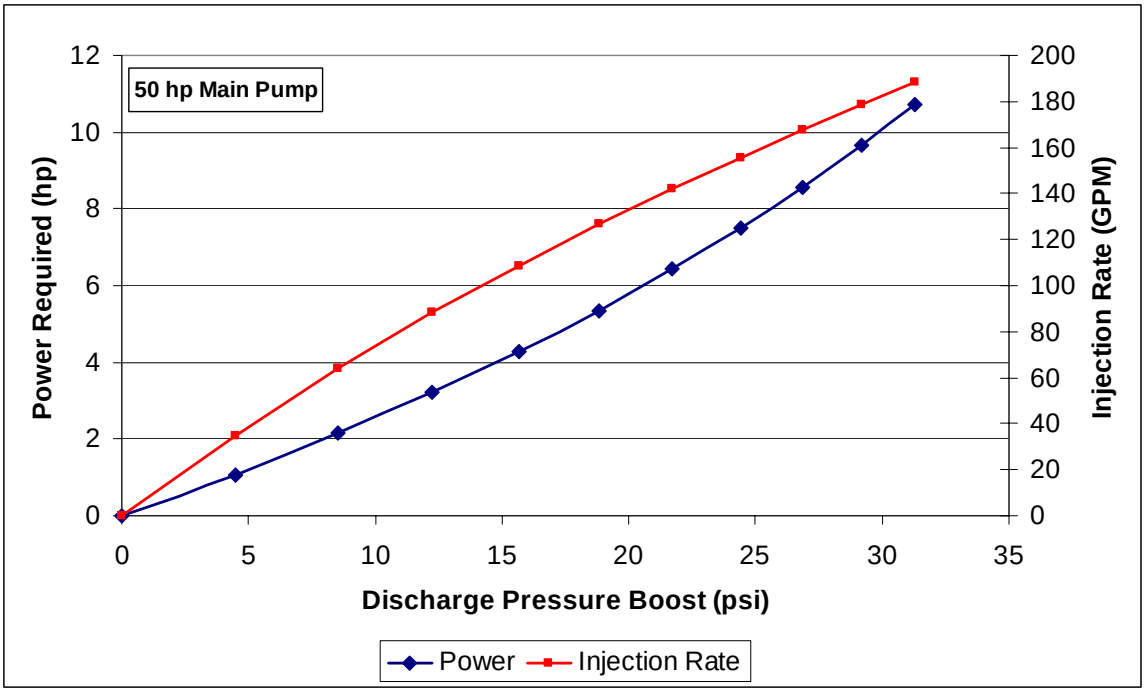

Fig. 6.7 – Discharge pressure boost (psi) versus power required (hp) and injection rate (GPM), 90% GVF, differential pressure 200 psi, 1800 RPM.

Fig. 6.7 illustrates the injection rate and horsepower needed to achieve a desired pressure boost at the discharge. For a 31 psi pressure increase, 180 GPM of injection using a little over 11 hp is required. This is a small amount of power compared to the twin-screw pump as a whole which uses only 50 hp.

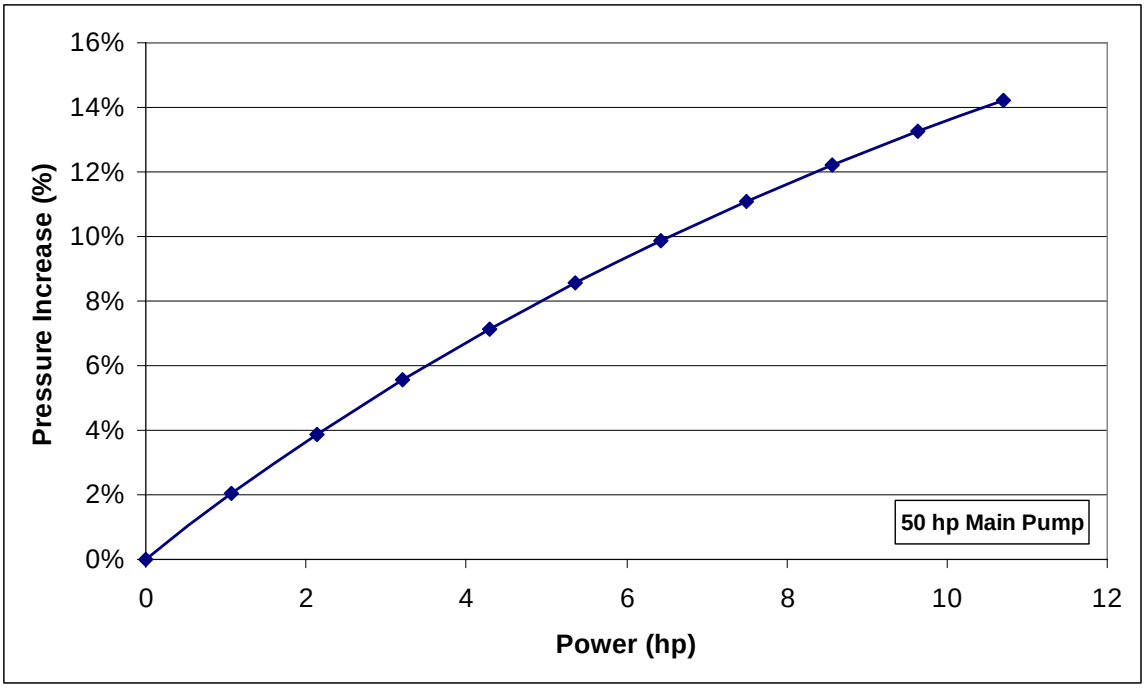

Fig. 6.8 – Power required (hp) versus pressure increase (%), 90% GVF, differential pressure 200 psi, 1800 RPM.

As more power is expended, a declining amount of pressure boost above 200 psi is observed. 11 hp is needed to increase the differential pressure provided by the twin-screw pump by about 14%, **Fig. 6.8**.

Similar results can be seen for 80% GVF, **Fig. 6.9** and **Fig. 6.10**, and 60% GVF, **Fig. 6.11** and **Fig. 6.12**. For injection at 80% GVF the results are almost identical to injection at 90%. The same basic trends are observed. Injection at 60% GVF begins to cause problems. At 60% GVF, the amount of the liquid already present in the pump is such that a given amount of injection has little effect on the chambers closer to the discharge. With a large amount of injection, the pressure profiles start to become more discontinuous and total pressure boost is reaches its limit.

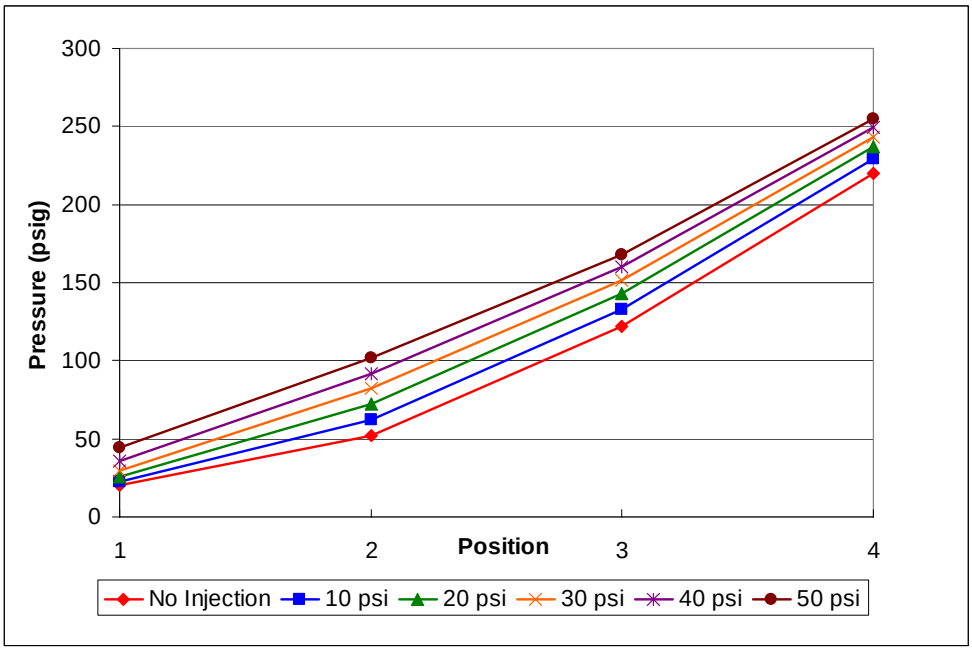

Fig. 6.9 – Pressure profiles (psig) with injection, 80% GVF, differential pressure 200 psi, 1800 RPM.

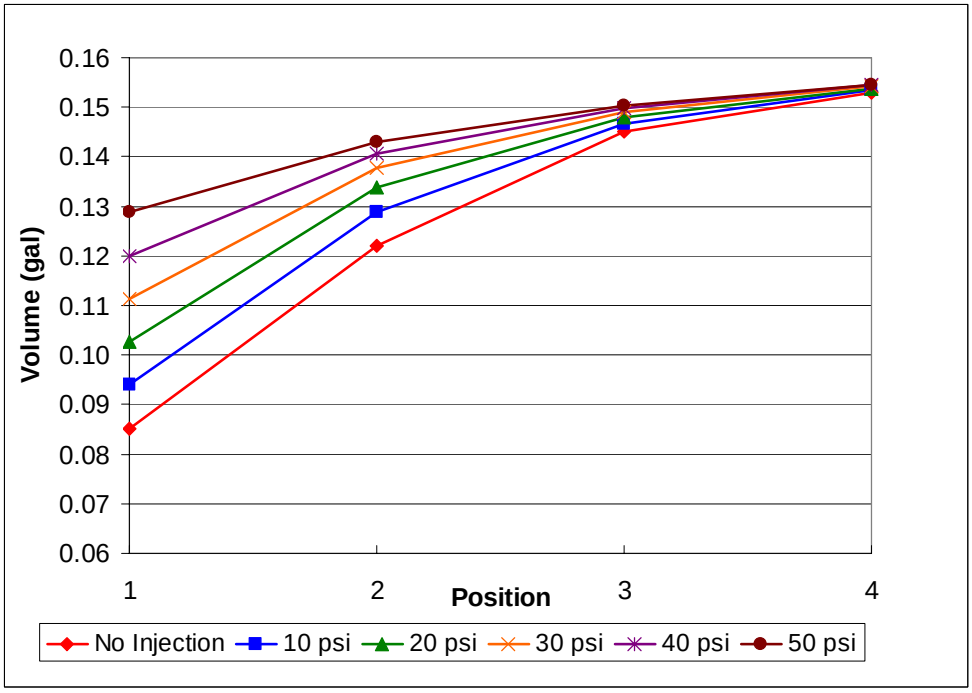

Fig. 6.10 – Liquid volume in chambers (gal) with injection, 80% GVF, differential pressure 200 psi, 1800 RPM.

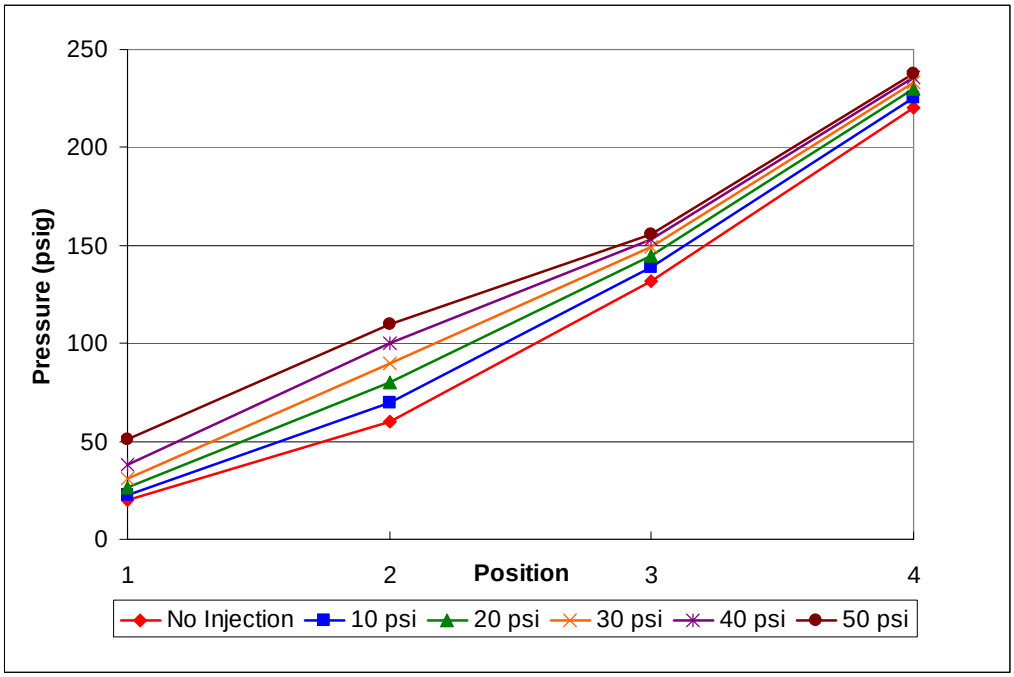

Fig. 6.11 – Pressure profiles (psig) with injection, 60% GVF, differential pressure 200 psi, 1800 RPM.

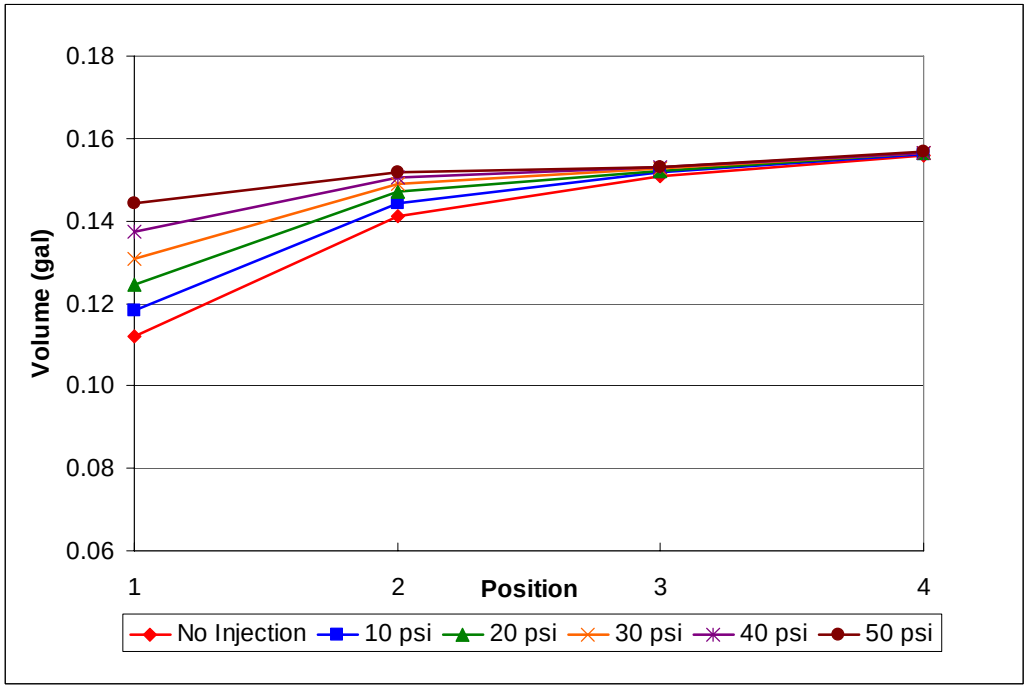

Fig. 6.12 – Liquid volume in chambers (gal) with injection, 60% GVF, differential pressure 200 psi, 1800 RPM.

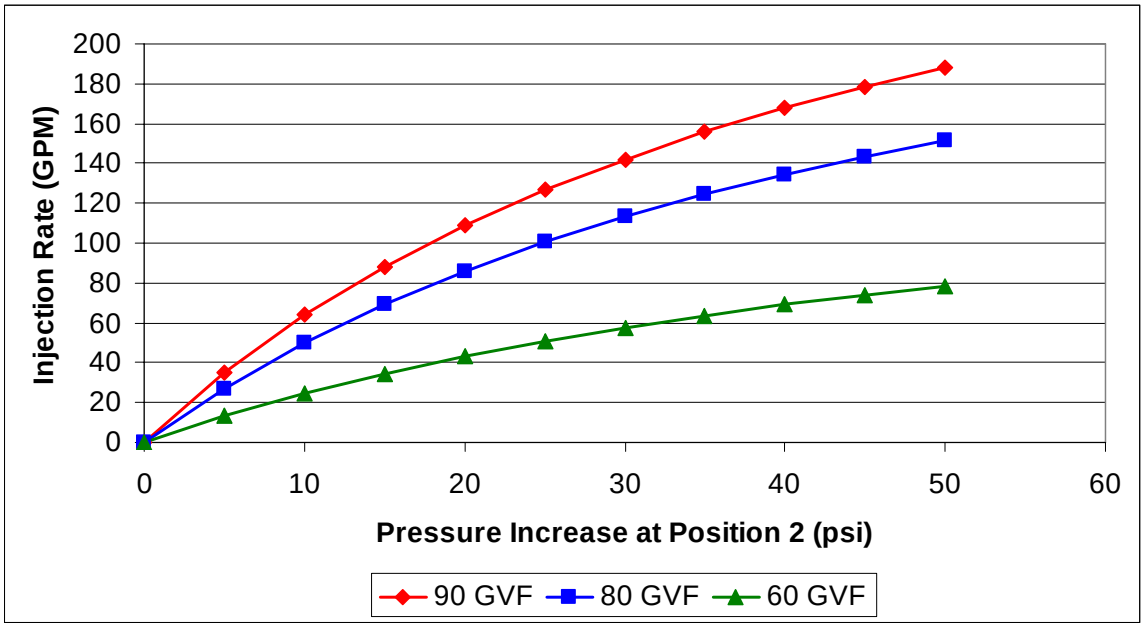

Fig. 6.13 – Pressure increase at position 2 (psi) versus injection rate (GPM), differential pressure 200 psi, 1800 RPM.

Fig. 6.13 displays the injection rate needed to produce the desired pressure increase at position 2. As GVF decreases less injection is required. This is due to the fact that there is more liquid present in each chamber at lower GVF.

To give a perspective of the amount of liquid needed. The total flow rate of the pump operating under the given conditions and at 90% GVF is 181.5 GPM. The total liquid flow rate is therefore only 18.15 GPM. The liquid injection needed can therefore be far larger than the liquid flow rate of the twin-screw pump.

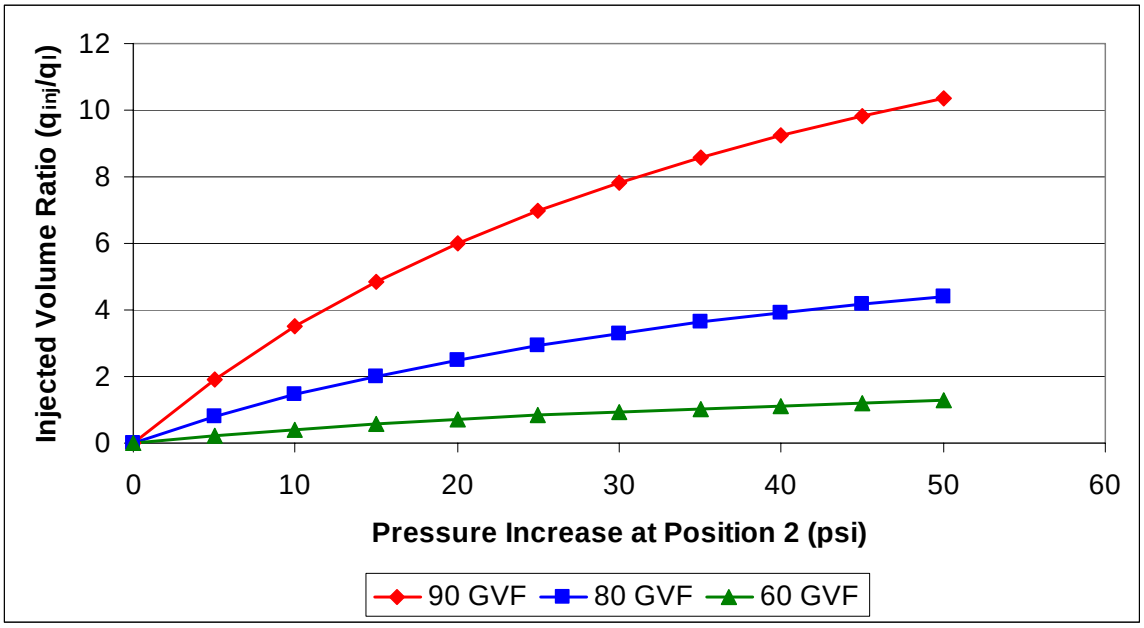

Fig. 6.14 – Pressure increase at position 2 (psi) versus injected volume ratio (q_{inj}/q_l), differential pressure 200 psi, 1800 RPM.

Fig. 6.14 illustrates how much liquid is needed for injection. For maximum pressure boost a 90% GVF, it is necessary to inject 10 times more liquid into the pump than would normally be present. At lower GVF this ratio between injection rate and liquid flow rate is much lower but still greater than one. At 80% GVF, the required injection rate may exceed four times the liquid flow rate. While at 60% GVF, the ratio is less than two. This large amount of liquid volume is needed for injection since we are in effect lowering the operating GVF of the pump.

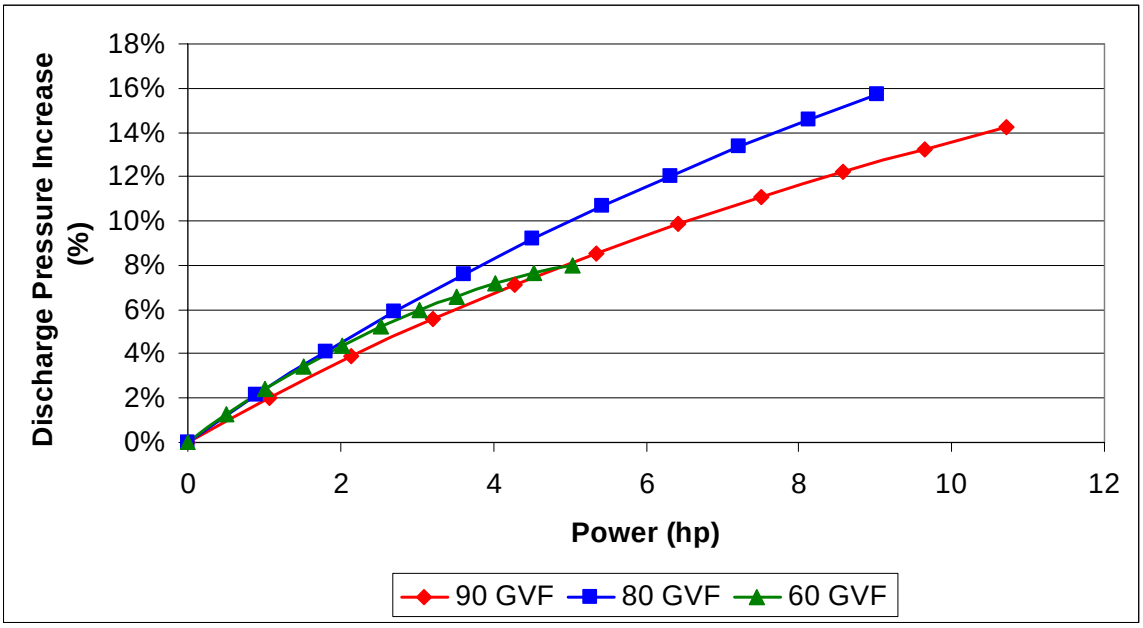

Fig. 6.15 – Power required (hp) versus pressure increase (%), differential pressure 200 psi, 1800 RPM.

Fig. 6.15 shows a comparison of the amount of pressure increase possible versus power needed starting at 90, 80, and 60% GVF. An interesting observation is that more pressure boost is possible using less power at 80% GVF as opposed to 90% GVF. At 80% GVF less liquid injection is needed to produce more compression. This suggests that there exists an optimum GVF for injection. At 60% GVF, the small amount of liquid needed for injection produces little total pressure boost due to reduced compression capacity.

6.3 Conclusions

The feasibility of through-casing injection has been demonstrated. This method has been shown capable of producing an increase in differential pressure of up to 16%. At high initial GVF, pressure profiles can become more linear with injection. The injection rate required to produce the pressure increases needed decreases as GVF decreases. The amount of liquid at the discharge is the limiting factor for the maximum injection rate possible.

The potential of this method has been shown. Further modeling studies and experimental tests should be conducted. The ability of this method to produce more linear pressure profiles may solve some of the vibration problems observed in the field at high GVF. This method also provides a means of producing more pressure boost from an existing pump. The use of injection of a cooler liquid to reduce internal temperature increases at high GVF is another possible application of this method that should be investigated.

CHAPTER VII
SUMMARY OF CONCLUSIONS AND RECOMMENDATIONS

This chapter summarizes the conclusions drawn from the experimental and modeling work performed for this project. Recommendations for future work on wet-gas compression are also given.

7.1 Pure-liquid Test

Tests conducted with pure liquid at elevated viscosity showed that increases in viscosity can have a significant impact on pump performance. Experimental data has shown that:

- Slip flow decreases as viscosity increases.
- Liquid flow rate and volumetric efficiency increase as viscosity increases.

7.2 Wet-gas Test

Efforts to replicate previous tests showing increases in total flow rate under wet-gas conditions with increased viscosity were unsuccessful. Our new experimental data does not confirm earlier findings. We can conclude that:

- At high GVF, viscosity is not the dominant parameter.

Possible explanations for the observed behavior include:

  - Thinning behavior of gel.
  - Loss of liquid sealing.
  - Multiphase flow in clearances.
  - Liquid recirculation.

7.3 Model Recommendations

The twin-screw pump model presented by Martin[8,9] could not produce adequate predictions of pump performance under wet-gas conditions with elevated viscosity. To improve model predictive ability, the following features should be implemented:

- Ability to use fluid property data.
- Multiphase slip-flow in clearances.

- Effective mixture viscosity of slip fluid.
    - Discussed by Cooper & Prang[13] and Vetter *et al.*[10,11]
- Bornemann pump liquid recirculation.
    - Discussed by Rausch *et. al*[14]

7.4 Experiment Recommendations

In order to fully explore wet-gas compression with twin-screw pumps and twin-screw pump behavior with high viscosity liquids further tests should be conducted with modifications to the experimental facility to accommodate:

- Higher boost pressures, > 150 psi.
- Higher viscosities, > 50 cp.

Additionally, the use of a non-temperature thinning, Newtonian liquid would eliminate the complications created by using guar gel.

7.5 Through-Casing Injection Feasibility

The modeling study of through casing injection has shown that:

- The feasibility of through-casing injection has been demonstrated.
- Discharge pressure can be boosted by a maximum of 16%.
- Pressure profiles can become more linear with injection.
- The required injection rate decreases with lower GVF.
- Amount of injection is limited by the volume of liquid in the final chamber.

NOMENCLATURE

A_c	circumferential area (ft^2)
c	radial clearance (in.)
c_c	circumferential clearance (in.)
C	effective clearance (dimensionless)
D	displacement per revolution (gal/rev)
D_c	screw external diameter (in.)
K	flow consistency index (cP^n)
l_h	circumferential gap (in.)
M	molecular weight (lb/lbmole)
$\dot{m}$	mass flow rate (lb/min)
N	pump speed (RPM)
n	flow behavior index (dimensionless)
n_t	number of threads (dimensionless)
n_u	number of chambers (dimensionless)
p	pressure (psi)
q	actual pump flow rate (GPM)
q_g	gas flow rate (GPM)
q_{inj}	injection flow rate (GPM)
q_l	liquid flow rate (GPM)
q_{slip}	slip flow rate (GPM)
q_{TH}	theoretical pump flow rate (GPM)
R	gas constant

s	pitch (in./rev)
T	temperature (°F)
V	volume (gallons)
v	velocity (ft/sec)
z	compressibility factor (dimensionless)
γ	shear rate (sec^{-1})
η_v	volumetric efficiency (dimensionless)
ρ_g	gas density (lb/gal)
ρ_l	liquid density (lb/gal)
μ	apparent viscosity (cP)

REFERENCES

1. Scott, S.L.: “Utilization of Multiphase Pumping in the Oil and Gas Industry,” paper presented at the 2004 Advances in Multiphase Separation and Multiphase Pumping Technologies Seminar, Aberdeen (June 30, 2004).

2. Scharf, A., Raush, T., Vauth, Th., and Mewes, D.: “Investigation on Conveying Characteristics of Multiphase Twin Screw Pumps,” presentation given at the 2005 Multiphase Pumping & Metering Technologies Conference, Manama, Bahrain (November 2005).

3. Martin, A.M. and Scott, S.L.: “Modeling Reservoir/Tubing/Pump Interaction Identifies Best Candidates for Multiphase Pumping,” paper SPE 77500 presented at the 2002 Annual Technical Conference and Exhibition, San Antonio, Texas, 29 September – 2 October.

4. Wilkinson, D.: “CNRL’s Twin Screw Multiphase Pump Experience 2002-2006,” presentation given at the 2006 Texas A&M Multiphase Pump User Roundtable- Canada, Calgary (June 12, 2006).

5. Dick, C. and Speirs, B.: “Imperial Oil Operating Experience with Multiphase and Mass Transfer Pumps in Wet Gas Compression at Cold Lake,” presentation given at the 2006 Texas A&M Multiphase Pump User Roundtable- Canada, Calgary (June 12, 2006).

6. Singh, A.: “Modeling Twin-Screw Multiphase Pump Performance during Periods of High Gas Volume Fraction,” MS thesis, Texas A&M U., College Station, Texas (2003).

7. Singh, A.: “Operability and Performance of Twin-Screw Multiphase Pumps During Wet-Gas Conditions,” presentation given at the 2005 National Engineering Laboratories, United Kingdom and Texas A&M Multiphase Pump User Roundtable- Europe, Aberdeen (August 31, 2005).

8. Martin, A.M.: “Multiphase Twin-Screw Pump Modeling for the Oil and Gas Industry,” PhD dissertation, Texas A&M U., College Station, Texas (2003).

9. Martin, A.M.: “Multiphase Twin-Screw Pump Modeling for the Oil and Gas Industry,” presentation given at the 2005 National Engineering Laboratories, United Kingdom and Texas A&M Multiphase Pump User Roundtable- Europe, Aberdeen (August 31, 2005).

10. Vetter, G. and Wincek, M.: “Performance Prediction of Twin-Screw Pumps for Two-Phase Gas/Liquid Flow,” *Pumping Machinery*, ASME (1993) FED **154**, 331-340.

11. Vetter, G., Wirth, W., Korner, H., and Pregler, S.: “Multiphase Pumping with Twin-Screw Pumps- Understand and Model Hydrodynamics and Hydroabrasive Wear,” *Proc*., 17th International Pump Users Symposium, Houston (1999) 153-169.

12. Egashira, K., Shoda, S., Tochikawa, T., and Furukawa, A.: “Backflow in Twin-Screw-Type Multiphase Pump,” *SPEPF* (February 1998) 64.

13. Prang, A.J. and Cooper, P.: “Enhanced Multiphase Predictions in Twin-Screw Pumps,” *Proc*., 21st International Pump Users Symposium, Houston (2004) 69-76.

14. Rausch, T., Vauth, Th., Brandt, J-U., and Mewes, D.: "A Model for the Delivering Characteristic of Multiphase Pumps," paper presented at the 4th Annual North American Conference on Multiphase Technology, Banff, Canada (June 3-4, 2004).

15. Toma, P.: "Analysis of Multiphase Pumping Instabilities Observed in Steam-Assisted Oil Recovery Fields," *Proc*., International Mechanical Engineers Congress and Exhibition, Orlando, Florida (2005) 1-14.

16. Rohlfing, G. and Muller-Link, D.: "Twin-Screw Rotors - 2nd Generation for Increased Efficiency," presentation given at the 2006 Texas A&M Multiphase Pump User Roundtable-Canada, Calgary (June 12, 2006).

17. "NPV Subsea Test Results," Nuovo Pignone SpA, Florence, Italy (June 2001).

18. Fraino and Santibanez: "Effect of Speed Increase and Clearance Reduction in the Performance of Multiphase Twin Screw Pumps," presentation given at the 2006 Texas A&M Multiphase Pump User Roundtable-Canada, Calgary (June 12, 2006).

APPENDIX A
STUDY OF TWIN-SCREW PUMP CLEARANCES

This section features a short study of pump clearance sizes using the model presented by Martin[8,9]. The Martin model uses linear regression on pure water performance data to determine a value for the effective clearance size, C, within a pump. The linear regression gives a value of C that is consistent with the equation for pump flow rate with turbulent slip flow in the clearances

$$q = q_{TH} - C \cdot \Delta p^{0.57} \tag{A.1}$$

For laminar flow C can also be calculated by:

$$C = 4 \cdot l_h \cdot c \cdot n_t \cdot \left(\frac{c^{1.25}}{\rho^{0.75} \mu^{0.25}} \frac{2 \cdot n_t}{0.066 \cdot s \cdot n_{ch}} \right) \tag{A.2}$$

In Eq, A.2, l_h, c, and s are all measurements of screw geometry. C is therefore a lumped parameter with no meaningful units. Nominally, the Bornemann pump examined has a C value of around 9.5. Unfortunately, reducing this C value to specific measurements of pump clearances cannot be easily done. So the effect of reducing the C value itself will be examined to give the effect of proportional changes in the clearance sizes.

As shown in **Fig. A.1** and **Fig. A.2**, reducing the C value produces increases in flow rate and decreases in slip flow rate at 0% GVF. Therefore volumetric efficiency increases as clearance are narrowed. **Fig. A.3** and **Fig. A.4** show similar results for 95% GVF. The effect of reducing clearances is even more pronounced at this higher GVF. **Fig. A.5** shows a comparison of the reduction of clearance sizes. Reducing the clearances by a third can more than double the flow rate possible.

Although narrower clearances produce more efficient pump performance, they are not necessary desirable. Pump clearances are a tradeoff between efficiency and reliability. A pump's ability to tolerate entrained solids such as sand is due in large part to the clearance sizes. Additionally, metal on metal contact due to shaft deflection is far more likely with narrower clearances. The results of this study are consistent with field data presented by Fraino & Santibanez[18].

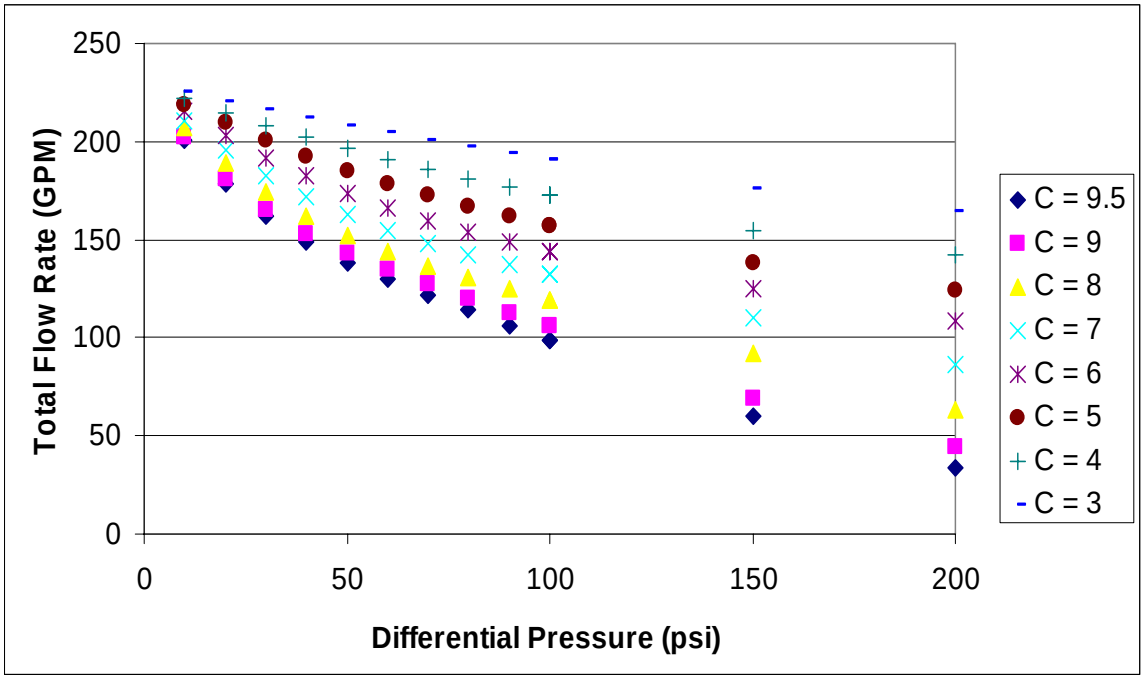

Fig. A.1 – Pump clearance effects, total flow rate (GPM) versus differential pressure (psi), 0% GVF, pump speed 1350 RPM, 1 cP.

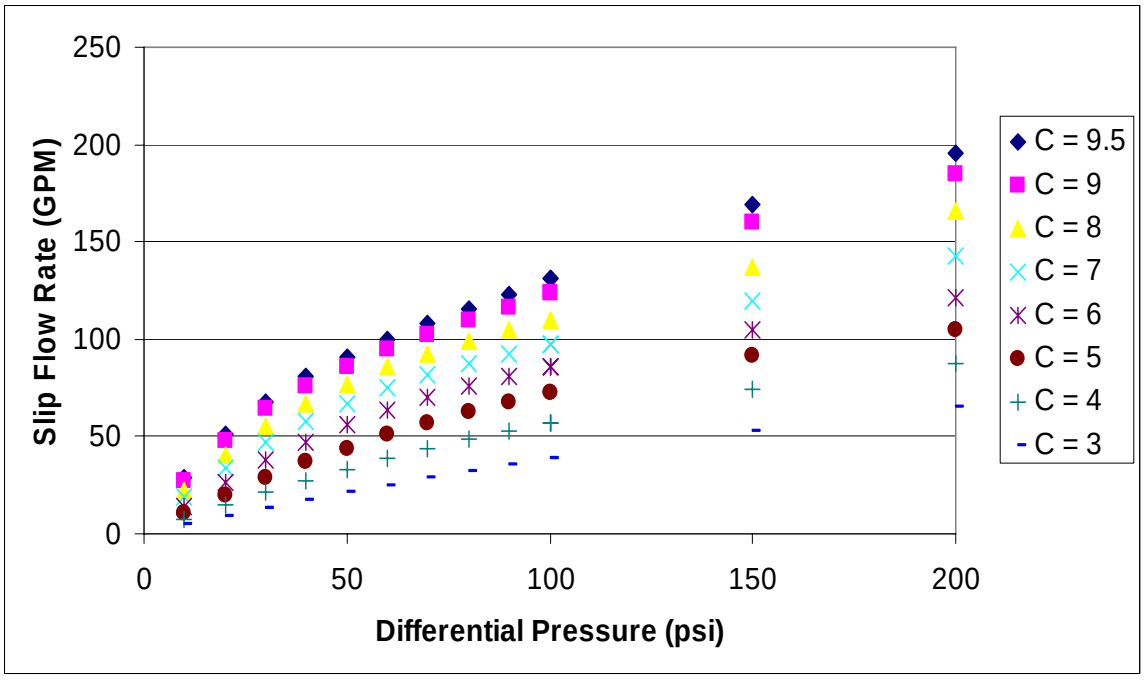

Fig. A.2 – Pump clearance effects, slip flow rate (GPM) versus differential pressure (psi), 0% GVF, pump speed 1350 RPM, 1 cP.

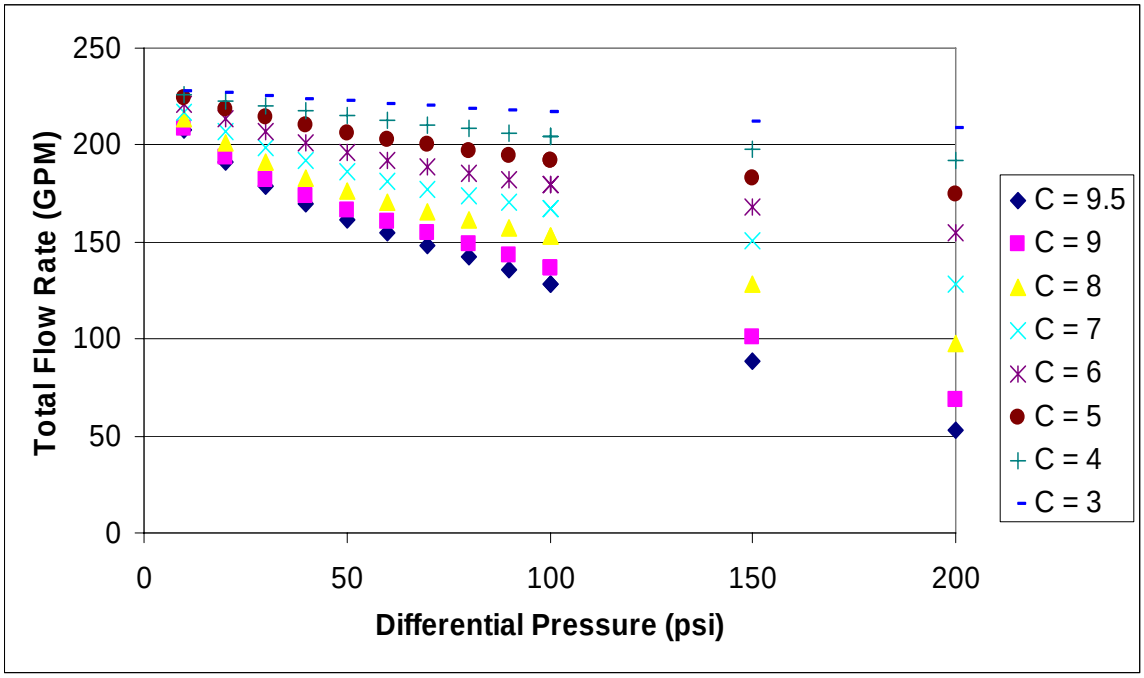

Fig. A.3 – Pump clearance effects, total flow rate (GPM) versus differential pressure (psi), 95% GVF, pump speed 1350 RPM, 1 cP.

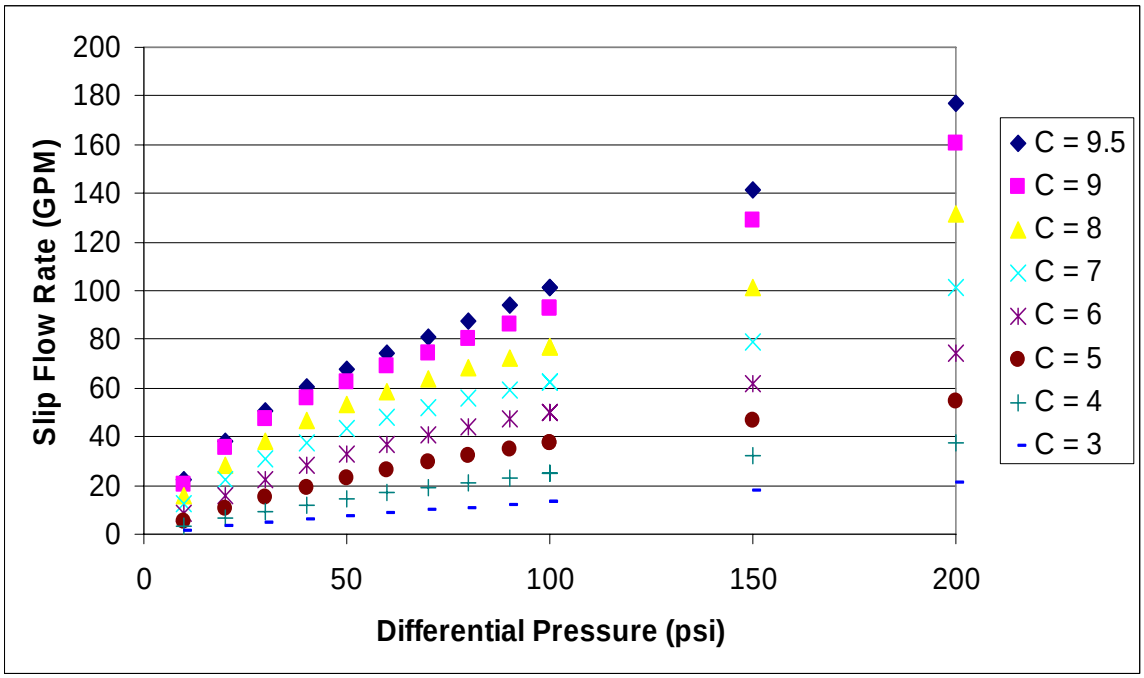

Fig. A.4 – Pump clearance effects, slip flow rate (GPM) versus differential pressure (psi), 95% GVF, pump speed 1350 RPM, 1 cP.

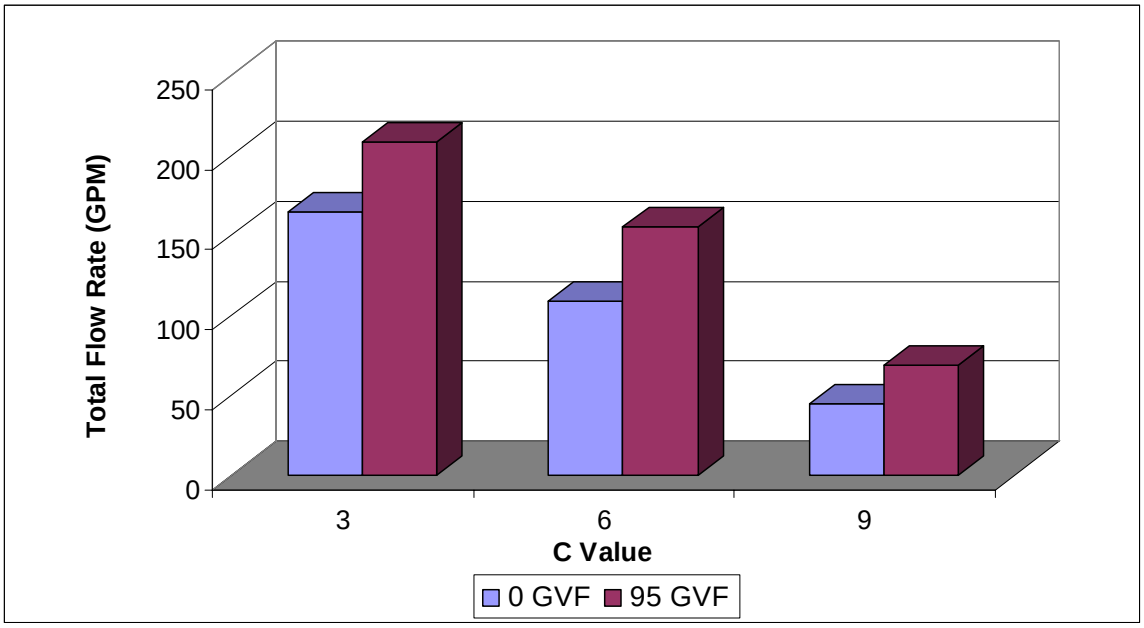

Fig. A.5 – Pump clearance effect comparison.

APPENDIX B

0% GVF DATA

Table B.1 – 1 cP, 0% GVF, 1350 RPM.

m_g (lbpm)	T (F)	m_l (lbpm)	ρ_l (ppg)	P_D (psi)	P_S (psi)	T_S (F)	T_D (F)	q_l (bbl/d)	q_g (bbl/d)	GVF	q_l (GPM)	q_g (GPM)	ΔP (psi)
0.027	88.24	1527.03	8.260	83.62	73.12	90.00	89.99	6339.58	19.41	0.003	185.12	0.57	10.50
0.023	88.71	1368.26	8.260	105.46	82.76	91.19	91.29	5680.04	14.85	0.003	165.86	0.43	22.70
0.026	88.77	1263.83	8.258	121.63	88.17	91.39	91.64	5247.81	15.27	0.003	153.24	0.45	33.47
0.020	89.33	1136.07	8.255	142.78	94.57	94.24	94.47	4718.98	11.22	0.002	137.79	0.33	48.22
0.022	88.82	1092.94	8.258	151.67	96.65	91.81	92.05	4538.16	12.04	0.003	132.51	0.35	55.01
0.019	88.94	961.55	8.259	177.31	102.17	92.38	92.52	3992.45	10.02	0.003	116.58	0.29	75.14
0.020	89.44	933.42	8.253	181.10	103.23	95.27	95.35	3878.25	10.23	0.003	113.24	0.30	77.88
0.019	89.05	856.82	8.257	199.27	106.03	92.93	93.26	3558.09	9.43	0.003	103.90	0.28	93.24
0.020	89.14	789.14	8.258	213.38	108.35	93.19	93.81	3276.94	9.89	0.003	95.69	0.29	105.03
0.021	89.23	671.41	8.255	239.90	111.74	93.72	94.56	2788.91	10.07	0.004	81.44	0.29	128.16
0.020	89.74	1370.38	8.252	70.34	47.72	95.67	95.70	5694.40	21.69	0.004	166.28	0.63	22.62
0.023	89.94	1246.87	8.251	86.93	52.33	96.01	96.13	5181.82	22.74	0.004	151.31	0.66	34.60
0.016	90.14	1096.63	8.251	110.42	57.24	96.30	96.31	4557.68	15.11	0.003	133.08	0.44	53.18
0.019	90.19	989.99	8.250	128.77	60.17	96.15	96.47	4114.83	16.83	0.004	120.15	0.49	68.61
0.017	90.22	793.62	8.249	166.80	64.82	96.20	96.88	3298.99	13.69	0.004	96.33	0.40	101.98
0.021	90.30	595.50	8.251	211.59	68.47	96.46	97.51	2474.93	16.55	0.007	72.27	0.48	143.13
0.007	93.71	1320.15	8.267	66.35	36.23	82.68	82.57	5476.02	9.99	0.002	159.90	0.29	30.12
0.008	93.81	1235.90	8.268	78.60	39.11	82.97	82.93	5125.64	9.94	0.002	149.67	0.29	39.50
0.006	93.75	1078.15	8.269	105.97	44.41	83.00	83.22	4470.66	6.67	0.001	130.54	0.19	61.55
0.007	93.55	946.43	8.269	132.83	48.26	83.60	83.73	3924.79	7.42	0.002	114.60	0.22	84.57
0.007	93.56	824.23	8.267	157.62	51.45	83.47	84.20	3418.72	6.75	0.002	99.83	0.20	106.17
0.009	93.63	740.89	8.268	177.57	53.45	83.97	84.57	3072.71	8.63	0.003	89.72	0.25	124.12
0.008	93.69	641.17	8.269	203.03	55.57	84.47	85.21	2658.87	7.91	0.003	77.64	0.23	147.45
0.013	95.61	1333.06	8.263	62.27	35.43	88.30	88.50	5531.92	19.05	0.003	161.53	0.56	26.83
0.014	95.82	1237.63	8.262	76.30	39.84	88.59	88.75	5136.27	18.21	0.004	149.98	0.53	36.46
0.016	95.94	1093.34	8.262	99.94	46.11	88.80	89.04	4537.77	17.84	0.004	132.50	0.52	53.83
0.016	95.99	965.41	8.263	124.65	51.64	88.86	89.27	4006.52	16.44	0.004	116.99	0.48	73.01
0.012	95.98	813.60	8.263	156.37	57.48	89.22	89.64	3376.23	10.50	0.003	98.59	0.31	98.89
0.013	95.99	719.09	8.262	177.70	60.57	89.13	90.03	2984.60	10.85	0.004	87.15	0.32	117.14
0.014	96.00	614.83	8.262	202.55	63.85	89.62	90.44	2551.75	11.68	0.005	74.51	0.34	138.69
0.011	95.94	529.46	8.261	224.18	66.07	89.66	90.94	2197.63	8.77	0.004	64.17	0.26	158.10

Table B.2 – 9 cP, 0% GVF, 1350 RPM.

m_g (lbpm)	T (F)	m_l (lbpm)	ρ_l (ppg)	P_D (psi)	P_S (psi)	T_S (F)	T_D (F)	q_l (bbl/d)	q_g (bbl/d)	GVF	q_l (GPM)	q_g (GPM)	ΔP (psi)
0.008	85.08	1403.35	8.271	63.82	37.53	87.09	87.00	5818.24	10.93	0.002	169.89	0.32	26.29
0.009	85.36	1275.57	8.269	83.23	42.21	87.16	87.14	5289.42	11.24	0.002	154.45	0.33	41.02
0.009	85.67	1214.19	8.271	94.85	45.40	87.03	87.27	5033.71	10.26	0.002	146.98	0.30	49.46
0.010	86.03	1113.04	8.271	113.80	49.42	87.40	87.46	4614.42	10.30	0.002	134.74	0.30	64.38
0.010	86.17	1009.84	8.270	134.04	53.39	87.34	87.60	4186.98	9.62	0.002	122.26	0.28	80.65
0.009	86.16	937.76	8.270	149.50	56.19	87.48	87.78	3888.13	7.91	0.002	113.53	0.23	93.31
0.009	85.94	839.55	8.270	170.99	59.30	87.56	88.08	3481.09	8.15	0.002	101.65	0.24	111.69
0.008	85.62	782.97	8.270	184.07	60.90	87.51	88.31	3246.44	7.09	0.002	94.80	0.21	123.17
0.008	85.26	721.95	8.269	197.63	62.34	87.85	88.67	2993.68	6.49	0.002	87.42	0.19	135.30
0.007	84.89	627.93	8.270	218.46	64.08	88.11	89.19	2603.54	6.05	0.002	76.02	0.18	154.37
0.007	84.62	548.47	8.271	234.75	64.89	88.47	89.69	2273.96	5.67	0.002	66.40	0.17	169.86

Table B.3 – 26 cP, 0% GVF, 1350 RPM.

m_g (lbpm)	T (F)	m_l (lbpm)	ρ_l (ppg)	P_D (psi)	P_S (psi)	T_S (F)	T_D (F)	q_l (bbl/d)	q_g (bbl/d)	GVF	q_l (GPM)	q_g (GPM)	ΔP (psi)
0.012	115.69	1550.63	8.244	104.69	91.32	104.97	104.89	6449.29	7.17	0.001	188.32	0.21	13.36
0.012	115.76	1402.92	8.245	126.19	97.61	104.97	105.02	5834.27	6.72	0.001	170.36	0.20	28.58
0.012	115.79	1266.16	8.245	148.88	102.99	105.34	105.46	5265.59	6.15	0.001	153.76	0.18	45.89
0.012	115.86	1168.76	8.245	166.23	106.42	105.43	105.66	4860.81	6.30	0.001	141.94	0.18	59.80
0.011	115.95	1049.02	8.244	188.40	110.15	105.93	106.22	4363.29	5.25	0.001	127.41	0.15	78.25
0.012	116.16	938.21	8.244	211.12	113.23	106.19	106.67	3902.33	5.64	0.001	113.95	0.16	97.89
0.011	116.35	811.96	8.245	238.19	116.42	106.70	107.30	3376.83	5.04	0.001	98.60	0.15	121.77
0.013	116.49	714.08	8.243	259.51	118.48	107.12	107.87	2970.49	5.92	0.002	86.74	0.17	141.04

Table B.4 – 40 cP, 0% GVF, 1350 RPM.

m_g (lbpm)	T (F)	m_l (lbpm)	ρ_l (ppg)	P_D (psi)	P_S (psi)	T_S (F)	T_D (F)	q_l (bbl/d)	q_g (bbl/d)	GVF	q_l (GPM)	q_g (GPM)	ΔP (psi)
0.006	102.15	1489.44	8.244	91.82	70.15	102.75	102.81	6195.09	4.38	0.001	180.90	0.13	21.67
0.008	102.05	1412.04	8.245	106.24	75.71	103.14	103.16	5872.30	5.93	0.001	171.47	0.17	30.53
0.016	102.08	1260.54	8.246	136.17	84.60	103.45	103.48	5241.52	10.08	0.002	153.05	0.29	51.57
0.013	102.11	1198.78	8.247	149.73	89.21	103.81	104.04	4984.25	7.65	0.002	145.54	0.22	60.52
0.019	102.07	1085.07	8.247	173.52	93.84	104.31	104.48	4511.73	10.98	0.002	131.74	0.32	79.67
0.019	102.08	976.20	8.247	197.77	98.50	104.60	104.90	4058.89	10.34	0.003	118.52	0.30	99.26
0.015	102.10	863.22	8.245	227.77	106.36	104.98	105.49	3589.88	7.65	0.002	104.82	0.22	121.41
0.017	102.07	785.78	8.245	246.28	109.18	105.35	106.03	3267.81	8.24	0.003	95.42	0.24	137.10

Table B.5 – 1 cP, 0% GVF, 1700 RPM.

m_g (lbpm)	T (F)	m_l (lbpm)	ρ_l (ppg)	P_D (psi)	P_S (psi)	T_S (F)	T_D (F)	q_l (bbl/d)	q_g (bbl/d)	GVF	q_l (GPM)	q_g (GPM)	ΔP (psi)
0.010	95.80	1681.97	8.265	89.16	46.96	85.04	85.10	6978.40	11.22	0.002	203.77	0.33	42.21
0.008	95.40	1623.42	8.266	100.10	50.37	85.45	85.54	6734.85	8.57	0.001	196.66	0.25	49.73
0.010	95.24	1500.43	8.265	126.32	59.97	86.03	86.12	6224.72	8.70	0.001	181.76	0.25	66.35
0.009	95.24	1387.65	8.264	151.55	67.76	86.24	86.56	5757.59	7.07	0.001	168.12	0.21	83.79
0.011	95.21	1314.06	8.264	169.51	73.38	86.52	86.88	5452.21	7.74	0.001	159.20	0.23	96.13
0.012	95.18	1242.58	8.264	188.27	78.50	86.77	87.33	5156.03	8.18	0.002	150.56	0.24	109.77
0.014	95.25	1159.77	8.264	208.65	83.50	87.44	87.77	4812.57	8.87	0.002	140.53	0.26	125.15
0.017	95.38	1087.62	8.263	227.23	87.64	87.43	88.20	4513.40	9.99	0.002	131.79	0.29	139.60
0.018	95.51	969.08	8.262	256.59	93.80	88.06	88.75	4021.83	9.91	0.002	117.44	0.29	162.79
0.031	95.65	902.32	8.262	272.30	97.25	88.33	89.29	3745.07	16.47	0.004	109.36	0.48	175.05

Table B.6 – 9 cP, 0% GVF, 1700 RPM.

m_g (lbpm)	T (F)	m_l (lbpm)	ρ_l (ppg)	P_D (psi)	P_S (psi)	T_S (F)	T_D (F)	q_l (bbl/d)	q_g (bbl/d)	GVF	q_l (GPM)	q_g (GPM)	ΔP (psi)
0.018	79.89	1729.51	8.268	89.29	45.77	88.93	89.05	7173.04	20.42	0.003	209.45	0.60	43.52
0.014	79.44	1649.39	8.268	105.13	51.06	88.97	89.19	6840.29	13.95	0.002	199.74	0.41	54.07
0.012	78.93	1546.64	8.269	128.29	59.18	89.20	89.33	6413.60	10.46	0.002	187.28	0.31	69.11
0.012	78.48	1458.56	8.268	149.92	66.08	89.33	89.58	6048.88	9.19	0.002	176.63	0.27	83.84
0.010	77.46	1365.96	8.268	172.33	71.46	89.72	90.07	5664.91	7.41	0.001	165.42	0.22	100.87
0.010	77.05	1267.60	8.268	198.44	78.87	90.03	90.32	5256.88	6.60	0.001	153.50	0.19	119.57
0.011	76.69	1203.46	8.267	215.67	83.23	90.08	90.60	4992.04	7.02	0.001	145.77	0.20	132.45
0.010	76.40	1122.04	8.268	238.00	88.41	90.35	90.91	4653.64	5.66	0.001	135.89	0.17	149.59
0.009	76.03	1022.63	8.267	267.34	94.90	90.65	91.39	4241.83	5.15	0.001	123.86	0.15	172.44

Table B.7 – 26 cP, 0% GVF, 1700 RPM.

m_g (lbpm)	T (F)	m_l (lbpm)	ρ_l (ppg)	P_D (psi)	P_S (psi)	T_S (F)	T_D (F)	q_l (bbl/d)	q_g (bbl/d)	GVF	q_l (GPM)	q_g (GPM)	ΔP (psi)
0.017	110.83	1880.22	8.233	101.51	73.80	109.94	109.95	7831.19	12.30	0.002	228.67	0.36	27.71
0.017	111.66	1739.86	8.234	127.66	82.31	109.55	109.83	7245.46	11.40	0.002	211.57	0.33	45.35
0.015	113.43	1641.39	8.235	146.77	87.47	109.17	109.51	6834.28	9.21	0.001	199.56	0.27	59.30
0.013	114.19	1558.17	8.235	164.00	91.72	108.97	109.31	6487.78	7.60	0.001	189.44	0.22	72.28
0.014	114.91	1472.41	8.237	182.14	95.74	108.81	109.14	6129.82	8.13	0.001	178.99	0.24	86.41
0.015	115.59	1388.43	8.238	201.08	99.24	108.47	108.82	5779.31	7.94	0.001	168.76	0.23	101.84
0.014	116.11	1296.93	8.240	222.51	102.73	108.30	108.59	5397.28	7.47	0.001	157.60	0.22	119.79
0.015	116.40	1184.02	8.242	250.34	106.79	107.56	108.15	4926.29	7.47	0.002	143.85	0.22	143.55

Table B.8 – 40 cP, 0% GVF, 1700 RPM.

m_g (lbpm)	T (F)	m_l (lbpm)	ρ_l (ppg)	P_D (psi)	P_S (psi)	T_S (F)	T_D (F)	q_l (bbl/d)	q_g (bbl/d)	GVF	q_l (GPM)	q_g (GPM)	ΔP (psi)
0.008	102.36	1604.01	8.236	151.13	81.25	108.62	108.87	6678.24	5.36	0.001	195.00	0.16	69.89
0.009	101.79	1562.43	8.233	143.52	66.79	108.00	108.41	6507.23	7.65	0.001	190.01	0.22	76.73
0.009	101.82	1423.03	8.237	180.43	77.44	107.50	107.74	5923.80	6.12	0.001	172.97	0.18	102.99
0.012	101.88	1318.31	8.241	218.24	94.28	106.84	107.38	5485.12	6.93	0.001	160.17	0.20	123.96
0.013	101.99	1134.55	8.244	267.30	103.38	105.90	106.70	4718.90	6.78	0.001	137.79	0.20	163.91

APPENDIX C

70% GVF DATA

Table C.1 – 1 cP, 70% GVF, 1350 RPM.

m_g (lbpm)	T (F)	m_l (lbpm)	ρ_l (ppg)	P_D (psi)	P_S (psi)	T_S (F)	T_D (F)	q_l (bbl/d)	q_g (bbl/d)	GVF	q_l (GPM)	q_g (GPM)	ΔP (psi)
5.504	108.02	496.27	8.263	62.75	59.69	87.30	87.54	2059.46	4798.07	0.700	60.14	140.10	3.06
5.317	113.58	426.04	8.262	76.07	63.07	88.00	88.25	1768.20	4392.28	0.713	51.63	128.25	13.00
5.075	117.91	355.28	8.261	105.61	68.42	88.77	89.50	1474.63	3869.78	0.724	43.06	113.00	37.18
4.588	119.89	332.03	8.260	132.89	71.12	89.74	90.90	1378.35	3371.87	0.710	40.25	98.46	61.78
3.955	119.96	289.49	8.258	156.48	71.03	90.67	92.54	1202.15	2914.70	0.708	35.10	85.11	85.45
3.293	114.76	264.19	8.254	175.76	71.12	92.70	94.95	1097.49	2432.56	0.689	32.05	71.03	104.64
2.883	118.75	211.25	8.256	201.04	71.27	91.46	95.06	877.38	2120.96	0.707	25.62	61.93	129.77

Table C.2 – 12 cP, 70% GVF, 1350 RPM.

m_g (lbpm)	T (F)	m_l (lbpm)	ρ_l (ppg)	P_D (psi)	P_S (psi)	T_S (F)	T_D (F)	q_l (bbl/d)	q_g (bbl/d)	GVF	q_l (GPM)	q_g (GPM)	ΔP (psi)
5.477	102.34	459.94	8.256	80.49	66.08	95.84	96.15	1910.25	4380.16	0.696	55.78	127.90	14.41
5.284	105.37	401.82	8.256	96.13	68.43	95.62	96.19	1668.82	4078.57	0.710	48.73	119.09	27.70
4.841	104.93	374.04	8.257	120.21	72.82	95.18	95.95	1553.27	3508.93	0.693	45.36	102.46	47.39
4.337	98.81	318.41	8.258	140.30	73.53	94.74	96.02	1322.18	3111.06	0.702	38.61	90.84	66.78
3.575	91.42	282.61	8.259	162.80	73.65	94.38	96.16	1173.32	2558.58	0.686	34.26	74.71	89.15
3.152	89.64	228.86	8.259	179.60	73.94	94.26	96.88	950.21	2246.31	0.703	27.75	65.59	105.66
2.431	88.72	191.08	8.259	206.84	74.31	94.55	98.36	793.36	1724.76	0.685	23.17	50.36	132.53

Table C.3 – 20 cP, 70% GVF, 1350 RPM.

m_g (lbpm)	T (F)	m_l (lbpm)	ρ_l (ppg)	P_D (psi)	P_S (psi)	T_S (F)	T_D (F)	q_l (bbl/d)	q_g (bbl/d)	GVF	q_l (GPM)	q_g (GPM)	ΔP (psi)
5.047	107.85	431.70	8.269	84.18	61.82	85.61	85.97	1790.07	4234.69	0.703	52.27	123.65	22.36
4.523	109.21	388.05	8.271	107.27	62.59	86.03	86.70	1608.79	3751.43	0.700	46.98	109.54	44.68
4.042	111.15	351.66	8.271	129.93	63.42	86.51	87.61	1457.97	3311.37	0.694	42.57	96.69	66.51
3.803	112.80	323.36	8.270	144.47	64.46	87.31	88.56	1340.76	3069.97	0.696	39.15	89.64	80.00
3.501	113.77	287.56	8.270	165.35	66.77	88.03	89.87	1192.34	2731.93	0.696	34.82	79.77	98.58
3.378	114.75	270.44	8.269	174.25	68.28	88.87	91.09	1121.48	2581.91	0.697	32.75	75.39	105.98
2.725	115.25	225.09	8.267	199.94	69.04	90.53	93.79	933.62	2065.55	0.689	27.26	60.31	130.90

Table C.4 – 1 cP, 70% GVF, 1700 RPM.

m_g (lbpm)	T (F)	m_l (lbpm)	ρ_l (ppg)	P_D (psi)	P_S (psi)	T_S (F)	T_D (F)	q_l (bbl/d)	q_g (bbl/d)	GVF	q_l (GPM)	q_g (GPM)	ΔP (psi)
5.823	111.31	549.94	8.247	80.28	55.47	97.18	97.64	2286.54	5560.57	0.709	66.77	162.37	24.81
5.731	112.30	529.04	8.248	92.44	56.74	97.17	97.81	2199.46	5350.50	0.709	64.22	156.23	35.70
5.549	113.01	536.61	8.248	106.63	58.24	97.03	97.74	2230.95	5045.40	0.693	65.14	147.33	48.39
5.443	113.40	510.40	8.247	123.51	59.54	96.70	97.64	2122.07	4837.74	0.695	61.96	141.26	63.97
5.054	112.37	469.98	8.249	159.65	61.53	96.25	97.79	1953.67	4343.72	0.690	57.05	126.84	98.12
4.867	111.08	426.76	8.249	185.20	63.45	95.68	97.67	1774.01	4051.99	0.695	51.80	118.32	121.75
4.824	110.54	388.19	8.250	198.37	64.10	95.19	97.63	1613.53	3972.35	0.711	47.12	115.99	134.26

Table C.5 – 12 cP, 70% GVF, 1700 RPM.

m_g (lbpm)	T (F)	m_l (lbpm)	ρ_l (ppg)	P_D (psi)	P_S (psi)	T_S (F)	T_D (F)	q_l (bbl/d)	q_g (bbl/d)	GVF	q_l (GPM)	q_g (GPM)	ΔP (psi)
5.977	99.15	577.96	8.254	79.33	56.20	96.22	96.60	2401.04	5623.97	0.701	70.11	164.22	23.13
5.724	101.37	532.79	8.255	102.29	58.96	96.39	97.07	2213.23	5135.68	0.699	64.63	149.96	43.33
5.627	100.91	516.46	8.254	110.70	59.90	96.45	97.21	2145.49	4969.47	0.698	62.65	145.11	50.80
5.387	97.91	467.54	8.254	131.98	61.75	96.40	97.42	1942.26	4614.36	0.704	56.71	134.74	70.23
5.049	94.24	420.22	8.256	159.67	64.09	95.87	97.50	1745.44	4163.29	0.705	50.97	121.57	95.58
4.956	96.07	397.44	8.255	169.36	65.25	96.02	97.93	1650.92	4014.63	0.708	48.21	117.23	104.11
4.320	90.76	351.28	8.256	196.90	66.32	95.34	97.94	1458.98	3439.33	0.702	42.60	100.43	130.59

Table C.6 – 20 cP, 70% GVF, 1700 RPM.

m_g (lbpm)	T (F)	m_l (lbpm)	ρ_l (ppg)	P_D (psi)	P_S (psi)	T_S (F)	T_D (F)	q_l (bbl/d)	q_g (bbl/d)	GVF	q_l (GPM)	q_g (GPM)	ΔP (psi)
5.793	114.01	561.20	8.253	83.09	55.52	97.80	98.31	2331.82	5532.46	0.703	68.09	161.55	27.57
5.682	114.05	549.81	8.253	97.73	57.68	97.63	98.27	2284.33	5222.09	0.696	66.70	152.49	40.05
5.601	113.16	514.03	8.254	110.63	58.80	97.31	98.22	2135.56	5046.34	0.703	62.36	147.35	51.83
5.477	113.20	496.70	8.254	120.49	59.57	97.18	98.15	2063.36	4870.03	0.702	60.25	142.20	60.92
5.243	114.16	452.22	8.256	141.53	61.02	96.74	98.03	1878.23	4548.07	0.708	54.84	132.80	80.52
5.252	113.14	423.10	8.257	150.68	61.72	96.21	97.64	1757.03	4499.59	0.719	51.31	131.39	88.96
4.700	113.20	415.07	8.258	178.25	62.81	95.33	97.29	1723.55	3950.95	0.696	50.33	115.37	115.45
4.395	113.39	393.16	8.260	198.19	64.08	94.25	96.70	1632.19	3614.42	0.689	47.66	105.54	134.11

APPENDIX D

95% GVF DATA

Table D.1 – 1 cP, 95% GVF, 1350 RPM.

m_g (lbpm)	T (F)	m_l (lbpm)	ρ_l (ppg)	P_D (psi)	P_S (psi)	T_S (F)	T_D (F)	q_l (bbl/d)	q_g (bbl/d)	GVF	q_l (GPM)	q_g (GPM)	ΔP (psi)
6.665	104.64	63.55	8.245	74.63	61.54	96.52	97.74	264.29	5730.55	0.956	7.72	167.33	13.09
6.150	104.40	65.45	8.245	87.86	61.97	97.93	101.55	272.20	5264.09	0.951	7.95	153.71	25.88
6.314	105.26	71.00	8.251	87.56	62.35	95.48	96.34	295.07	5348.81	0.948	8.62	156.19	25.21
5.451	103.63	73.71	8.250	92.26	56.73	94.19	97.76	306.36	5063.10	0.943	8.95	147.84	35.52
5.200	104.39	53.68	8.249	117.19	59.57	95.05	99.20	223.14	4606.44	0.954	6.52	134.51	57.62
5.166	107.16	29.89	8.239	134.12	62.74	96.88	106.37	124.42	4359.53	0.972	3.63	127.30	71.37
5.123	107.75	36.50	8.243	166.75	69.93	98.57	106.54	151.84	3890.18	0.962	4.43	113.59	96.82
3.669	101.84	51.08	8.242	158.92	52.34	96.97	109.83	212.52	3713.74	0.946	6.21	108.44	106.59
5.233	100.39	120.47	8.258	26.99	26.75	92.03	91.77	500.21	10286.94	0.953	14.61	300.38	0.24
4.275	100.84	63.17	8.260	62.00	41.82	91.71	95.45	262.23	5361.71	0.953	7.66	156.56	20.18
4.139	102.02	59.41	8.259	91.65	45.96	91.93	96.12	246.67	4725.78	0.950	7.20	137.99	45.70
3.712	100.99	54.06	8.259	130.30	46.68	91.57	100.13	224.45	4169.83	0.949	6.55	121.76	83.61
3.617	101.20	50.16	8.261	151.91	48.90	91.51	103.09	208.20	3878.40	0.949	6.08	113.25	103.01
3.550	100.86	46.59	8.258	164.14	50.91	91.57	105.51	193.46	3657.39	0.950	5.65	106.80	113.23
3.383	100.09	41.24	8.259	179.98	53.58	91.62	108.39	171.23	3311.29	0.951	5.00	96.69	126.40
3.005	95.92	38.41	8.260	203.09	55.03	90.71	112.81	159.44	2858.68	0.947	4.66	83.47	148.06
2.619	100.84	28.88	8.260	256.50	66.96	97.19	116.87	119.89	2071.45	0.945	3.50	60.49	189.54
5.105	102.24	49.73	8.261	162.49	67.82	90.62	99.59	206.43	3940.24	0.950	6.03	115.05	94.67
4.193	102.06	36.52	8.260	207.26	71.10	90.64	104.10	151.60	3087.43	0.953	4.43	90.15	136.16
3.574	101.59	26.88	8.259	238.04	74.10	97.76	109.17	111.61	2557.62	0.958	3.26	74.68	163.94
3.291	100.62	21.18	8.259	250.34	75.61	102.28	116.17	87.94	2326.59	0.964	2.57	67.94	174.73

Table D.2 – 9 cP, 95% GVF, 1350 RPM.

m_g (lbpm)	T (F)	m_l (lbpm)	ρ_l (ppg)	P_D (psi)	P_S (psi)	T_S (F)	T_D (F)	q_l (bbl/d)	q_g (bbl/d)	GVF	q_l (GPM)	q_g (GPM)	ΔP (psi)
6.067	96.73	76.32	8.268	57.19	53.74	88.07	89.51	316.53	5884.16	0.949	9.24	171.82	3.46
5.800	97.04	68.68	8.269	76.75	56.98	87.93	90.67	284.82	5302.78	0.949	8.32	154.84	19.77
5.716	96.65	64.06	8.269	87.83	59.44	87.76	91.71	265.67	5007.44	0.950	7.76	146.22	28.38
5.444	96.51	57.51	8.268	105.00	61.70	87.36	92.88	238.50	4591.91	0.951	6.96	134.08	43.30
4.755	94.09	49.16	8.270	136.80	64.90	87.31	96.17	203.85	3812.29	0.949	5.95	111.32	71.90
4.681	94.08	44.18	8.270	154.47	69.59	86.87	98.88	183.18	3497.41	0.950	5.35	102.12	84.88
4.309	94.79	37.12	8.270	179.18	74.65	86.66	101.73	153.92	3000.22	0.951	4.49	87.61	104.53
3.592	94.83	25.68	8.270	206.30	78.90	86.42	106.29	106.46	2365.06	0.957	3.11	69.06	127.39
3.021	92.84	18.25	8.274	222.75	81.80	96.53	116.13	75.65	1954.26	0.963	2.21	57.06	140.95

Table D.3 – 24 cP, 95% GVF, 1350 RPM.

m_g (lbpm)	T (F)	m_l (lbpm)	ρ_l (ppg)	P_D (psi)	P_S (psi)	T_S (F)	T_D (F)	q_l (bbl/d)	q_g (bbl/d)	GVF	q_l (GPM)	q_g (GPM)	ΔP (psi)
5.800	117.79	86.98	8.257	62.21	55.57	98.84	99.31	361.21	5547.20	0.939	10.55	161.98	6.64
5.811	116.46	62.99	8.257	79.57	58.13	99.03	100.96	261.56	5313.82	0.953	7.64	155.16	21.44
5.710	115.77	57.98	8.257	92.48	60.15	98.89	102.98	240.78	5044.79	0.954	7.03	147.31	32.34
5.227	117.56	45.58	8.258	125.95	63.42	99.34	105.60	189.26	4383.16	0.959	5.53	127.99	62.53
4.767	115.45	51.78	8.256	131.63	62.57	100.15	108.53	215.07	4057.67	0.950	6.28	118.48	69.06
4.552	116.60	46.65	8.258	151.27	65.74	99.95	109.99	193.72	3686.32	0.950	5.66	107.64	85.53
4.270	118.07	39.40	8.256	178.76	71.69	99.90	113.44	163.64	3170.32	0.951	4.78	92.57	107.08
3.707	118.72	28.06	8.259	209.61	76.11	100.22	118.41	116.49	2594.34	0.957	3.40	75.75	133.50
3.329	118.35	21.19	8.255	225.73	78.83	100.38	126.37	88.02	2250.08	0.962	2.57	65.70	146.90

Table D.4 – 40 cP, 95% GVF, 1350 RPM.

m_g (lbpm)	T (F)	m_l (lbpm)	ρ_l (ppg)	P_D (psi)	P_S (psi)	T_S (F)	T_D (F)	q_l (bbl/d)	q_g (bbl/d)	GVF	q_l (GPM)	q_g (GPM)	ΔP (psi)
6.130	112.24	81.57	8.274	58.05	52.97	88.90	89.42	338.04	6041.49	0.947	9.87	176.41	5.08
5.750	113.39	65.53	8.275	85.03	57.72	89.86	91.85	271.53	5207.46	0.950	7.93	152.06	27.30
5.415	112.03	62.30	8.272	96.11	56.73	90.93	95.21	258.25	5000.07	0.951	7.54	146.00	39.38
5.191	114.39	55.18	8.273	125.76	61.49	91.45	97.30	228.72	4426.44	0.951	6.68	129.25	64.28
4.980	116.72	47.27	8.272	152.37	66.64	91.87	100.67	195.96	3920.43	0.952	5.72	114.48	85.72
4.794	116.20	41.67	8.273	171.07	69.79	92.08	104.12	172.74	3605.34	0.954	5.04	105.28	101.28
4.309	115.26	29.02	8.273	196.05	73.37	92.50	111.22	120.27	3084.79	0.962	3.51	90.08	122.68
3.742	113.55	26.12	8.273	224.17	76.17	92.50	116.85	108.27	2580.70	0.960	3.16	75.36	148.00

Table D.5 – 50 cP, 95% GVF, 1350 RPM.

m_g (lbpm)	T (F)	m_l (lbpm)	ρ_l (ppg)	P_D (psi)	P_S (psi)	T_S (F)	T_D (F)	q_l (bbl/d)	q_g (bbl/d)	GVF	q_l (GPM)	q_g (GPM)	ΔP (psi)
5.876	106.95	74.63	8.247	63.65	56.10	104.71	105.91	310.29	5626.24	0.948	9.06	164.29	7.54
5.616	108.72	64.25	8.249	89.53	60.20	104.45	107.78	267.08	5006.36	0.949	7.80	146.19	29.32
5.482	109.11	58.24	8.248	105.78	61.67	104.47	109.10	242.15	4771.43	0.952	7.07	139.33	44.12
5.177	109.78	47.32	8.249	129.63	64.81	104.32	111.63	196.71	4285.71	0.956	5.74	125.14	64.82
4.771	110.60	41.15	8.252	163.49	69.28	104.20	115.55	171.00	3694.01	0.956	4.99	107.87	94.21
4.588	109.79	30.05	8.253	179.60	72.28	104.18	119.92	124.87	3404.45	0.965	3.65	99.41	107.33
3.757	106.36	33.31	8.256	198.70	68.84	103.90	124.95	138.36	2926.03	0.955	4.04	85.44	129.86

Table D.6 – 1 cP, 95% GVF, 1700 RPM.

m_g (lbpm)	T (F)	m_l (lbpm)	ρ_l (ppg)	P_D (psi)	P_S (psi)	T_S (F)	T_D (F)	q_l (bbl/d)	q_g (bbl/d)	GVF	q_l (GPM)	q_g (GPM)	ΔP (psi)
6.333	104.78	95.98	8.268	45.96	40.61	86.34	85.84	398.07	8101.24	0.953	11.62	236.56	5.35
6.279	105.79	92.72	8.267	55.61	42.15	87.04	87.17	384.58	7746.96	0.953	11.23	226.21	13.46
6.243	106.30	87.53	8.267	76.83	45.07	86.95	88.98	363.04	7202.92	0.952	10.60	210.33	31.75
6.218	106.78	82.17	8.267	102.24	48.43	87.58	91.41	340.81	6684.08	0.951	9.95	195.18	53.80
6.158	108.22	77.60	8.267	127.63	51.36	87.63	93.80	321.87	6242.12	0.951	9.40	182.27	76.27
6.125	108.96	73.32	8.268	144.79	53.55	87.63	96.16	304.07	5954.51	0.951	8.88	173.87	91.23
5.864	110.41	65.73	8.267	175.48	56.64	87.60	99.56	272.65	5389.58	0.952	7.96	157.38	118.84
5.339	106.99	62.02	8.264	187.26	54.55	90.99	103.21	257.34	5127.53	0.952	7.51	149.72	132.71
5.196	104.62	54.53	8.264	202.66	56.29	93.77	107.61	226.26	4860.04	0.956	6.61	141.91	146.37
4.903	108.91	51.68	8.263	229.31	58.70	97.19	108.15	214.44	4424.61	0.954	6.26	129.20	170.61

Table D.7 – 10 cP, 95% GVF, 1700 RPM.

m_g (lbpm)	T (F)	m_l (lbpm)	ρ_l (ppg)	P_D (psi)	P_S (psi)	T_S (F)	T_D (F)	q_l (bbl/d)	q_g (bbl/d)	GVF	q_l (GPM)	q_g (GPM)	ΔP (psi)
6.538	118.71	95.63	8.259	51.74	45.38	96.96	96.84	397.06	7630.50	0.951	11.59	222.81	6.36
6.423	119.93	91.31	8.258	72.17	46.60	97.22	98.56	379.13	7302.94	0.951	11.07	213.25	25.57
6.271	119.94	83.93	8.259	97.40	49.28	97.85	101.29	348.49	6748.97	0.951	10.18	197.07	48.12
6.153	119.95	78.15	8.258	115.40	51.05	98.06	103.40	324.51	6395.73	0.952	9.48	186.76	64.35
5.661	119.94	75.94	8.256	137.20	51.24	99.18	106.58	315.39	5873.97	0.949	9.21	171.52	85.96
5.512	119.95	69.49	8.255	161.27	54.45	99.19	109.05	288.64	5382.15	0.949	8.43	157.16	106.82
5.359	119.94	63.27	8.256	185.33	58.46	99.28	112.09	262.78	4873.94	0.949	7.67	142.32	126.86
5.178	119.96	55.46	8.256	208.92	63.60	99.33	116.69	230.34	4329.81	0.949	6.73	126.43	145.32

Table D.8 – 26 cP, 95% GVF, 1700 RPM.

m_g (lbpm)	T (F)	m_l (lbpm)	ρ_l (ppg)	P_D (psi)	P_S (psi)	T_S (F)	T_D (F)	q_l (bbl/d)	q_g (bbl/d)	GVF	q_l (GPM)	q_g (GPM)	ΔP (psi)
6.366	119.60	102.07	8.250	52.29	46.11	103.01	103.55	424.25	7394.08	0.946	12.39	215.91	6.18
6.281	119.99	96.07	8.250	79.97	48.53	103.23	105.90	399.29	6930.30	0.946	11.66	202.36	31.44
6.116	119.99	82.19	8.250	110.36	51.22	103.70	108.96	341.64	6400.30	0.949	9.98	186.89	59.14
6.021	119.98	77.14	8.250	126.34	53.18	103.59	110.75	320.66	6067.08	0.950	9.36	177.16	73.16
5.798	119.96	69.95	8.250	149.45	55.46	103.61	113.06	290.76	5601.69	0.951	8.49	163.57	93.99
5.687	119.98	64.61	8.249	165.68	57.93	104.02	115.72	268.59	5264.14	0.951	7.84	153.71	107.75
5.253	119.98	52.40	8.247	201.50	61.71	104.10	120.37	217.90	4565.42	0.954	6.36	133.31	139.79

Table D.9 – 40 cP, 95% GVF, 1700 RPM.

m_g (lbpm)	T (F)	m_l (lbpm)	ρ_l (ppg)	P_D (psi)	P_S (psi)	T_S (F)	T_D (F)	q_l (bbl/d)	q_g (bbl/d)	GVF	q_l (GPM)	q_g (GPM)	ΔP (psi)
6.801	117.44	99.21	8.264	54.54	47.78	94.89	95.72	411.68	7511.70	0.948	12.02	219.34	6.76
6.629	117.52	93.98	8.263	68.93	50.58	95.83	97.51	390.00	6926.52	0.947	11.39	202.25	18.35
6.294	116.94	90.48	8.263	89.09	47.98	96.35	99.98	375.50	6939.72	0.949	10.96	202.64	41.11
6.237	118.02	86.75	8.264	105.29	49.38	96.52	101.56	359.99	6684.19	0.949	10.51	195.18	55.91
6.060	118.65	78.11	8.262	139.04	53.37	96.79	104.57	324.21	6010.36	0.949	9.47	175.50	85.67
5.857	118.84	70.57	8.264	164.98	56.30	97.13	107.61	292.84	5510.38	0.950	8.55	160.90	108.68
5.679	118.81	62.83	8.263	187.02	59.22	97.22	111.79	260.73	5080.02	0.951	7.61	148.34	127.79
5.525	118.22	57.94	8.264	202.15	60.95	97.28	113.99	240.40	4803.36	0.952	7.02	140.26	141.21

Table D.10 – 50 cP, 95% GVF, 1700 RPM.

m_g (lbpm)	T (F)	m_l (lbpm)	ρ_l (ppg)	P_D (psi)	P_S (psi)	T_S (F)	T_D (F)	q_l (bbl/d)	q_g (bbl/d)	GVF	q_l (GPM)	q_g (GPM)	ΔP (psi)
6.522	104.78	93.57	8.253	54.59	47.39	101.29	102.56	388.79	7347.01	0.950	11.35	214.53	7.20
6.307	105.98	84.38	8.253	69.03	50.52	101.25	103.61	350.57	6663.00	0.950	10.24	194.56	18.51
6.363	105.87	84.73	8.252	89.33	50.13	101.10	105.34	352.08	6771.01	0.951	10.28	197.71	39.19
6.138	106.69	76.55	8.253	119.15	52.28	101.47	107.90	318.06	6268.02	0.952	9.29	183.03	66.87
5.776	104.85	75.61	8.257	139.18	52.86	100.02	109.73	314.03	5818.11	0.949	9.17	169.89	86.31
5.615	106.27	69.32	8.258	163.17	55.02	99.41	111.08	287.84	5428.34	0.950	8.40	158.51	108.16
5.546	106.90	62.58	8.259	188.62	59.07	99.29	114.35	259.83	4992.68	0.951	7.59	145.79	129.55
5.090	108.06	47.43	8.258	236.05	64.16	99.63	120.11	196.95	4221.11	0.955	5.75	123.26	171.89

APPENDIX E

100% GVF DATA

Table E.1 – 1 cp, 100% GVF, 1350 RPM.

m_g (lbpm)	T (F)	m_l (lbpm)	ρ_l (ppg)	P_D (psi)	P_S (psi)	T_S (F)	T_D (F)	q_l (bbl/d)	q_g (bbl/d)	GVF	q_l (GPM)	q_g (GPM)	ΔP (psi)
6.628	102.89	2.52	8.252	68.30	60.38	95.51	98.09	10.47	5797.58	0.998	0.31	169.29	7.91
4.113	110.39	2.67	8.253	91.05	73.50	97.20	101.09	11.10	2966.00	0.996	0.32	86.61	17.55
3.449	94.71	4.18	8.260	179.62	54.08	90.06	117.78	17.36	3338.30	0.995	0.51	97.48	125.54
5.718	99.11	3.19	8.277	76.80	53.55	81.90	86.94	13.21	5501.93	0.998	0.39	160.66	23.26
5.220	100.50	3.00	8.274	93.26	53.37	84.00	95.67	12.42	5058.60	0.998	0.36	147.71	39.90
5.097	101.62	2.57	8.271	110.98	56.61	85.42	104.60	10.65	4668.51	0.998	0.31	136.32	54.37
4.718	103.27	2.90	8.272	139.42	58.71	86.54	112.25	12.02	4175.20	0.997	0.35	121.92	80.71
5.977	101.81	2.96	8.260	67.62	52.91	91.12	96.94	12.28	5918.55	0.998	0.36	172.82	14.70
5.753	103.34	2.74	8.259	100.50	59.78	91.93	100.68	11.40	5049.55	0.998	0.33	147.45	40.72
5.065	103.44	2.87	8.259	161.94	68.20	92.27	108.78	11.94	3899.91	0.997	0.35	113.88	93.74
4.074	103.35	2.92	8.259	191.91	72.04	92.08	118.37	12.11	2968.24	0.996	0.35	86.67	119.87
3.202	102.76	2.96	8.259	211.10	75.86	92.29	128.65	12.31	2216.53	0.994	0.36	64.72	135.24

Table E.2 – 9 cp, 100% GVF, 1350 RPM.

m_g (lbpm)	T (F)	m_l (lbpm)	ρ_l (ppg)	P_D (psi)	P_S (psi)	T_S (F)	T_D (F)	q_l (bbl/d)	q_g (bbl/d)	GVF	q_l (GPM)	q_g (GPM)	ΔP (psi)
6.487	94.11	3.78	8.269	79.15	61.13	87.55	94.75	15.67	5524.77	0.997	0.46	161.32	18.02
6.177	95.37	3.80	8.270	95.59	64.23	87.66	97.76	15.76	5007.73	0.997	0.46	146.23	31.36
5.766	96.55	3.57	8.270	118.53	67.56	87.68	102.48	14.82	4444.14	0.997	0.43	129.77	50.97
4.852	98.10	3.76	8.271	141.69	75.11	87.77	107.91	15.58	3363.91	0.995	0.46	98.23	66.57
4.865	90.50	3.71	8.268	133.54	62.41	86.44	102.63	15.40	4050.70	0.996	0.45	118.28	71.13
3.641	92.91	3.94	8.270	208.34	78.37	86.94	113.34	16.32	2417.01	0.993	0.48	70.58	129.97
0.744	90.82	3.64	8.270	246.88	89.39	87.12	125.89	15.09	432.75	0.966	0.44	12.64	157.49

VITA

Evan Chan
3907 Flintrock Ln.
Sugar Land, Texas 77479
Phone: (281) 980-6038
Email: evanchan13@gmail.com

Education

Texas A&M University, College Station, Texas
Master of Science, Petroleum Engineering, August 2006
GPA: 3.84/4.00

Brown University, Providence, Rhode Island
Bachelor of Science, Chemical Engineering, 2004